GLASS FORMATION BOUNDARY APPROACH TO THE SINTERING OF ALUMINA

BY

THOMAS LAM

A THESIS
SUBMITTED TO THE FACULTY OF

ALFRED UNIVERSITY

IN PARTIAL FULFILLMENT OF THE REQUIREMENTS
FOR THE DEGREE OF

DOCTOR OF PHILOSOPHY

IN

CERAMICS

ALFRED, NEW YORK
DECEMBER, 2010

GLASS FORMATION BOUNDARY APPROACH TO THE SINTERING OF ALUMINA

BY

THOMAS LAM

B.S. ALFRED UNIVERSITY (2004)

M.S. ALFRED UNIVERSITY (2007)

SIGNATURE OF AUTHOR (SIGNATURE ON FILE)

APPROVED BY (SIGNATURE ON FILE)
WILLIAM M. CARTY, ADVISOR

(SIGNATURE ON FILE)
VASANTHA R. AMARAKOON, ADVISORY COMMITTEE

(SIGNATURE ON FILE)
MATTHEW M. HALL, ADVISORY COMMITTEE

(SIGNATURE ON FILE)
WILLIAM C. LACOURSE, ADVISORY COMMITTEE

(SIGNATURE ON FILE)
CHAIR, ORAL THESIS DEFENSE

ACCEPTED BY (SIGNATURE ON FILE)
DOREEN D. EDWARDS, DEAN
KAZUO INAMORI SCHOOL OF ENGINEERING

ACCEPTED BY (SIGNATURE ON FILE)
NANCY J. EVANGELISTA, ASSOCIATE PROVOST
FOR GRADUATE AND PROFESSIONAL PROGRAMS
ALFRED UNIVERSITY

ACKNOWLEDGEMENTS

I would first like to thank my advisor, Dr. Carty. Dr. Carty, it has been a privilege to learn from you and work on this research thesis topic. Dr. Amarakoon, Dr. Hall, and Dr. LaCourse thank you for being on my committee.

I would like to thank the National Energy Technology Laboratory (NETL) for my appointment as a student trainee in the Minority Mentoring Internship Program. From NETL, I would first like to thank Dr. Christopher Cowen for being a great friend and informing about the Minority Mentoring Internship Program. I would like to thank Dr. Kyei-Sing Kwong for being my mentor, Dr. Jinichiro Nakano for giving me lessons in FactSage™ and the educational discussions on thermodynamic modeling, and John Sears for teaching me the operation and sample preparation in TEM.

Within Dr. Carty's group, I would like to thank Keith DeCarlo for being my roommate and his help with SEM of thermal etch samples, Hyojin Lee for sending out the chemical analysis, Dave Finkelnburg for his editorial assistance, and Mindy Friday for helping me get the thesis on display.

At Scholes Library, I would like to thank Jane Brown for handling my out of state book renewals, Beverly Crowell and Pat LaCourse for their help with interlibrary loan and reference citations.

Gerald Wynick, thank you for the wavelength dispersive spectroscopy data and all of the numerous technical discussions on electron microscopy.

I would also like to thank Dr. Jake Amoroso John Rich, and Kara Vaneck for their friendship, scientific discussions, company during late night research sessions. Not to mention the friendship of Dr. Aladdin Geleil, Martin Chao, James Kelly, Dr. Eric Nichols and many other graduate students, faculty within the program, and the undergraduate students (especially from the SEM classes) who helped make this a memorable experience.

Lastly, I would like to thank my family who is always there for me.

TABLE OF CONTENTS

LIST OF TABLES

LIST OF FIGURES

ABSTRACT

Sintering in alumina has been extensively studied with a wide range of compositions and a correspondingly large variability of reported chemistries and mineralogy in the grain boundaries. Even with recent advances in the understanding kinetics of grain growth and grain boundary structures, only a few studies have attempted to interpret the evolution of the grain boundary phases and chemistries in alumina sintering potentially due to the fact that sintering of ceramics is a decidedly non-equilibrium process. Expanding on a concept used to successfully explain mineralogy of fired porcelain, the glass formation boundary approach is introduced to predict grain boundary evolution in sintered alumina. Microstructural evolution and grain boundary phases were investigated for four $CaO:SiO_2$ ratios in isochronal sintering studies at 1400°C, 1600°C, and 1700°C.

The microstructural analysis showed that additive ratios of high silica to calcia ratios yielded amorphous grain boundaries containing anorthite and mullite as secondary phases. A glass formation boundary was applied to explain the formation of mullite without the presence of anorthite. Anorthite found in the samples sintered at 1400°C were proposed to be caused by localized low temperature solid state reactions. A similar argument was used to explain anorthite and gehlenite precipitation at 1400°C at higher CaO ratios. At temperatures above 1600°C amorphous grain boundaries of invert glass compositions and anorthite were found at the grain boundaries and were explainable by an invert glass formation boundary.

The glass formation boundary approach adequately provides an explanation for secondary phases reported in the literature and allows for the prediction of grain boundary chemistry in steady-state non-equilibrium conditions experienced when sintering alumina in the presence of a liquid phase (as would be expected in situations with alumina containing silica, alkali, and alkaline earth impurities). The volume of the secondary phases observed correlates with the grain boundary chemistry at the triple points also consistent with the glass formation boundary approach. Furthermore, it is shown that impurities can be viewed as localized concentrations where the volume of secondary phases is directly limited by the concentration of additives. Although this

study has addressed CaO and SiO_2 as the impurity chemistry, it is expected that this idea can be more globally applied to explain grain boundary evolution in alumina.

1. INTRODUCTION

1.1. ADDITIVES IN SINTERING OF ALUMINA

The literature shows numerous studies in the sintering of alumina with particular use of additives, or more commonly, impurities, and their influence on sintering behavior and microstructure evolution. In most cases the impurities present will segregate to the grain boundary due to the limited solubility of ions within the alumina lattice.[1]

Studies have shown that amorphous or disordered grain boundaries typically result in the sintering of impure alumina. Studies that focused specifically on calcia and silica additives on grain growth kinetics and solid state single crystal conversion have lead to advances in understanding microstructures in the sintering of alumina.[2-23] Recently, six types of grain boundaries called "complexions" have been proposed in the grain growth kinetics associated with sintering in alumina. The theoretical understanding of complexions is derived from force balance arguments that address the attractive forces from London dispersion forces and repulsive forces of steric constraints within the grain boundary and results in varying degrees of disorder within a grain boundary.[24] The degree of disorder correlates with grain boundary thickness and grain growth kinetics and provide an explanation for slight deviations from the bulk thermodynamics.[25] Though it is assumed that complexions can be applied to more complex chemistries (additive systems greater than a binary system) and can explain some of the thermodynamic deviations found in the sintering of alumina, the chemistry of the grain boundary and resulting secondary phases were not the primary focus of these studies.[24, 25]

Systematic investigations of grain boundary chemistries and the corresponding secondary phases have rarely been studied, particularly in systems outside of simple binary component system, possibly due the apparent inconsistencies of the grain boundary phases and chemistries reported from study to study.[26-32] The disorder within grain boundaries could still be attributed to glass forming abilities of segregated impurities. Segregation of impurities, potentially aggravated by heat treatment conditions, could also give rise to localized concentration of impurities, thus further confusing a comprehensive analysis of grain boundary chemistries.[33, 34] It is proposed that

the glass formation boundary can be used to explain previous observations and predict the grain boundary chemistry in alumina.

1.2. GLASS FORMATION

Glass formation theory was approached from three perspectives based on structural, thermodynamic, and kinetic models.[35] The industrial (traditional) ceramic systems to which the glass formation boundary approach has been applied to have been typically alkali and alkaline earth silicates and alumino-silicates.[36, 37]

Sun's single bond strength criterion is an example thermodynamic approach that helps to classify the role of oxides in glass formation.[35] Sun's concept calculates quantifiable values for the strength of single oxygen-cation bonds and relates those bond strengths to the inability of liquid (melt) structures to rearrange for crystallization. The resulting bond strength calculations give rise to the general classifications of network formers (with bond strengths >80kcal/mol), intermediates (60-80kcal/mol), and network modifiers (i.e., fluxes, <60kcal/mol).[38] In addition to Sun's single bond strength criterion, Rawson pointed out the importance of the liquidus temperature for the breaking of atomic bonds within a multicomponent system which in some cases helps to selectively explain somewhat more unexpected glass forming regions, ie. glass formation in the low temperature regions in calcium aluminates.[39] Much of the work on ternary systems and glass formation are readily available for alkali and alkaline earth aluminosilicate systems.[40-42] Figure 1.1 shows an example of the large areas of glass formation within the CaO-Al_2O_3-SiO_2 system tested to the limits of the 1600°C liquidus (the $CaO{\cdot}SiO_2$ composition did not form a glass). Sun's single bond strength criterion is consistent with the role of the oxides in glass structures, where SiO_2 is a network forming oxide, Al_2O_3 acts as an intermediate, and Na_2O, K_2O, and CaO serve as modifiers (fluxes). It should be noted that Al_2O_3 can also adopt a coordination number of four (or five), allowing Al_2O_3 to also function as a network former in some cases.[38, 43]

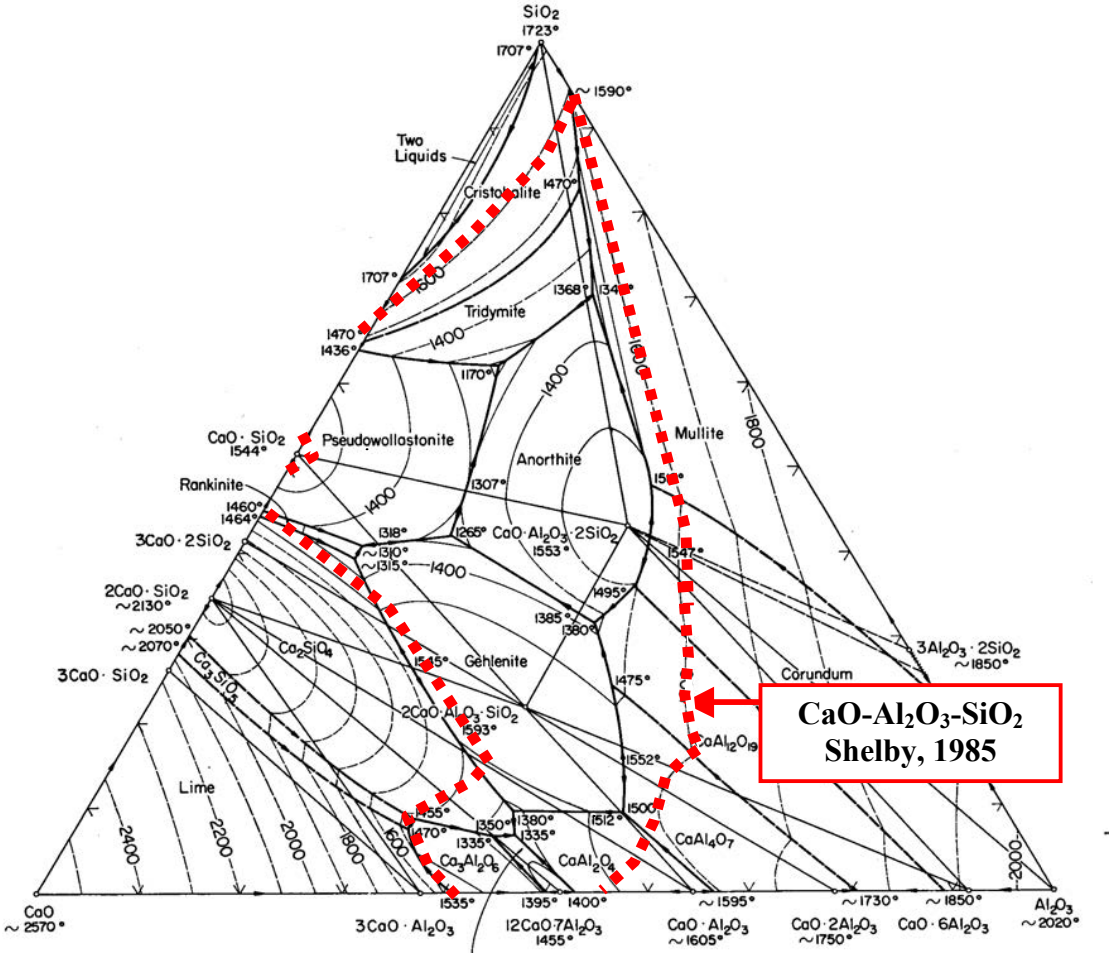

Figure 1.1. Example of glass formation region in $CaO\text{-}Al_2O_3\text{-}SiO_2$ system as adapted from Shelby.[41, 44]

The kinetic approach defines glass formation by the rate of cooling or quenching needed to prevent crystallization.[38] However, glass formation as applied to industrial ceramics relies on what has been termed as an intrinsic glass formation boundary. Industrial cooling rates, typically dictated by thermal shock restrictions, range from 1.7 K/sec to 0.12 K/sec which will likely lead to a smaller compositional region of glass formation.[36]

1.3. GLASS FORMATION BOUNDARY FOR CERAMIC GLAZES

To develop a way to look at ceramic compositions, and in particular glazes for porcelain and temperature measurement, Hermann Seger developed a glaze nomenclature based on molar oxide ratios. This glaze nomenclature has historically been referred to as a Seger Formula, but more recently known as the Unity Molecular Formula (UMF).[36, 45, 46] This approach groups oxides by their valence: R_2O (alkali), RO (alkaline earth), R_2O_3 (typically Al_2O_3, and erroneously B_2O_3 and Fe_2O_3), and RO_2 (typically SiO_2). Using the UMF approach, the batch composition is evaluated in terms of the moles for each component. The overall chemistry is represented as a molar ratio to the sum of the moles of flux (R_2O+RO). Using this approach, Stull mapped the trends in glaze texture by plotting behavior as a function of alumina and silica levels in the glaze (against a background of R_2O+RO as unity).[47] Quinlan demonstrated that the glaze surface quality predicted by Stull correlates with the glass formation boundary at or below SiO_2:Al_2O_3 ratios of 5:1, and that matte glazes fall outside the boundary and gloss glazes within the glass formation boundary (as illustrated in Figure 1.2). Matte glazes can also be produced at SiO_2:Al_2O_3 ratios greater than (about) 15:1, representing an apparent contradiction to the glass formation boundary idea. Stull's nomenclature, that these glazes are "devitrified" further adds to this confusion (Stull's work, nonetheless, remains one of the most important glaze research studies ever conducted and is still one of the most commonly referenced and widely used both within industry and the art ceramics community.) However, analysis by Quinlan demonstrated that these matte glazes had not actually completely melted, evidenced by the presence of quartz in these glazes after firing, and quartz is not a possible crystallization product under the firing conditions used to create the samples. The crystallization products in matte glazes are typically in the albite-anorthite solid solution region due to the fact that these glazes lie in the anorthite phase field and because there is typically both CaO and Na_2O in the glaze. If the alumina level is lower, wollastonite crystallizes, indicating that the glaze chemistry lies in the wollastonite phase field.[36] This behavior in glazes gives an indication of the applicability of the glass formation boundary approach to grain boundary phases in alumina. The

precipitation of crystalline phases in the grain boundary should correspond to the phase field where the grain boundary chemistry resides.

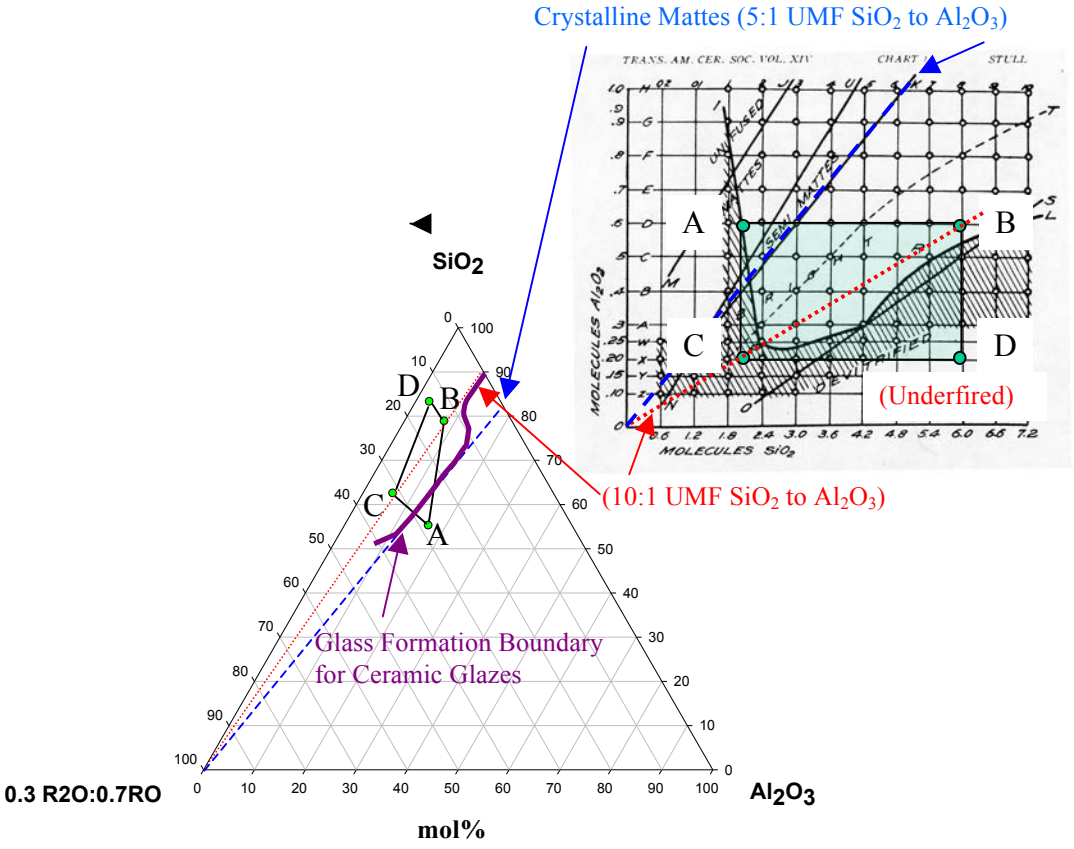

Figure 1.2. Stull diagram (created at Cone 11, 1335°C) in relation to the glass formation boundary plotted on the ternary phase diagram (mol%) with corresponding compositional points of A, B, C, and D.[36, 47]

1.4. GLASS FORMATION BOUNDARY FOR PORCELAINS

The mineralogy and microstructure of porcelain can be explained through the use of the glass formation boundary concept.[37] The composition of all porcelains can be plotted on a portion of the K_2O-Al_2O_3-SiO_2 phase diagram by locating meta-kaolin and appropriately compensating for the dehydroxylation of kaolinite (shown in Figure 1.3).[48, 49] For the region of interest, the K_2O-Al_2O_3-SiO_2 and Na_2O-Al_2O_3-SiO_2 are essentially identical when plotted on a molar diagram phase diagram.[50] The mineralogy of porcelain, are composed of quartz, mullite and glass would be in general agreement with the phase diagram, with the obvious exception that glass is not an equilibrium phase.[49] The

calculation of mullite by the lever rule, however, results in an overestimation of the mullite level observed in porcelain because some of the alumina is soluble in the glass phase, and this is consistent with experimental measurements.[37, 51]

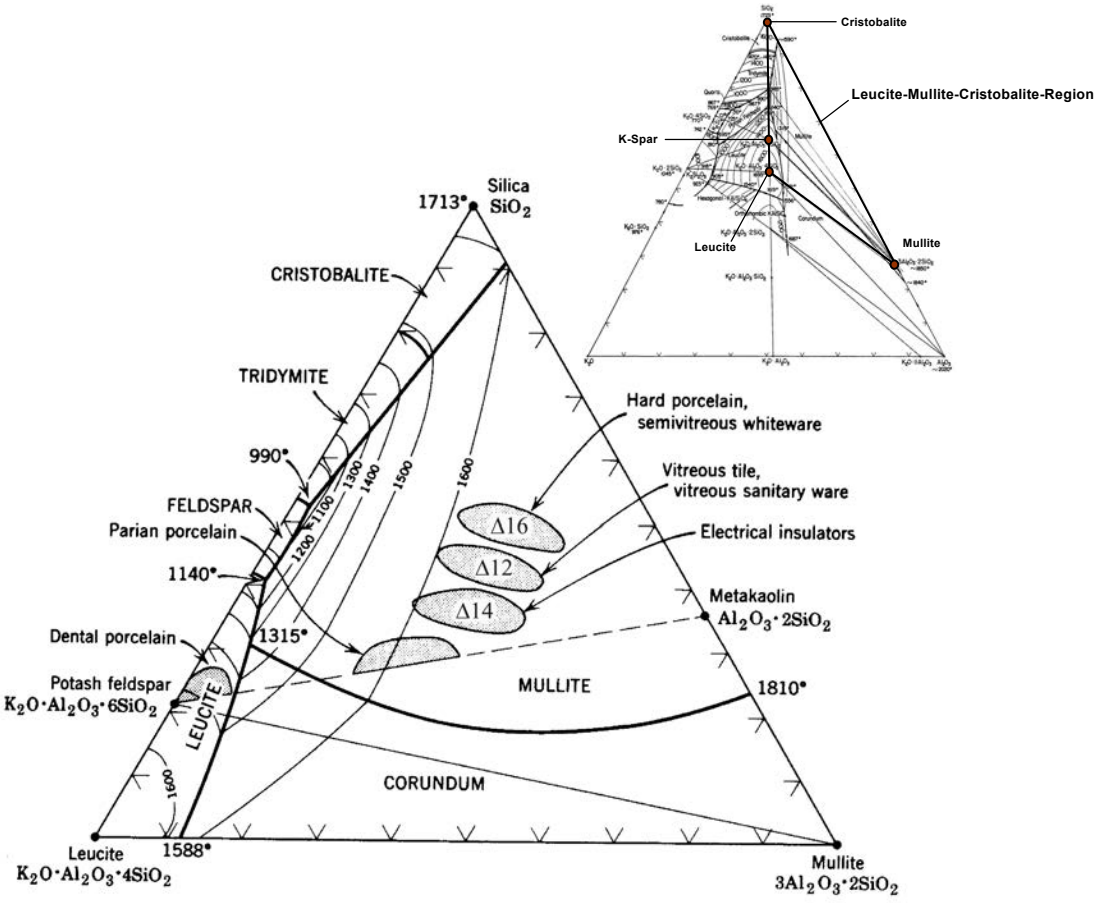

Figure 1.3. The porcelain compositions on leucite-mullite-cristobablite region, with inset of the K_2O-Al_2O_3-SiO_2 phase diagram.[48, 49]

The reported mineralogy of fired porcelain varies widely: 10-25% mullite, 5-25% quartz and 55-80 volume percent of a viscous alkali-aluminosilicate glass.[52-54] Based on the glass formation boundary results, the glass phase compositions reported in the literature all appear to be incorrect. The level of alumina in the glass phase is limited by the alumina solubility in the glass. Any additional alumina forms mullite, explaining the inability of the phase diagram to be used to calculate the mullite levels directly. Essentially, the glass formation boundary allows the phase diagram to be used to predict

non-equilibrium conditions within porcelain. Furthermore, the crystallization of mullite has been shown to be complete by 1150°C.[37, 55] The alumina saturation level in the glass is constant at a ratio of 1.19 (±0.1):1.0 Al_2O_3:R_2O+RO (alkali plus alkaline earth oxides).[37, 56] It is proposed the saturated glass within a given composition range follows a constant molar ratio of flux (R_2O+RO) to alumina with changing silica levels shown in Figure 1.4A.[57] The flux to alumina ratio may be dictated by a charge coupling situation with Al^{3+} ions assuming the role of Si^{4+} ions in four-fold coordinated positions.[37] The solubility of quartz dissolution into the glass phase is a function of firing temperature and has also been experimentally demonstrated to reach steady state within one to four hours.[58, 59] The concentration of dissolved silica in the glass phase is therefore dependent on the firing temperature of the porcelain as shown in Figure 1.4B.[37] The solubility of quartz in the alkali-aluminosilicate glasses at a specific firing temperature is dependent on the SiO_2 to flux ratio. The application of the lever rule with the glass formation boundary as an interrupted path within the compatibility triangle allows for a more accurate calculation to the steady state experimental observations.[37] In essence, after firing, feldspar no longer exists, but has been replaced by the glass phase, forming the third composition anchor in conjunction with mullite and cristobalite.

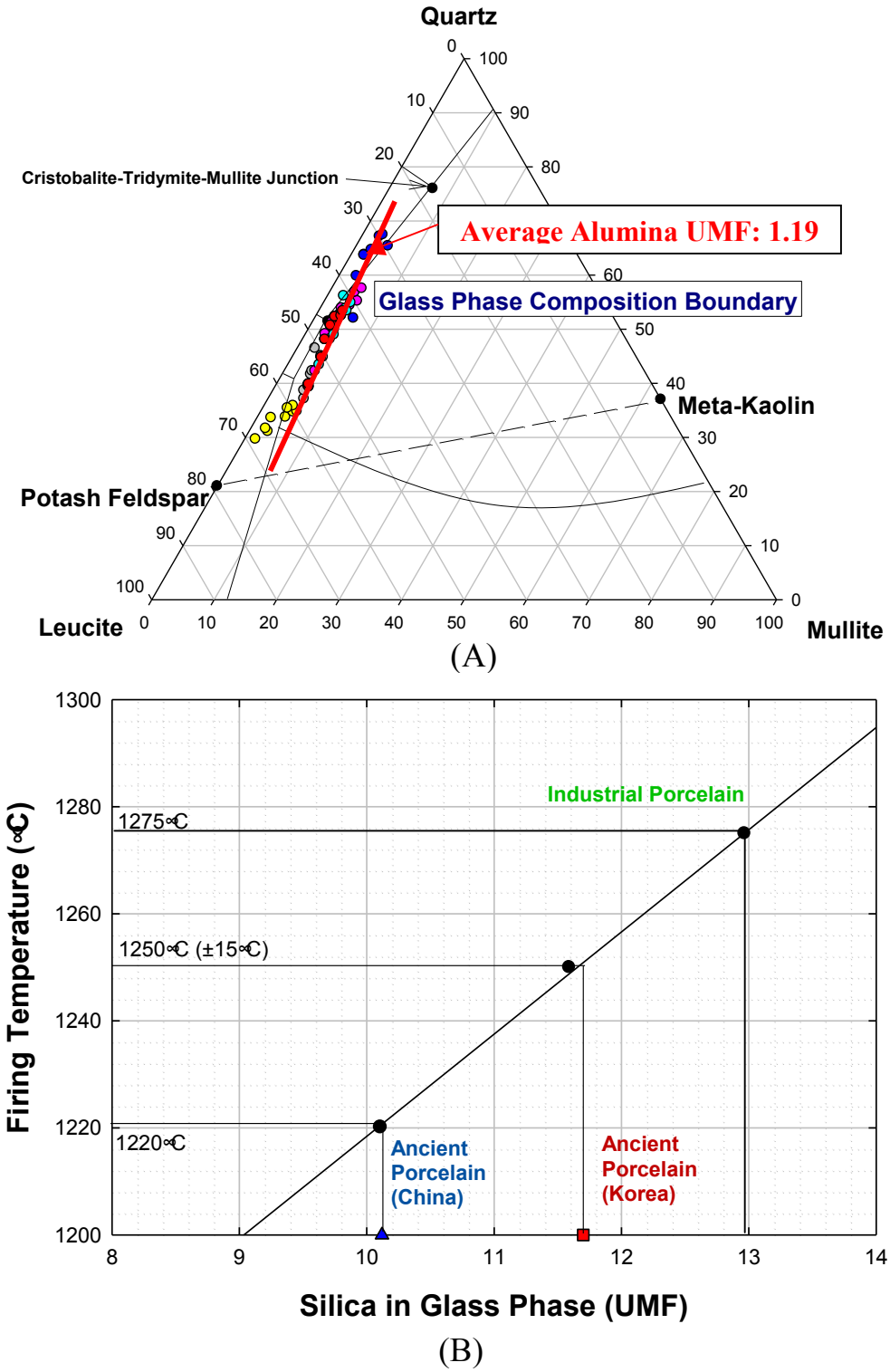

Figure 1.4. (A) Experimental glass phase chemistries showing glass a constant alumina UMF average of 1.19. (B) Quartz solubility in relation to firing temperature.[57]

An initial microstructural characterization study questioned the homogeneity of the glass phase, based on the range of index of refraction measurements on thin sections.[54] Iqbal and Lee pointed out the difficulties in resolving the amount of crystalline mullite within even small glass regions and suggested that the conclusions regarding inhomogeneity may be unreliable. Their compositional analysis by transmission electron microscopy concluded variability to be region dependent within the microstructure (the variability caused as result of surrounding mullite) and the glass is much more uniform the previously believed.[52, 54] The conclusion of which is in agreement with Hermansson's and Carlsson's electron microscopy study.[60] A glass phase with a uniform bulk chemistry is supportive to the applicability of the glass formation boundary concept that has been proposed by Carty.[37] A slight discrepancy of exact concentration of alumina within the glass phase of porcelain exists. Electron microscopy studies suggest a slightly higher concentration of alumina within glass phase of the porcelain than proposed by Carty.[37, 52, 60] The composition of the glass phases proposed by Carty was calculated using a method of finding the difference from the bulk chemical analysis and the concentration of crystalline phases determined by quantitative X-ray diffraction.[37] Iqbal and Lee did conclude that mullite crystals would contribute to errors in determining the exact composition of the glass.[52] By the use of calculated glass property predictions and experimental confirmations, Skovira also demonstrated the properties (densities and coefficient of thermal expansions) of the proposed alumina saturated glass compositions with the crystalline components of mullite and quartz follows the rule of mixtures.[61]

1.5. POSSIBILITIES OF GLASS FORMATION BOUNDARY TO SINTERING IN ALUMINA

The diffusion couple study of DeCarlo et al. provided a quantitative understanding of alumina dissolution into a typical soda-lime-silica glass that mimicked grain boundary chemistries and indicated that alumina would likely react with localized impurities to form amorphous grain boundaries during sintering.[34] Based on Dillon and Harmer's definition of complexions, glass forming additives would form grain boundaries of the highest disorder and volume width classified as complexion VI.[25] It remained only to be demonstrated that the grain boundary would behave similarly to the bulk glass diffusion studies.

Additives of Na_2O and K_2O were not chosen for the study due to the high potential for alkali migration by the electron beam.[62] MgO was not tested as an additive due to foreseeable issues in quantifying the MgO solubility within an alumina lattice at the alumina grain edges and the complex issues surrounding the exact role of MgO in alumina, which is not fully understood.[1, 63-65] A sufficient amount of sintering literature was available for a direct comparison of these results with the sintering of alumina containing the co-dopants CaO and SiO_2.[27, 28, 31, 66-76]

To produce representative microstructures that would be applicable to industrial systems and for comparisons with the literature, samples were not quenched, not subsequently heat treated (annealed), or cooled with a slow programmed cooling (with excessive time or dwells to crystallize the sample). The samples were sintered at ambient pressure at a heating rate of 10K/min with a one hour dwell. The furnace was cooled under normal conditions by simply shutting off power to the elements (i.e., it was not a controlled cooling cycle). Considering the well established glass formation boundary in the $CaO\text{-}Al_2O_3\text{-}SiO_2$ system, a revisit in the microstructural evolution involving CaO and SiO_2 additives was an ideal system to test the hypothesis that the grain boundary chemistry should reside on the glass formation boundary within a given system.[41]

1.6. REFERENCES

1. J.E. Blendell and C.A. Handwerker, "Effect of Chemical Composition on Sintering Ceramics," *J. Cryst. Growth,* **75** [1] 138-60 (1986).

2. S. Baik and C.L. White, "Anisotropic Calcium Segregation to the Surfaces of Aluminum Oxide," *J. Am. Ceram. Soc.,* **70** [9] 682-8 (1987).

3. S. Baik and J.H. Moon, "Effects of Magnesium Oxide on the Grain Boundary Segregation of Calcium During Sintering of Alumina," *J. Am. Ceram. Soc.,* **74** [4] 819-22 (1991).

4. R.F. Cook and A.G. Schrott, "Calcium Segregation to Grain Boundaries in Alumina," *J. Am. Ceram. Soc.,* **71** [1] 50-8 (1988).

5. S.M. Mukhopadhyay, A.P. Jardine, J.M. Blakley, and S. Baik, "Segregation of Magnesium and Calcium to the Prismatic Surface of Magnesium Implanted Sapphire," *J. Am. Ceram. Soc.,* **71** [5] 358-62 (1988).

6. W.D. Kaplan, H. Muellejans, M. Ruehle, J. Roedel, and N. Claussen, "Ca Segregation to the Basal Surfaces," *J. Am. Ceram. Soc.,* **78** [10] 2841-4 (1995).

7. A. Altay and M.A. Gülgün, "Microstructrual Evolution of Calcium-doped Alumina," *J. Am. Ceram. Soc.,* **86** [4] 623-9 (2003).

8. J. Jung and S. Baik, "Abnormal Grain Growth of Alumina: CaO Effect," *J. Am. Ceram. Soc.,* **86** [4] 644-9 (2003).

9. S.J. Dillon and M.P. Harmer, "Relating Grain-boundary Complexion to Grain Boundary Kinetics I: Calcia-doped Alumina," *J. Am. Ceram. Soc.,* **91** [7] 2304-23 (2008).

10. J. Bae and S. Baik, "Abnormal Grain Growth in Alumina," *J. Am. Ceram. Soc.,* **80** [5] 1149-56 (1997).

11. J.H. Yoo, J.C. Nam, and S. Baik, "Quantitative Evaluation of Glass-forming Impurities in Alumina," *J. Am. Ceram. Soc.,* **82** [8] 2233-8 (1999).

12. M.J. Kim, S.M. Kim, and D.Y. Yoon, "Singular Grain Boundaries in Alumina Doped with Silica," *J. Am. Ceram. Soc.,* **87** [3] 507-9 (2004).

13. C.W. Park and D.Y. Yoon, "Effects of SiO_2, CaO, and MgO Additions on the Grain Growth of Alumina," *J. Am. Ceram. Soc.,* **83** [10] 2605-9 (2000).

14. Y.-M. Kim, S.-H. Hong, and D.-Y. Kim, "Anisotropic Grain Growth in TiO_2/SiO_2-doped Alumina," *J. Am. Ceram. Soc.,* **83** [11] 2809-12 (2000).

15. O.S. Kwon, S.H. Hong, J.H. Lee, U.J. Chung, D.Y. Kim, and N.M. Hwang, "Microstructural Evolution During the Sintering of TiO_2/SiO_2-doped Alumina. Mechanism of Anisotropic Abnormal Grain Growth," *Acta Mater.,* **50** [19] 4865-72 (2002).

16. J.E. Blendell, W.C. Carter, and C.A. Handwerker, "Faceting and Wetting Transitions of Anisotropic Interfaces and Grain Boundaries," *J. Am. Ceram. Soc.,* **82** [7] 1899-900 (1999).

17. H. Ahn, J.-H. Lee, S.-H. Hong, N.-M. Hwang, and D.-Y. Kim, "Effect of Liquid-forming Additive Content on the Kinetics of Abnormal Grain Growth in Alumina," *J. Am. Ceram. Soc.,* **86** [8] 1421-3 (2003).

18. S.J. Dillon and M.P. Harmer, "Relating Grain Boundary Complexion to Grain Boundary Kinetics II: Silica-doped Alumina," *J. Am. Ceram. Soc.,* **91** [7] 2314-20 (2008).

19. S.J. Dillon and M.P. Harmer, "Diffusion Controlled Abnormal Grain Growth in Ceramics," *Mater. Sci. Forum,* **558-559**, 1227-36 (2007).

20. C. Scott, M. Kaliszewski, C. Greskovich, and L. Levinson, "Conversion of Polycrystalline Al_2O_3 into Single Crystal Sapphire by Abnormal Grain Growth," *J. Am. Ceram. Soc.,* **85** [5] 1275-80 (2002).

21. G.S. Thompson, P.A. Henderson, M.P. Harmer, G.C. Wei, and W.H. Rhodes, "Conversion of Polycrystalline Alumina to Single-crystal Sapphire by Localized Codoping with Silica," *J. Am. Ceram. Soc.,* **87** [10] 1879-81 (2004).

22. S.J. Dillon and M.P. Harmer, "Direct Observations of Multilayer Adsorption on Alumina Grain Boundaries," *J. Am. Ceram. Soc.,* **90** [3] 996-8 (2007).

23. S.J. Dillon and M.P. Harmer, "Mechanism of "Solid State" Single Crystal Conversion in Alumina," *J. Am. Ceram. Soc.,* **90** [3] 993-5 (2007).

24. S.J. Dillon and M.P. Harmer, "Multiple Grain Boundary Transitions in Ceramics: A Case Study of Alumina," *Acta Mater.,* **55** [15] 5247-54 (2007).

25. S.J. Dillon, M. Tang, W.C. Carter, and M.P. Harmer, "Complexion: A New Concept for Kinetic Engineering in Material Science," *Acta Mater.,* **55** [18] 6208-18 (2007).

26. D.S. Phillips and Y.R. Shiue, "Grain Boundary Microstructure in Alumina Ceramics," *Adv. Ceram.,* **10**, 357-67 (1983).

27. C.A. Powell-Dogan and A.H. Heuer, "Microstructure of 96% Alumina Ceramics: III, Crystallization of High-calcia Boundary Glasses," *J. Am. Ceram. Soc.,* **73** [12] 3684-91 (1990).

28. R. Brydson, S.-C. Chen, F.L. Riley, S.J. Milne, X. Pan, and M. Rühle, "Microstructure and Chemistry of Intergranular Glassy Films in Liquid-phase-sintered Alumina," *J. Am. Ceram. Soc.,* **81** [2] 369-79 (1998).

29. A. Nakajima and G.L. Messing, "Liquid-phase Sintering of Alumina Coated with Magnesium Aluminosilicate Glass," *J. Am. Ceram. Soc.,* **81** [5] 1163-72 (1998).

30. R.E. Chinn, M.J. Haun, C.Y. Kim, and D.B. Price, "Microstructures and Properties of Three Composites of Alumina, Mullite, and Monoclinic $SrAl_2Si_2O_8$," *J. Am. Ceram. Soc.,* **83** [11] 2668-72 (2000).

31. M.M. Seabaugh, G.L. Messing, and M. Vaudin, "Texture Development and Microstructure Evolution in Liquid-phase-sintered α-Alumina Ceramics Prepared by Templated Grain Growth," *J. Am. Ceram. Soc.,* **83** [12] 3109-16 (2000).

32. H.-Y. Kim, J.-A. Lee, and J.-J. Kim, "Densification Behaviors of Fine-alumina and Coarse-alumina Compacts during Liquid-phase Sintering with the Addition of Talc," *J. Am. Ceram. Soc.,* **83** [12] 3128-34 (2000).

33. T. Lam, "Glass Melts as Indicators for Liquid Phase Sintering in Alumina"; M.S. Thesis. Alfred University, Alfred, NY, 2007.

34. K.J. DeCarlo, T.F. Lam, and W.M. Carty, "Dissolution of Alumina in Silicate Glasses and the Glass Formation Boundary," *Ceram. Trans.,* **209**, 61-9 (2010).

35. D.R. Uhlmann, "Glass Formation, a Contemporary View," *J. Am. Ceram. Soc.,* **66** [2] 95-100 (1983).

36. B. Quinlan, "The Unity Molecular Formula Approach to Glaze Development"; M.S. Thesis. Alfred University, Alfred, NY, 2002.

37. W.M. Carty, "Observations on the Glass Phase Composition in Porcelains," *Ceram. Eng. Sci. Proc.,* **23** [2] 79-94 (2002).

38. A.K. Varshneya, *Fundamentals of Inorganic Glasses;* pp. 27-59. Academic Press, New York, 1994.

39. H. Rawson, *Inorganic Glass-forming Systems;* pp. 11-29. Academic Press, New York, 1967.

40. P.W. McMillian, *Glass-ceramics;* p. 22. Academic Press, New York, 1964.

41. J.E. Shelby, "Formation and Properties of Calcium Aluminosilicate Glasses," *J. Am. Ceram. Soc.,* **68** [3] 155-8 (1985).

42. P. Richet, M. Roskosz, and J. Roux, "Glass Formation in Silicates: Insights from Composition," *Chem. Geol.,* **225** [3-4] 388-401 (2006).

43. S.H. Risbud, R.J. Kirkpatrick, A.P. Taglialavore, and B. Montez, "Solid-State NMR Evidence of 4-, 5-, and 6- Fold Aluminum Sites in Roller-quenched SiO_2-Al_2O_3 Glasses," *J. Am. Ceram. Soc.,* **70** [1] C–10-2 (1987).

44. Phase Diagrams for Ceramists, Vol. 1; Fig. 630. Edited by E.F. Osborn and A. Muan. American Ceramic Society, Westerville, OH, 1964.

45. H.A. Seger, *The Collected Writings of Herman August Seger,* Vol. 1*;* pp. 242-5. Chemical Publishing, Easton, PA, 1902.

46. W.M. Carty, M. Katz, and J. Gill, "Unity Molecular Formula Approach to Glaze Development," *Ceram. Eng. Sci. Proc.,* **21** [2] 95-107 (2000).

47. R.T. Stull, "Influence of Variable Silica and Alumina on the Porcelain Glazes of Constant RO," *Trans. Am. Ceram. Soc.,* **XIV**, 62-72 (1912).

48. W.D. Kingery, H.K. Bowen, and D.R. Ulhmann, *Introduction to Ceramics,* 2nd ed.*;* p. 533. John Wiley and Sons, New York, 1976.

49. Phase Diagrams for Ceramists, Vol 1; Fig. 407. Edited by E.F. Osborn and A. Muan. American Ceramic Society, Westerville, OH, 1964.

50. S. Reagan, "Pyroplastic Deformation of Whitewares"; M.S. Thesis. Alfred University, Alfred, NY, 1998.

51. Phase Diagrams for Ceramists, Vol. 1; p. 7. Edited by E.M. Levin, C.R. Robbins, and H.F. McMurdie. American Ceramic Society, Westerville, OH, 1964.

52. Y. Iqbal and W.E. Lee, "Fired Porcelain Microstructures Revisited," *J. Am. Ceram. Soc.,* **82** [12] 3584-90 (1999).

53. J. Oldenburgh, "Analysis of Glass Phase Composition in Porcelains"; B.S. Thesis. Alfred University, Alfred, NY, 2002.

54. S.T. Lundin, "Microstructure of Porcelain," *Natl. Bur. Stand. (U.S), Misc. Publ.,* **257**, 93-106 (1964).

55. D.I. Seymour, "Phase Evolution in Electrical Porcelains During Firing"; M.S. Thesis. Alfred University, Alfred, NY, 2000.

56. A. Shah, "Glass Formation Boundary in Porcelains"; M.S. Thesis. Alfred University, Alfred, NY, 2007.

57. H. Lee and W.M. Carty, "Glass Phase Composition in Porcelains and Correlation with Firing with Temperature," *Presentation at ACerS Annual Meeting,* 2004 (unpublished).

58. B. Pinto and W. Carty, "The Effect of Filler Size on Strength of Porcelain Bodies," *Ceram. Eng. Sci. Proc.,* **23** [2] 95-105 (2002).

59. B. Earley, "Effect of Time on Quartz Dissolution in Porcelain Bodies"; B.S. Thesis. Alfred University, Alfred, NY, 2002.

60. L. Hermansson and R. Carlsson, "On the Crystallisation of the Glassy Phase in Whitewares," *Trans. J. Br. Ceram. Soc.,* **77** [2] 32-9 (1978).

61. E. Skovira, "Properties of the Porcelain Glass Phase"; M.S. Thesis. Alfred University, Alfred, NY, 2006.

62. A.K. Varshneya, A.R. Cooper, and M. Cable, "Changes in Composition During Electron-microprobe Analysis of K_2O-SrO-SiO_2 Glass," *J. Appl. Phys.,* **75** [4] 2199-2202 (1966).

63. S.J. Bennison and M.P. Harmer, "A History of the Role Magnesia in the Sintering of α-Alumina," *Ceram. Trans.,* **7**, 13-49 (1990).

64. W. Jo, D.-Y. Kim, and N.-M. Hwang, "Effect of Interface Structure on the Microstructural Evolution of Ceramics," *J. Am. Ceram. Soc.,* **89** [8] 2369-80 (2006).

65. S.J. Dillon and M.P. Harmer, "Comment on "Effect of Interface Structure on the Microstructural Evolution of Ceramics," *J. Am. Ceram. Soc.,* **90** [7] 2291-2 (2007).

66. J.R. Floyd, "Effect of Secondary Crystalline Phases on Dielectric Losses in High-alumina Bodies," *J. Am. Ceram. Soc.,* **47** [11] 539-43 (1964).

67. S.J. Wu, L.C. DeJonghe, and M.N. Rahaman, "Subeutectic Densification and Second-phase Formation in Al_2O_3-CaO," *J. Am. Ceram. Soc.,* **68** [7] 385-8 (1985).

68. E. Kostić, S.J. Kiss, and S. Bošković, "Liquid Phase Sintering of Alumina," *Powder Metall. Int.,* **19** [4] 41-3 (1987).

69. J.E. Marion, C.H. Hsueh, and A.G. Evans, "Liquid-phase Sintering of Ceramics," *J. Am. Ceram. Soc.,* **70** [10] 708-13 (1987).

70. H. Song and R.L. Coble, "Morphology of Platelike Abnormal Grains in Liquid-phase-sintered Alumina," *J. Am. Ceram. Soc.,* **73** [7] 2086-90 (1990).

71. C.A. Powell-Dogan and A.H. Heuer, "Microstructure of 96% Alumina Ceramics: I, Characterization of the As-sintered Materials," *J. Am. Ceram. Soc.,* **73** [12] 3670-6 (1990).

72. N.P. Padture and H.M. Chan, "Improved Flaw Tolerance in Alumina Containing 1 vol% Anorthite via Crystallization of the Intergranular Glass," *J. Am. Ceram. Soc.,* **75** [7] 1870-5 (1992).

73. E. Kostić, S. Bošković, and S.J. Kiss, "Reaction Sintering of Al_2O_3 in the Presence of the Liquid Phase," *Ceram. Int.,* **19** [4] 235-40 (1993).

74. M.J. Kim and D.Y. Yoon, "Effect of Magnesium Oxide Addition on Surface Roughening of the Alumina Grains in Anorthite Liquid," *J. Am. Ceram. Soc.,* **86** [4] 630-3 (2003).

75. P. Švancárek, D. Galusek, F. Loughran, A. Brown, R. Brydson, A. Atkinson, and F. Riley, "Microstructure-stress Relationships in Liquid-phase Sintered Alumina Modified by the Addition of 5 wt.% of Calcia-silica Additives," *Acta Mater.,* **54** [18] 4853-63 (2006).

76. A.P. Goswami, S. Roy, M.K. Mitra, and G.C. Das, "Influence of Powder, Chemistry and Intergranular Phases on the Wear Resistance of Liquid-phase-sintered Al_2O_3," *Wear,* **244** [1-2] 1-14 (2000).

2. GRAIN BOUNDARY CHEMISTRIES IN THE SINTERING OF ALUMINA WITH CALCIA AND SILICA ADDITIVES REVISITED: HIGH SILICA TO CALCIA RATIOS AND THE GLASS FORMATION BOUNDARY

2.1. ABSTRACT

It is proposed that the glass formation boundary concept can explain grain boundary evolution in the sintering of alumina. To demonstrate this hypothesis, alumina samples with additive ratios of $CaO:8SiO_2$ and $CaO:4SiO_2$ were sintered at 1400°C, 1600°C, and 1700°C. Scanning electron microscopy, wavelength dispersive spectroscopy and transmission electron microscopy were used in the microstructural evaluation. Amorphous grain boundaries, anorthite, and mullite were observed. The observed phases fit within the proposed model of the glass formation boundary and explain secondary phases in the steady state non-equilibrium condition of sintering in alumina with additives of high silica to calcia ratios.

2.2. INTRODUCTION

A review of the literature shows that various compositions of additives (K_2O, Li_2O, Na_2O, MgO, CaO, BaO, SrO, ZnO, CoO, Y_2O_3, SiO_2,and B_2O_3) have been used in the sintering of alumina; this has resulted in a variety of secondary phases at the grain boundary, either from sintering or heat treatments (Table 2.I).[1-20] It is interesting to note that only a few studies attempt to interpret the evolution of the grain boundary phases and chemistries in the sintering of alumina. In these studies, the calculation of phases from cooling path analyses does not correlate with the observed microstructures in the liquid phase sintering of alumina.[21] In the sintering of alumina with calcia and silica additives, the literature reports anorthite and gehlenite as commonly observed phases at the grain boundaries, rather than calcium hexaluminate which has been reported to have a tendency for resorption.[7, 11-15] Differences between the reported microstructures and the thermodynamic calculations can be explained by the non-equilibrium nature of liquid phase sintering. The sintering of ceramics is unlike the solidification processes observed in metals, since the system never completely melts. Without obtaining a 100% liquid

phase, crystallization upon cooling occurs from a system of a non-homogenous composition.[22]

Table 2.I. Crystalline Phases Observed at the Grain Boundaries in Sintered Alumina

Chemical Formula	Mineral Name	Reference Number
SiO_2	cristobalite	1
$3Al_2O_3{\cdot}2SiO_2$	mullite	1-5
$Na_2O{\cdot}Al_2O_3{\cdot}6SiO_2$	albite	6-8
$11Al_2O_3{\cdot}xNa_2O$, $1.0 \leq x \geq 1.6$	beta-alumina	9, 10
$CaO{\cdot}Al_2O_3{\cdot}SiO_2$	fassaite	11
$CaO{\cdot}Al_2O_3{\cdot}2SiO_2$	anorthite	2, 6-8, 11-14
$2CaO{\cdot}Al_2O_3{\cdot}SiO_2$	gehlenite	2, 7, 11, 14, 15
$CaO{\cdot}2Al_2O_3$	grossite	14, 16
$Ca_3Al_2Si_3O_{12}$	grossularite	7, 11
$CaO{\cdot}Al_2O_3$	calcium aluminate	16
$CaO{\cdot}6Al_2O_3$	calcium hexaluminate	2, 7, 9, 10, 16-19
$(Al)MgSiO_3$	orthoenstatite	6
$2MgO{\cdot}SiO_2$	forsterite	3, 6
$Mg_3Al_2Si_3O_{12}$	pyrope	7
$2MgO{\cdot}2Al_2O_3{\cdot}5SiO_2$	α-cordierite	4, 6
$5MgO{\cdot}4Al_2O_3{\cdot}2SiO_2$	sapphirine	1, 4, 6
$MgO{\cdot}Al_2O_3$ or $ZnO{\cdot}Al_2O_3$, $CoO{\cdot}Al_2O_3$	spinel	1-4, 6-11, 17, 18
$Ca(Fe, Mg)Si_2O_6$	augite	11
$BaO{\cdot}Al_2O_3{\cdot}2SiO_2$ or $SrO{\cdot}Al_2O_3{\cdot}2SiO_2$	hexa-celsian	2, 5, 6, 9, 20
$3Y_2O_3{\cdot}5Al_2O_3$	garnet	17

Phillips and Shiue reported triple point compositions of 40% Al_2O_3, 30% SiO_2, and 30% CaO (wt%) from transmission electron microscopy energy dispersive spectroscopy (TEM EDS) were somewhat unexpected from the viewpoint of cooling from a bulk composition.[23] Kingery suggests the unexpected result found by Phillips and Shiue could be cause by non-equilibrium cooling or by processing below the required

temperature.[24] In a templated grain growth study of alumina, Seabaugh et al. were also in agreement with the viewpoint that sintering above the 1380°C puts the expected secondary phases in the gehlenite ($2CaO{\cdot}Al_2O_3{\cdot}SiO_2$), anorthite ($CaO{\cdot}Al_2O_3{\cdot}2SiO_2$), and calcium hexaluminate ($CaO{\cdot}6Al_2O_3$) compatibility triangle.[13]

TEM EDS compositional analysis by Powell-Dogan and Heuer suggests the triple point chemistry to be within the pseudowollastonite-anorthite-cristobalite compatibility triangle. Anorthite was the main secondary phase crystallized upon heat treatments. Phases of gehlenite, grossular garnet (solid solution of $Ca_3Al_2Si_3O_{12}$ and $Mg_3Al_2Si_3O_{12}$), calcium hexaluminate, and spinel ($MgO{\cdot}Al_2O_3$) were also observed.[7] The grossular garnet phase formed due to the additional 0.4 wt% magnesium present. The high amount of anorthite observed was similar to that of crystallization from the bulk glass, supporting the compositional triple point of the liquid to be in the pseudowollastonite-anorthite-cristobalite compatibility triangle. The absence of wollastonite ($CaSiO_3$) was proposed to be due to a kinetic restraint resulting from the presence of Na_2O and MgO in the glass phase.[7]

Brydson et al. observed alumina dissolution into grain boundaries only using calcia and silica as additives. This suggests that alumina dissolution into the intergranular liquid occurs in the initial sintering stage. They propose the grain boundary to be a "transient" liquid that slowly disappears with time. The transient liquid changes composition until the final equilibrium phases are reached which is not revealed in the early stages of sintering.[15]

Sintering alumina by the use low melting/eutectic glasses and raw materials containing some amount of alumina also resulted in crystallization of higher alumina content phases at the grain boundaries.[1, 4, 5, 20] Many of the authors of these findings also support the viewpoint of alumina dissolution into a non-equilibrium "transient" grain boundary.[1, 4, 5]

In a hot pressing study at 1450°C, Švančárek et al. reported secondary phases of anorthite, gehlenite, and grossite ($CaO{\cdot}2Al_2O_3$) that correlated with the six different calcia to silica ratios used.[14] Temperature is clearly important, since a number of these studies of high silica to calcia ratios report amorphous grain boundaries at higher sintering temperatures.[9, 12, 18, 25, 26]

The glass formation boundary approach for sintering in alumina proposes that the additives should be viewed as a localized concentration in contact with alumina particles.[22, 27] Figure 2.1 shows a schematic of alumina dissolution into the additives (R_2O, RO, and SiO_2) segregated at the grain boundary. The initial localized concentration of additives will start as a ratio of the summation of fluxes (R_2O:RO):SiO_2. The alumina in the system will react with the additives of (R_2O:RO):SiO_2 to form a low melting liquid, which follows the reaction paths to the nearest invariant point, as described in Stage I of liquid phase sintering.[22, 28]

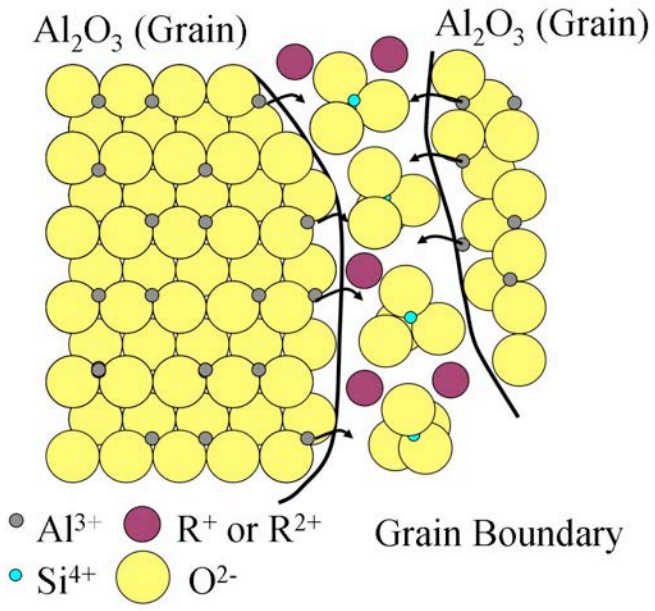

Figure 2.1. Schematic of alumina dissolution into glass forming impurities at the grain boundary to sinter the system.

The formation of low temperature melts are dependent on the initial ratios of (R_2O:RO):SiO_2 additives at the grain boundary. Figure 2.2 shows the formation of two low temperature melts at different compositions at different temperatures, demonstrated by two independent systems with additive ratios of CaO:8SiO_2 (C8S) and CaO:4SiO_2 (C4S). The starting ratio of C8S will follow a direct reaction path to the peritectic at

1368°C. The starting ratio of C4S will follow reaction path in the direction of the eutectic at 1170°C.

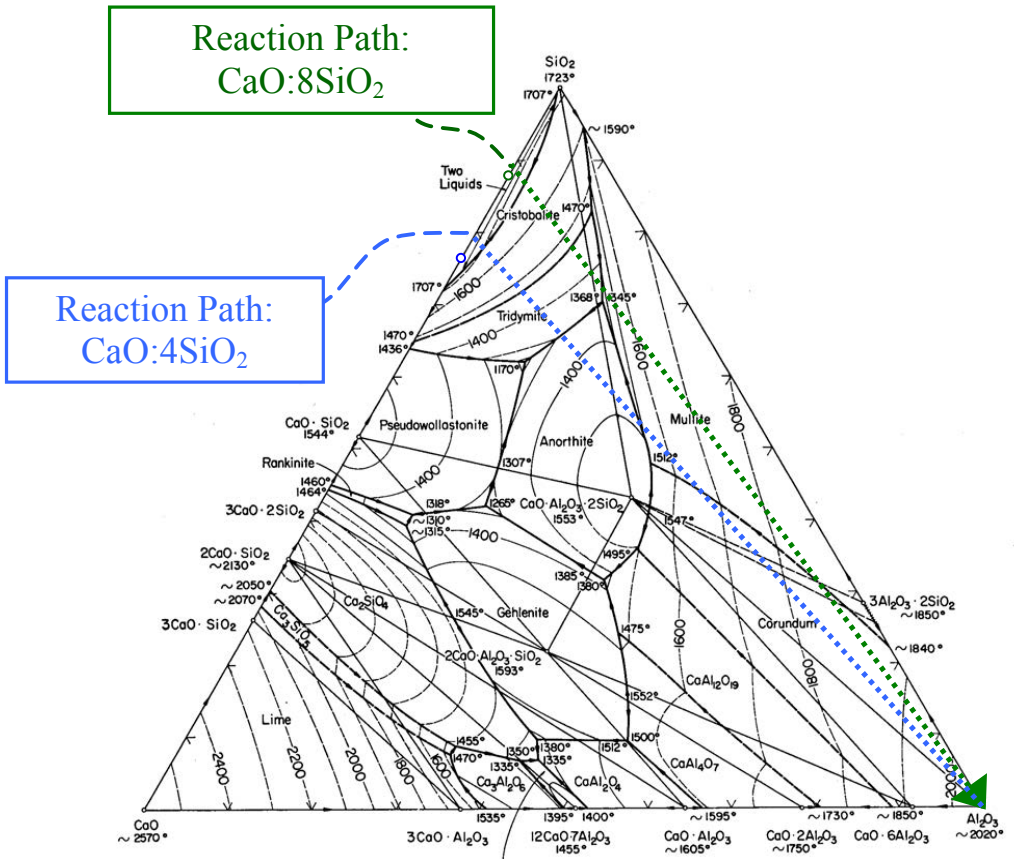

Figure 2.2. Reaction paths to form a low temperature liquid for the additive ratios $CaO:8SiO_2$ (C8S) and $CaO:4SiO_2$ (C4S), adapted from Osborn and Muan.[21]

As Brydson et al. suggested, alumina dissolution that occurs in Stage II will then change grain boundary compositions.[15, 28] Švančárek et al. showed that varying calcia to silica ratios yields different secondary phases and thus further supports the assertion that alumina dissolution into impurity liquid at the grain boundary is a driving reaction in sintering alumina using calcia and silica additives.[14] In a diffusion couple study of fuse cast alumina with a soda lime silicate glass (representative of a grain boundary) by DeCarlo et al., it was quantitatively shown that the amount of alumina dissolution is temperature dependent (Figure 2.3A) and the distance of the diffusion is time dependent but the concentration is not time dependent (Figure 2.3B). It was proposed that the rate-

controlling step governing alumina dissolution is the diffusion of aluminum ions through the glass, therefore the dissolution of alumina into glass is a "diffusion-controlled" process rather than a "dissolution-rate controlled" process. In this case, grain size and grain morphology do not affect the grain boundary chemistry during sintering.[27] The dissolution of alumina will be temperature dependent and follow the reaction path in the direction of increasing alumina concentration. According to the glass formation boundary approach, prediction of the "transient" grain boundary chemistry is possible based on alumina dissolution and will not allow a "random" composition to be present at the grain boundary.[22, 27]

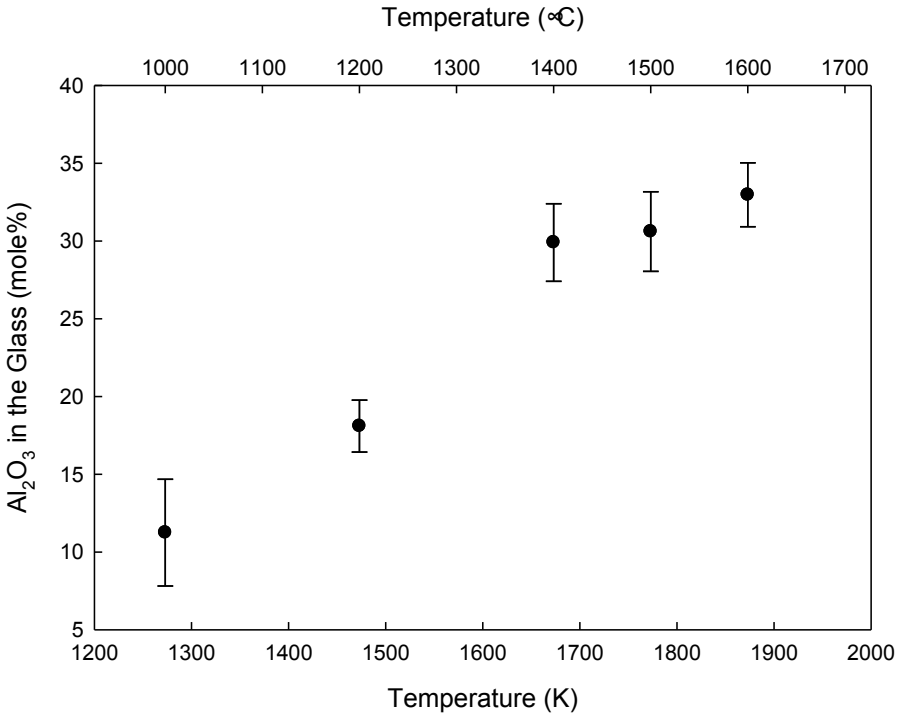

(A)

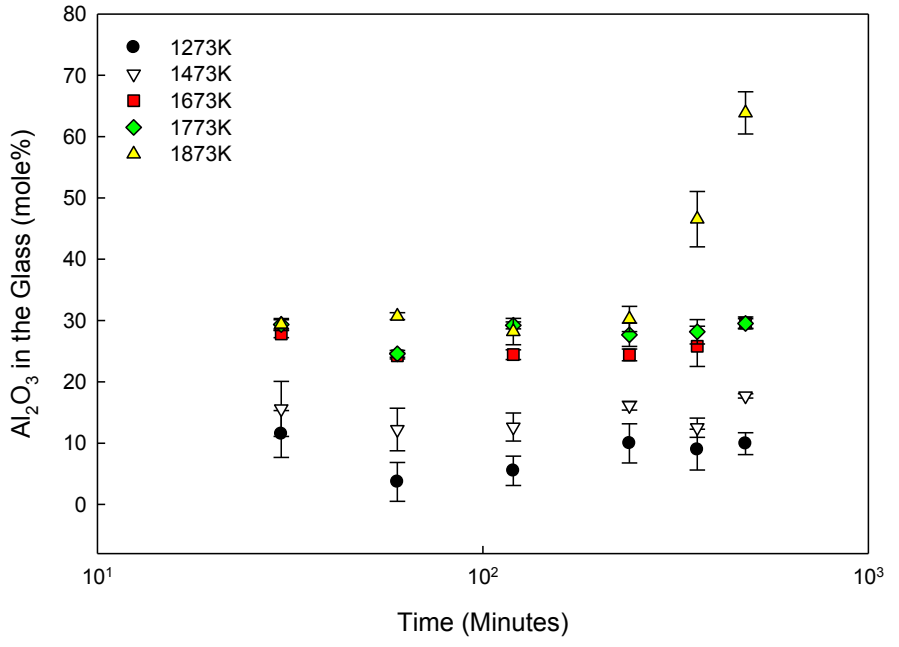

(B)

Figure 2.3. Measured alumina concentration in the glass as a function of (A) soak temperature (B) soak time.[27]

By visualizing the grain boundary impurities as a localized concentration, it is apparent that the liquid formed at these boundaries must follow the rules of glass formation upon cooling.[22] Compositional data at which glass forms within alkali, alkaline earth, rare earth aluminosilicate systems (ternary aluminosilicate base glasses were the specific glasses of interest in this study) and many other systems are well documented.[29-32] With the slower cooling rates observed in industrial ceramics (1.7 K/sec to 0.12 K/sec), the glass formation region will likely be reduced in area.[33]

However, general trends within the glass pertaining to higher SiO_2 concentrations will remain. These correspond to a constant Al_2O_3 molar ratio saturation limit of approximately 1.19 Al_2O_3:(R_2O:RO).[34] Figure 2.4 shows a comparison of a glass formation boundary region for CaO-SiO_2-Al_2O_3 for a system of quenched melts from Shelby, glass formation boundaries from porcelain and glazes of slow cooled systems.[30, 33, 34]

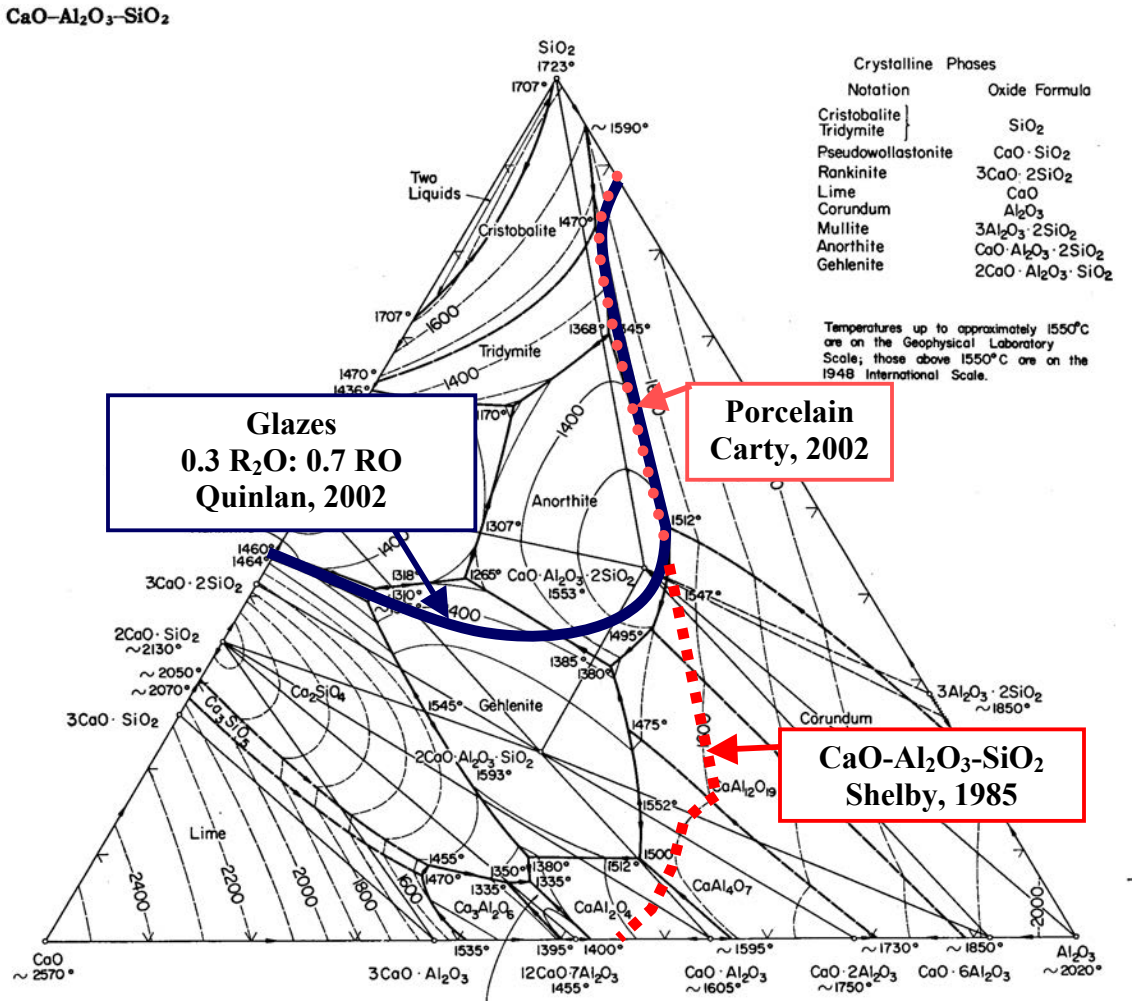

Figure 2.4. Glass formation boundary of traditional ceramics with an industrial cool in comparison to the quench system. [21, 30, 33, 34]

As the sintering temperature increases (consistent with the isotherms), alumina dissolution will shift the localized composition of a grain boundary out of the glass formation region. Upon cooling, the compositions outside the glass formation boundary will crystallize based on the resident phase fields and compatibility triangle due to the alumina saturation in the glass. Phases within the glass formation boundary do not crystallize. Using this approach, the compositions of glasses and crystalline phases found in the literature can be explained.[22] Based on the glass formation boundary approach, the boundary represents a metastable equilibrium boundary.[34]

The review of the literature shows that there has been no study focused on the evolution of the microstructure in alumina involving varying co-dopants of additives of calcia and silica for an A7 and A8 grade alumina as classified by Morrell or complexion VI as termed by Dillon and Harmer.[35, 36] A7 grade is classified as 94.5-96.5 wt% alumina and the typical applications are insulators and wear parts. A8 grade alumina is 86.0-94.5 wt% alumina and is typically used for insulators, wear parts and refractories.[35] This series of microstructurual evolution studies attempts to resolve the gaps in the literature and test the glass formation boundary hypothesis.

2.3. EXPERIMENTAL PROCEDURE

Aqueous suspensions were prepared from high purity alumina powder of 99.99 wt% (Sumitomo, AKP-15, Sumitomo Chemical, Tokyo, Japan). Coatings of colloidal silica (Ludox® TM-50, Sigma Aldrich, St. Louis, MO) on alumina were produced (or obtained using) through a heterocoagulation process.[37] Samples were slip cast and dried. Calcium chloride hexahydrate ($CaCl_2 \cdot 6H_2O$, Fisher Scientific, Ottawa, Canada) solutions were added to the porous alumina compact to obtain the desired dopant ratios of calcia versus silica. To obtain samples representative of microstructures of an industrial sample for comparison with the literature, the samples were not quenched, not subsequently heat treated (annealed), or cooled with programmed cool down. The samples were pressure-less sintered to 1400°C, 1600°C, and 1700°C at heating rates of 10K/min with a one hour dwell in SiC or $MoSi_2$ furnaces (Alfred University, Alfred, NY) and allowed to cool under ambient pressure following a power-law cooling curve.

Chemical analysis was determined by a $LiBO_2$ fusion using inductively couple plasma emission spectroscopy (ICP-ES) (ACME Analytical Laboratories Ltd., Vancouver, Canada). Scanning electron microscopy (SEM) was conducted on polished cross sections (Quanta FEG 200 and Inspect F, FEI, Hillsboro, OR). Selected samples were thermally etched at 50K below the sintering temperature for 10 minutes. Elemental chemical intensity maps for calcium and silicon were obtained by wavelength dispersive spectroscopy (WDS) on carbon coated polished cross sections (JEOL model JXA-820OF Electron Probe Microanalyzer, JEOL, Ltd., Tokyo, Japan). Transmission electron microscopy (TEM) samples were produced from dimpling to ~20 μm bridge (Model

2000 Specimen Prep, E.A. Fischione Instruments, Inc., Export, PA) and ion milling (691 Precision Ion Polishing System (PIPS™), Gatan, Pleasanton, CA) of 3 mm diameter discs of ~100 μm thickness, with an additional carbon coating (CM200, Philips, Eindhoven, Netherlands). Chemical analysis in TEM was performed by acquisition of energy dispersive spectroscopy (EDS) (CM-200 RTEM 147-5, EDAX, Mahwah, NJ). Selected area and convergent beam electron diffraction (SAED and CBED, respectively) were used to confirm secondary phases. Electron diffraction patterns were analyzed using simulated patterns from JEMS software.[38] Pseudobinary diagrams were created using FactSage™ 6.1 thermodynamic modeling program.[39] FT oxide and FACT 53 were the databases applied for the calculations.

2.4. RESULTS

Table 2.II presents the chemistries of the samples attained from ICP-ES in mole percent (mol%) oxides and the reference nomenclature that will be used for the remainder of the paper. Samples A, B, and C correspond to the C8S series. Samples D, E, and F belong to the C4S series. The heterocoagulation process with Ludox® TM-50 yielded suspensions with an average of 8.13 ± 0.32 mol% silica (91.87 mol% alumina). The experimental scatter was observed in samples of the C8S series due to the low amount of CaO required to satisfy this ratio. Samples A, B, and C of the C8S series were at least of C6S molar ratio and higher.

Table 2.II. ICP-ES Chemistries of the Sintered Samples

Sample	Average Mole Ratio	Actual Mole Ratio	Sintering Temperature	Al_2O_3 (mol%)	CaO (mol%)	SiO_2 (mol%)	Other (mol%)
A	C8S	8.18	1400°C	90.18	1.05	8.56	0.21
B	C8S	6.06	1600°C	90.76	1.28	7.73	0.22
C	C8S	9.37	1700°C	91.00	0.86	8.04	0.10
D	C4S	4.47	1400°C	89.81	1.85	8.25	0.09
E	C4S	4.06	1600°C	89.9	1.95	7.91	0.24
F	C4S	4.20	1700°C	90.64	1.78	7.58	0.06

Figure 2.5 presents the bright-field TEM micrographs of both C8S and C4S additive ratio and labeled according to sample nomenclature as referenced in Table II. The formation of amorphous grain boundaries were observed in Sample A which was sintered at 1400°C (Figure 2.5A). In the bright-field images the amorphous regions do not have diffraction contrast, further verified by convergent beam electron diffraction (CBED) pattern. Sample B, sintered at 1600°C, was mainly amorphous grain boundaries and some areas of mullite matrix with alumina inclusions. Exaggerated grain growth was observed and can be seen in the lower right hand quadrant in Figure 2.5B. The triple points within Sample B are larger in comparison to Sample A. Areas of alumina within a mullite matrix (upper portion of the micrograph in Figure 2.5C with the sintered alumina matrix at the bottom of the micrograph) were also observed in Sample C (1700°C), in addition to amorphous triple points.

In Sample D, sintered at 1400°C, regions of anorthite and amorphous grain boundaries were found as the secondary phases. As referenced by Powell-Dogan and Heuer, anorthite as a secondary phase is observed as a twinned microstructure seen in Figure 2.5D.[7] Sample E, sintered at 1600°C, showed no anorthite and contained predominately amorphous grain boundaries as shown in Figure 2.5E. An instance of mullite formation in Sample E was observed, a TEM micrograph and an electron diffraction pattern in the family <110> directions is presented in Figure 2.6. Similar to the C8S samples, Samples D and E for C4S also observed an increase in triple point size with increasing temperature. Sample F (Figure 2.5F) sintered at 1700°C, contained both regions of mullite and amorphous grain boundaries.

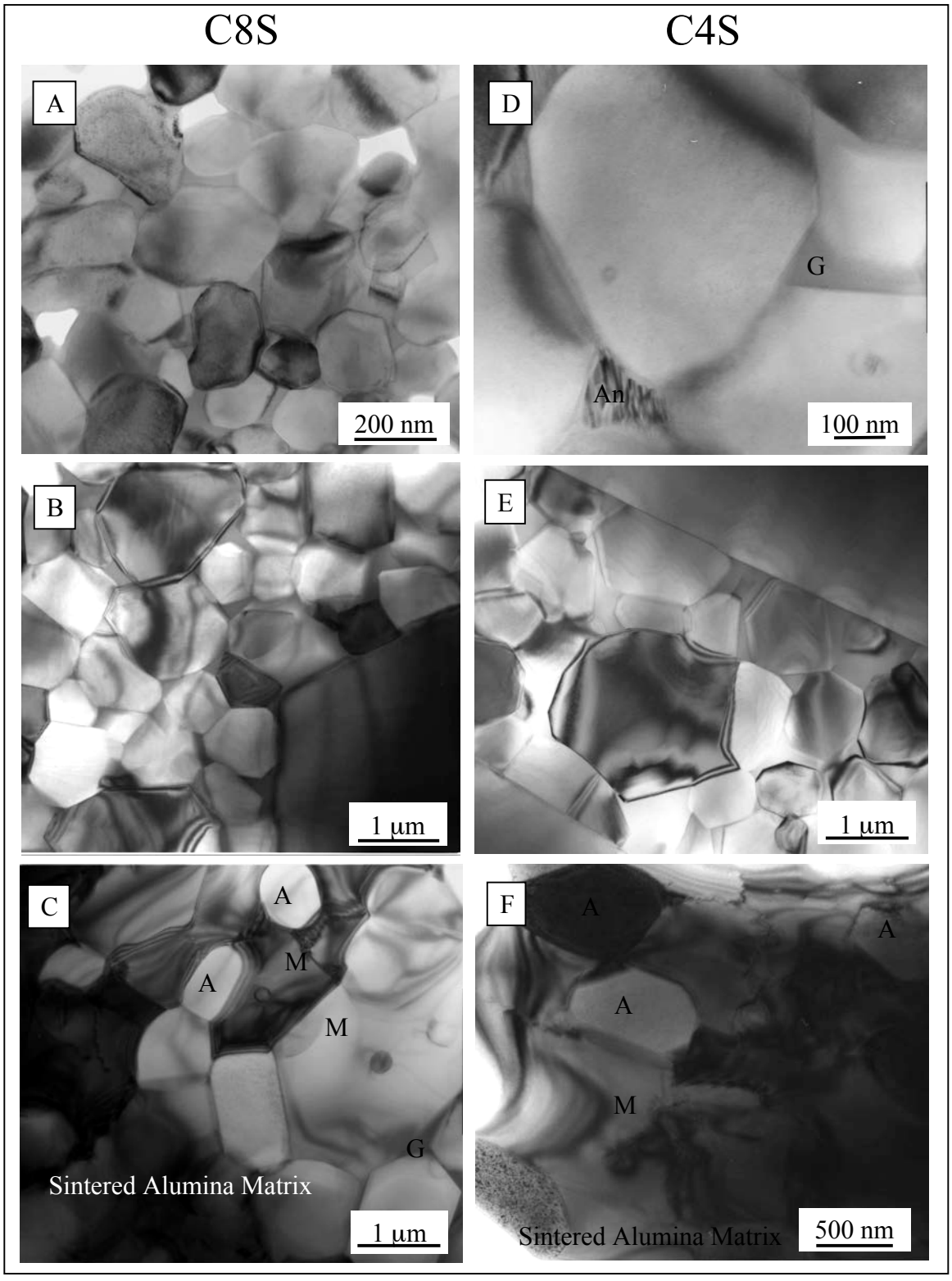

Figure 2.5. Bright-field TEM micrographs for C8S (left column) and C4S (right column) with phases of A - alumina, G - amorphous glassy triple points, An - anorthite and M - mullite matrix.

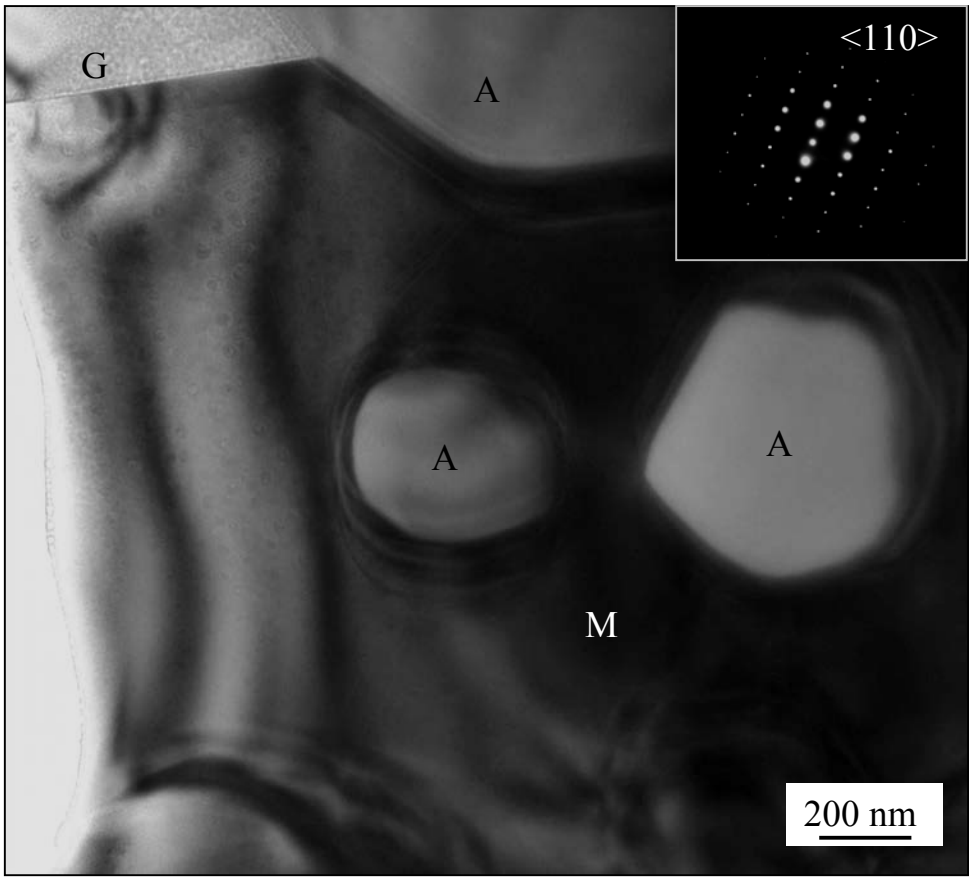

Figure 2.6. TEM micrograph of the secondary phase of mullite in diffraction in the family <110> direction in Sample E with phases A - alumina, M - mullite matrix, and G - amorphous glassy triple point.

Table 2.III tabulates the amorphous triple point TEM EDS chemistries (wt%). The triple point analyses plotted in Figure 2.7A and 2.7B show high values of standard deviations (as also shown in Table 2.III) that were also observed by Švančárek et al.[14] Figure 2.7A corresponds triple analysis of samples in the C8S additive ratio. Figure 2.7A shows a general increase in alumina concentration from Sample A to B. A slight decrease or saturation of alumina in the amorphous triple point is observed in sample C. Figure 2.7B shows the triple point analysis of the amorphous phase for the C4S ratio to be of approximately similar chemistry for Samples D, E, and F. A higher standard deviation is observed in Sample D in comparison to the samples sintered at the higher temperatures of 1600°C and 1700°C (Samples E and F, respectively). It should be noted

that calcium migration at 200kV electron was observed as a problematic issue and care was taken in collection of the TEM EDS data to avoid this effect. As noted by Kibbel and Heuer, variability of alumina content in triple point glass within a matrix containing surrounding alumina can be caused by X-ray Fluorescence, X-ray Absorption, excitation of the matrix grains by inelastic scattering.[40] Due to the smaller triple points, Samples A, B, D and E are most prone to migration errors that cause variability in alumina concentration, so the actual alumina concentration may be less than reported. Therefore, the differences between triple points in Samples A and B and Samples C and D may actually be greater.

Table 2.III. TEM EDS Analysis of the Triple Points

Sample	Al_2O_3 (wt%)	CaO (wt%)	SiO_2 (wt%)
A	15.47 ± 3.79	4.011 ± 1.21	80.52 ± 4.08
B	24.74 ± 5.66	7.74 ± 2.66	67.52 ± 6.73
C	21.48 ± 3.72	9.88 ± 3.04	68.64 ± 6.38
D	24.68 ± 5.48	9.71 ± 2.28	65.61 ± 7.49
E	23.49 ± 3.34	9.00 ± 1.99	67.51 ± 3.31
F	23.28 ± 1.24	11.42 ± 1.88	65.30 ± 2.86

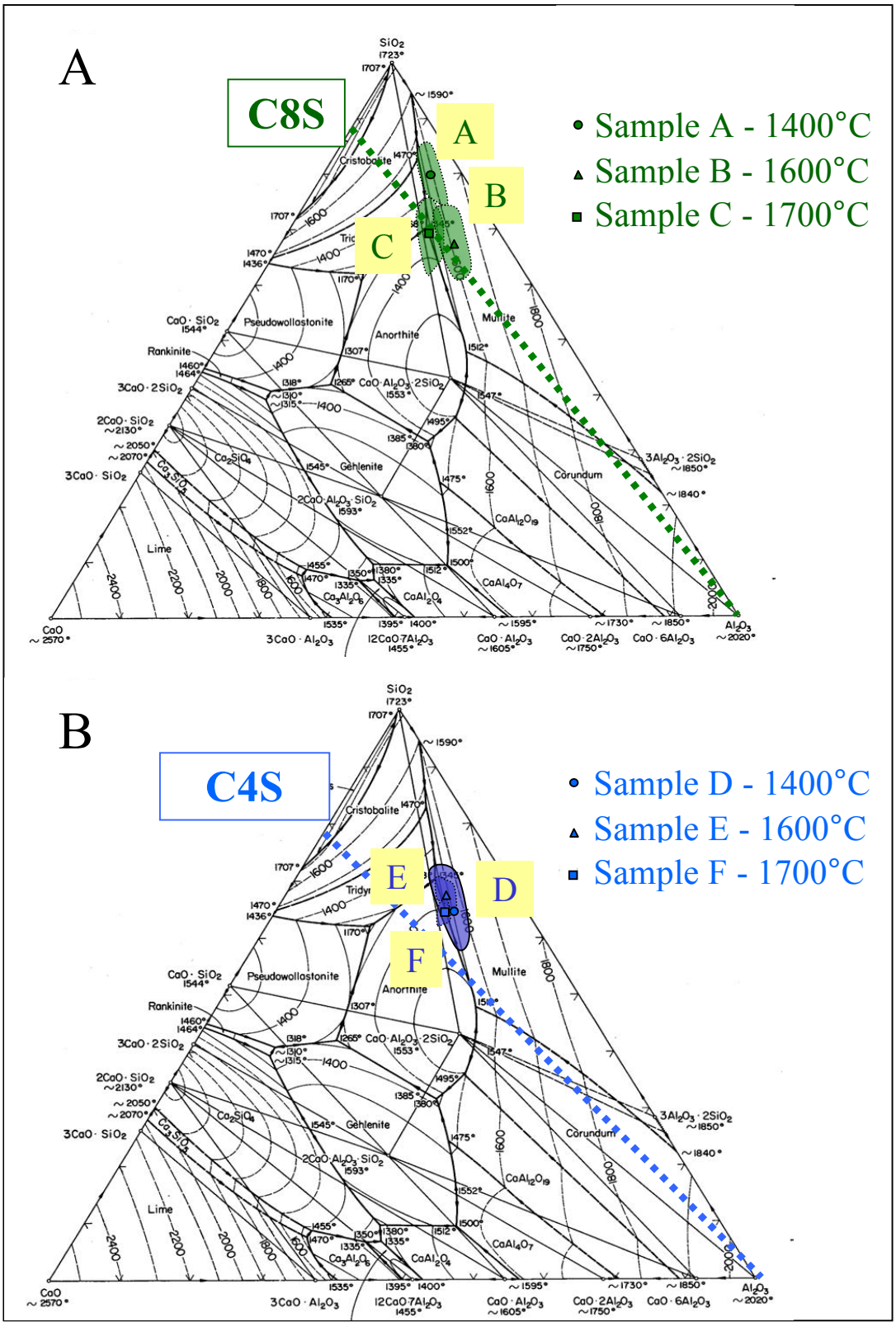

Figure 2.7. TEM EDS chemistries of the triple point analysis of the samples for the additive ratio of (A) C8S and (B) C4S.[21]

WDS chemical intensity maps were used to confirm the regions of mullite. Figure 2.8 shows the chemical intensity maps for calcium and silicon with black/blue as low, green as intermediate, and red as a high chemical concentration region for the individual maps. Areas in which only Al and Si were detected were concluded to be mullite. Similar to the findings in the TEM, regions of mullite with alumina inclusions within the sintered alumina were identified in Sample C.

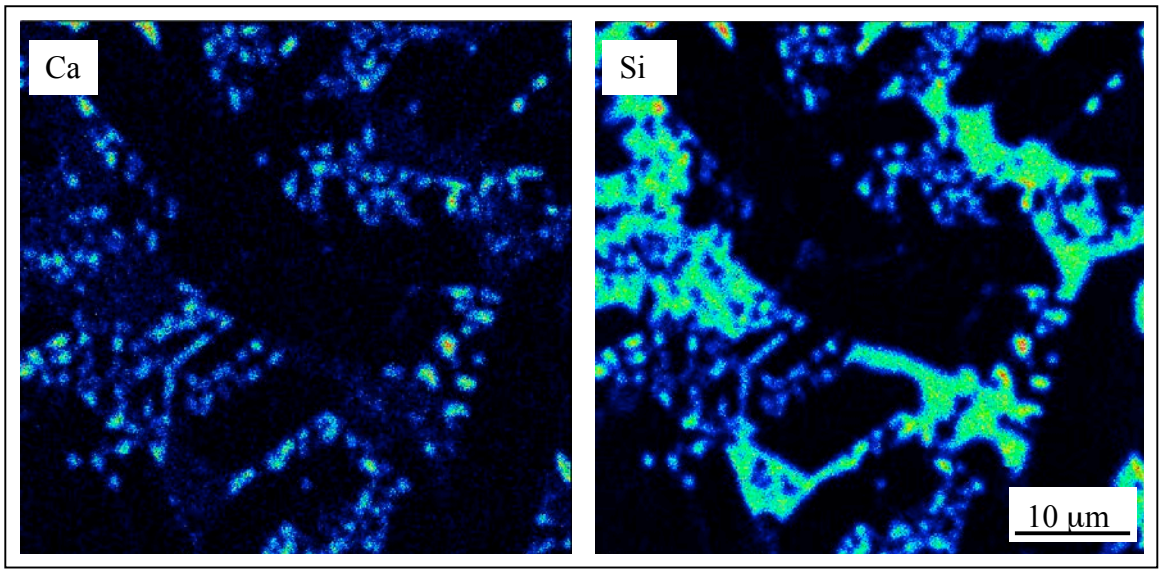

Figure 2.8. WDS chemical intensity element maps of calcium and silicon for Sample C. Black/blue as low, green as intermediate, and red as a high chemical concentration region for the individual maps.

SEM analysis in Figure 2.9A and 2.9D showed that no grain growth was observed for samples sintered at 1400°C for either series of C8S and C4S (sample A and D). Abnormal grain growth was present in the samples sintered at 1600°C and 1700°C shown in Figures 2.9B, C, E, and F. The thickness and volume of the amorphous grain boundaries and grain size shows an increasing trend with increasing sintering temperatures shown in Figures 2.9A-C for the C8S and for D-F in the C4S series. In Figure 2.9B and E, the lower contrast phase in backscatter electron mode is regions of mullite matrices with alumina inclusions, which were of similar morphologies presented in the TEM and WDS data. It should be noted the high volume of mullite observed in Figure 2.9B and 2.9E may be attributed to further crystallization during the thermal etch

process. Similar morphologies of mullite matrices as secondary phase can also be seen in Sample C (Figure 2.9C). In Sample E, (Figure 2.9E) the morphologies of mullite matrices are less frequent.

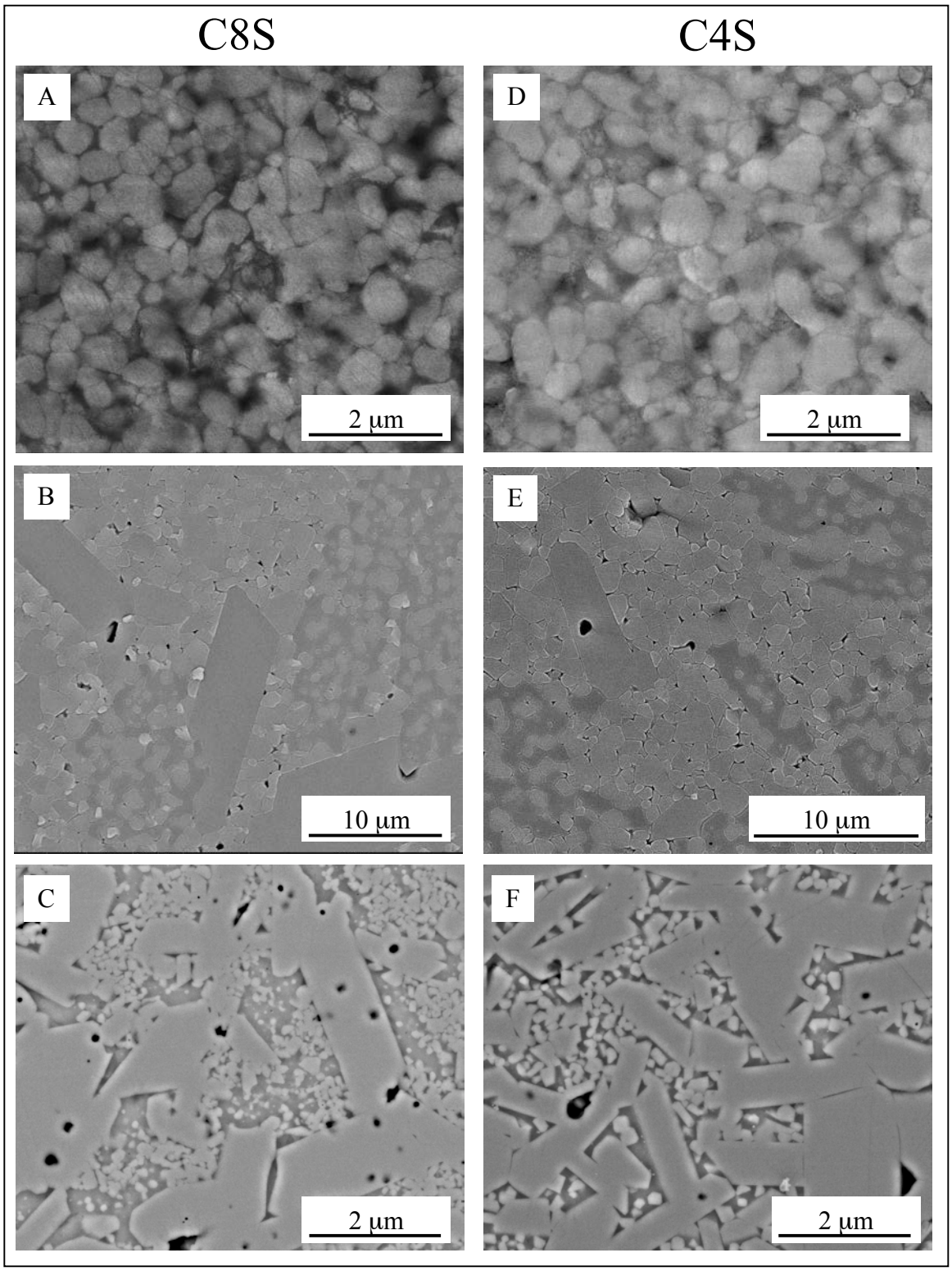

Figure 2.9. Backscatter electron micrographs for C8S (left column) and C4S (right column). (A and D) Thermally etched and imaging was performed in low vacuum mode. (B and E) Thermally etched with Au-Pd coating. (C and F) Polished with carbon coating.

2.5. DISCUSSION

Sample A, of the C8S ratio sintered at 1400°C, shows amorphous grain boundaries because the composition is within the glass formation boundary. For samples B and C for the C8S ratio as a function of increasing sintering temperature demonstrates mullite crystallization due to the saturation of alumina in grain boundaries, causing the composition to move outside the glass formation boundary.

Sample D, of the C4S ratio sintered at 1400°C, showed both anorthite and amorphous triple points. Even though anorthite was formed within Sample D it is proposed that grain boundary composition is still within the glass formation boundary. Based on the calculated pseudobinaries shown in Figure 2.10, if taken to equilibrium, phases of tridymite, wollastonite, and anorthite will form under 1170°C. Being that tridymite is a sluggish reaction, it will be an unlikely phase to form in the sintering conditions applied.[24] Figures 2.10 A & B are a comparison of dissolution paths of alumina of C6S and C3S which would be similar to C8S and C4S, respectively since it's proposed they would intersect adjacent phase fields. From the proposed dissolution paths, the chemistry of the grain boundary chemistry will move outside the phase fields allowable for wollastonite formation, thus wollastonite has not been reported as a phase at the grain boundary. However, if anorthite forms by solid state reactions (below 1170°C), similar to that observed in reactions of calcium carbonate with kaolinite at 1100°C, the phase will require further alumina dissolution to break down the anorthite and would require increasing temperatures up to 1553°C.[21, 41] Following the isotherms, Figure 2.10A shows the proposed path of alumina dissolution in C6S system that at 1400°C takes the reaction to the region of only mullite and liquid. Mullite was not observed in Sample A because the grain boundary composition, based on the location of the isotherms is within the glass formation boundary. Figure 2.10B shows a proposed path of alumina dissolution for the C3S system. At 1400°C the proposed path of the reaction is in a region of anorthite and liquid. If it were possible to increase the temperature while holding the chemistry constant a glass would be the result. However, alumina dissolution is a dynamic reaction that follows isotherms of the system. Even in the application of the glass formation boundary to ceramic glazes, anorthite has been found in under-fired matte glazes.[33] It is therefore proposed that the anorthite in Sample

D was not crystallized from the melt but is rather a product of a low temperature solid state reaction in the early process of alumina dissolution into the grain boundary.

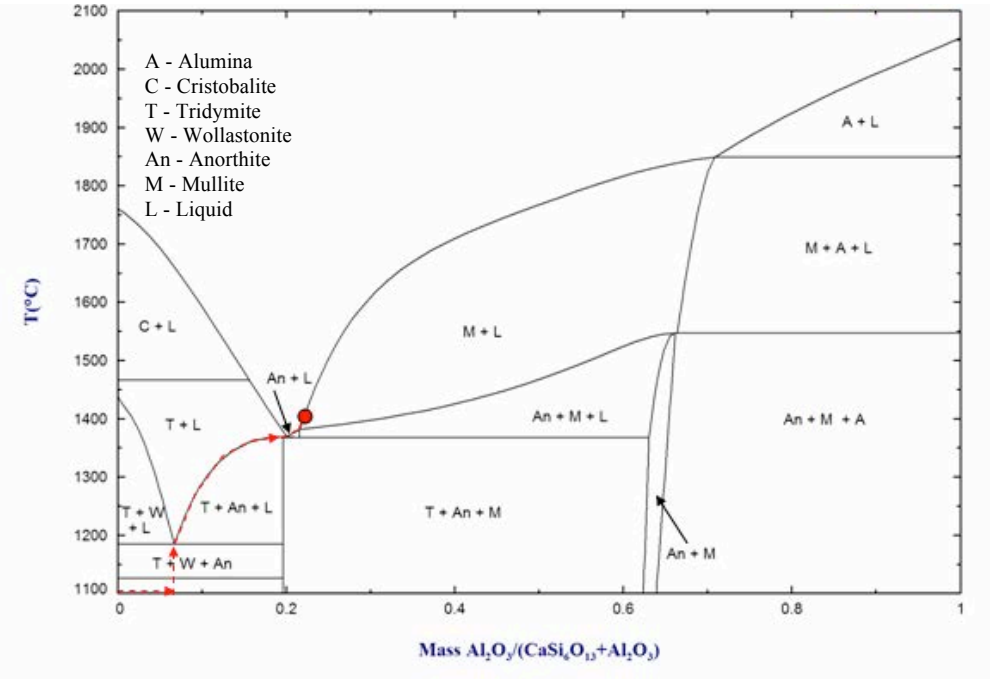

(A)

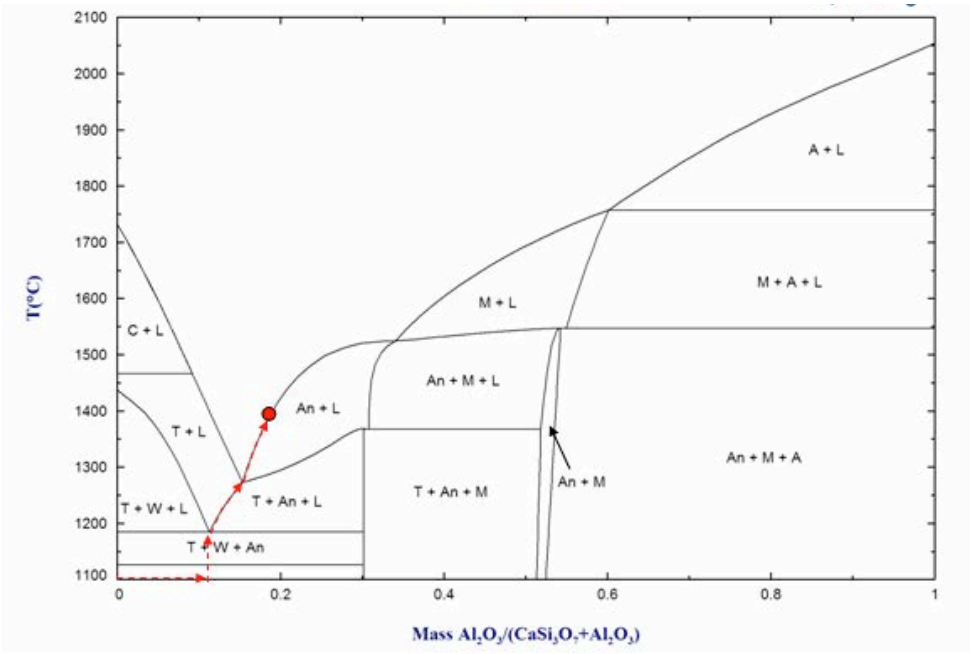

(B)

Figure 2.10. Pseudobinaries of (A) C6S-Al_2O_3 and (B) C3S-Al_2O_3 generated by FactSage™ software and the proposed change in chemistry by alumina dissolution.

The microstructures observed in Samples D and E were of particular interest. Based on the glass formation boundary approach the secondary phases result from the saturation of the glass with alumina. It is therefore unexpected to observe anorthite formation at 1400°C (Sample D) and mullite formation at 1600°C (Sample E). Based on thermodynamic phase calculations, anorthite would be expected to form along with mullite. The observance of only mullite without anorthite in Sample E is consistent and supports the glass formation boundary approach. Glass being a metastable phase and the sintering of ceramics not being an equilibrium condition, the crystallization of both phases is not expected unless the sintered sample was subjected to heat treatments allowing phases inside the glass formation boundary to crystallize similar to experiments performed by Powell et al.[6-8] The relative amount of amorphous boundaries in Sample E present compared to Sample D would also suggest the glass formation boundary to be closer to Sample E.

The microstructural phases of anorthite and amorphous grain boundaries observed in Sample D at 1400°C are consistent with the observations in hot pressing studies by Švančárek et al. (in comparison to the C5S ratio in their study).[14] The pressures produced in hot pressing are not great enough to affect the crystallization of secondary phases.[28] Samples A and D are proposed to be within the glass formation boundary and can be crystallized by heat treatments or annealing processes which enable nucleation and growth.[6-8, 12] Based on the results of this study a glass formation boundary was proposed as shown in Figure 2.11.

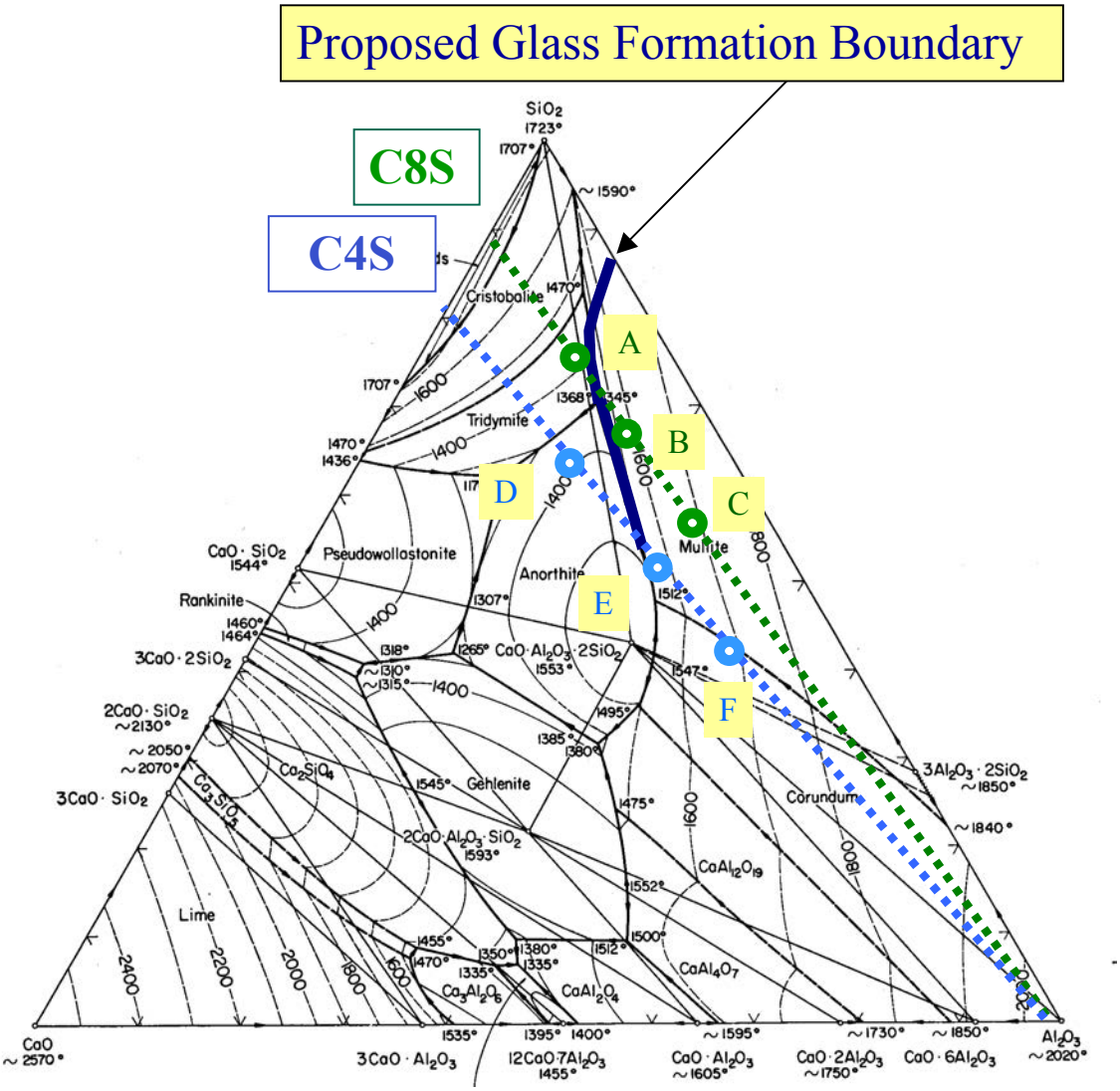

Figure 2.11. Proposed glass formation boundary in the sintering of alumina.[21]

Phases outside of the glass boundary that did not appear from sintering will not crystallize at the heat treatment temperatures within the glass formation boundary. This provides an explanation for why Powell-Dogan et al. did not find mullite as a crystallized phase in their heat treatment studies.[6-8] The glass formation boundary approach allows for an understanding of the transient grain boundary which is dependent on sintering temperature. Sintering temperature dictates the alumina dissolution level, allowing for the composition to change through the different phase fields and explaining the varying triple point chemistries and phases cited in the literature.

2.6. CONCLUSION

The observed phases of this microstructural evolution study fits the proposed model of the glass formation boundary allowing for the explanation of secondary phase predictions in a steady state non-equilibrium conditions of sintering in alumina high silica to calcia ratio additives. Anorthite was proposed to be a competing low temperature reaction resulting from the early stages of alumina dissolution and was discussed in detail through pseudobinaries. Saturation of the glass by alumina dissolution was demonstrated that resulted in the crystallization of mullite at the grain boundaries. The model is consistent with low temperature hot pressing data of other authors and gives an explanation for the observed phases upon heat treatments sintered alumina.

2.7. REFERENCES

1. H.-Y. Kim, J.-A. Lee, and J.-J. Kim, "Densification Behaviors of Fine-alumina and Coarse-alumina Compacts during Liquid-phase Sintering with the Addition of Talc," *J. Am. Ceram. Soc.,* **83** [12] 3128-34 (2000).

2. J.R. Floyd, "Effect of Secondary Crystalline Phases on Dielectric Losses in High-alumina Bodies," *J. Am. Ceram. Soc.,* **47** [11] 539-43 (1964).

3. S.J. Kiss and E. Kostić, "Densification of Ceramics in the Presence of the Reactive Liquid Phase," *Sci. Ceram.,* **10**, 333-40 (1980).

4. A. Nakajima and G.L. Messing, "Liquid-phase Sintering of Alumina Coated with Magnesium Aluminosilicate Glass," *J. Am. Ceram. Soc.,* **81** [5] 1163-72 (1998).

5. R.E. Chinn, M.J. Haun, C.Y. Kim, and D.B. Price, "Microstructures and Properties of Three Composites of Alumina, Mullite, and Monoclinic $SrAl_2Si_2O_8$," *J. Am. Ceram. Soc.,* **83** [11] 2668-72 (2000).

6. C.A. Powell-Dogan and A.H. Heuer, "Microstructure of 96% Alumina Ceramics: II, Crystallization of High-magnesia Boundary Glasses," *J. Am. Ceram. Soc.,* **73** [12] 3677-83 (1990).

7. C.A. Powell-Dogan and A.H. Heuer, "Microstructure of 96% Alumina Ceramics: III, Crystallization of High-calcia Boundary Glasses," *J. Am. Ceram. Soc.,* **73** [12] 3684-91 (1990).

8. C.A. Powell-Dogan, A.H. Heuer, and H.M. O'Bryan, "Devitrification of the Grain Boundary Glassy Phase in a High-alumina Ceramic Substrate," *J. Am. Ceram. Soc.,* **77** [10] 2593-8 (1994).

9. H. Song and R.L. Coble, "Morphology of Platelike Abnormal Grains in Liquid-phase-sintered Alumina," *J. Am. Ceram. Soc.,* **73** [7] 2086-90 (1990).

10. C.A. Powell-Dogan and A.H. Heuer, "Microstructure of 96% Alumina Ceramics: I, Characterization of the As-sintered Materials," *J. Am. Ceram. Soc.,* **73** [12] 3670-6 (1990).

11. A.P. Goswami, S. Roy, M.K. Mitra, and G.C. Das, "Influence of Powder, Chemistry and Intergranular Phases on the Wear Resistance of Liquid-phase-Sintered Al_2O_3," *Wear,* **244** [1-2] 1-14 (2000).

12. N.P. Padture and H.M. Chan, "Improved Flaw Tolerance in Alumina Containing 1 vol% Anorthite via Crystallization of the Intergranular Glass," *J. Am. Ceram. Soc.,* **75** [7] 1870-5 (1992).

13. M.M. Seabaugh, G.L. Messing, and M. Vaudin, "Texture Development and Microstructure Evolution in Liquid-phase-sintered α-Alumina Ceramics Prepared by Templated Grain Growth," *J. Am. Ceram. Soc.,* **83** [12] 3109-16 (2000).

14. P. Švancárek, D. Galusek, F. Loughran, A. Brown, R. Brydson, A. Atkinson, and F. Riley, "Microstructure-stress Relationships in Liquid-phase Sintered Alumina Modified by the Addition of 5 wt.% of Calcia-silica Additives," *Acta Mater.,* **54** [18] 4853-63 (2006).

15. R. Brydson, S.-C. Chen, F.L. Riley, S.J. Milne, X. Pan, and M. Rühle, "Microstructure and Chemistry of Intergranular Glassy Films in Liquid-phase-sintered Alumina," *J. Am. Ceram. Soc.,* **81** [2] 369-79 (1998).

16. S.J. Wu, L.C. DeJonghe, and M.N. Rahaman, "Subeutectic Densification and Second-phase Formation in Al_2O_3-CaO," *J. Am. Ceram. Soc.,* **68** [7] 385-8 (1985).

17. E. Kostić, S. Bošković, and S.J. Kiss, "Reaction Sintering of Al_2O_3 in the Presence of the Liquid Phase," *Ceram. Int.,* **19** [4] 235-40 (1993).

18. E. Kostić, S.J. Kiss, and S. Bošković, "Liquid Phase Sintering of Alumina," *Powder Metall. Int.,* **19** [4] 41-3 (1987).

19. J. Echeberría, F. Castro, and F.L. Riley, "Grain Growth in Liquid-phase-sintered Alumina," *Mater. Sci. Forum,* **113-115**, 579-84 (1993).

20. Y.-Q. Wu, Y.-F. Zhang, G. Pezzotti, and J.-K. Guo, "Effect of Glass Additives on the Strength and Toughness of Polycrystalline Alumina," *J. Eur. Ceram. Soc.,* **22** [2] 159-64 (2002).

21. Phase Diagrams for Ceramists, Vol. 1; Fig. 630. Edited by E.F. Osborn and A. Muan. American Ceramic Society, Westerville, OH, 1964.

22. T. Lam, "Glass Melts as Indicators for Liquid Phase Sintering in Alumina"; M.S. Thesis. Alfred University, Alfred, NY, 2007.

23. D.S. Phillips and Y.R. Shiue, "Grain Boundary Microstructure in Alumina Ceramics," *Adv. Ceram.,* **10**, 357-67 (1983).

24. W.D. Kingery, H.K. Bowen, and D.R. Uhlmann, *Introduction to Ceramics;* p. 317. John Wiley & Sons, New York, 1976.

25. M.J. Kim and D.Y. Yoon, "Effect of Magnesium Oxide Addition on Surface Roughening of the Alumina Grains in Anorthite Liquid," *J. Am. Ceram. Soc.,* **86** [4] 630-3 (2003).

26. J.E. Marion, C.H. Hsueh, and A.G. Evans, "Liquid-phase Sintering of Ceramics," *J. Am. Ceram. Soc.,* **70** [10] 708-13 (1987).

27. K.J. DeCarlo, T.F. Lam, and W.M. Carty, "Dissolution of Alumina in Silicate Glasses and the Glass Formation Boundary," *Ceram. Trans.,* **209**, 61-9 (2010).

28. M.N. Rahaman, *Ceramic Processing and Sintering;* p. 667. Marcel Dekker, New York, 1995.

29. P.W. McMillian, *Glass-ceramics;* p. 22. Academic Press, New York, 1964.

30. J.E. Shelby, "Formation and Properties of Calcium Aluminosilicate Glasses," *J. Am. Ceram. Soc.,* **68** [3] 155-8 (1985).

31. P. Richet, M. Roskosz, and J. Roux, "Glass Formation in Silicates: Insights from Composition," *Chem. Geol.,* **225** [3-4] 388-401 (2006).

32. M.J. Hyatt and D.E. Day, "Glass Properties in the Yttria-Alumina-Silica System," *J. Am. Ceram. Soc.,* **70** [10] C–283-7 (1987).

33. B. Quinlan, "The Unity Molecular Formula Approach to Glaze Development"; M.S. Thesis. Alfred University, Alfred, NY, 2002.

34. W.M. Carty, "Observations on the Glass Phase Composition in Porcelains," *Ceram. Eng. Sci. Proc.,* **23** [2] 79-94 (2002).

35. P. Auerkari, "Mechanical and Physical Properties of Engineering Alumina Ceramics" (1996) Technical Research Centre, Research Notes 1792. Accessed on: December 2010. Available at <http://www.vtt.fi/inf/pdf/tiedotteet/1996/T1792.pdf >

36. S.J. Dillon, M. Tang, W.C. Carter, and M.P. Harmer, "Complexion: A New Concept for Kinetic Engineering in Material Science," *Acta Mater.,* **55** [18] 6208-18 (2007).

37. J.E. Webb, "Processing of Mullite for Use as Ceramic-ceramic Composite Matrix Material"; M.S. Thesis. University of Washington, Seattle, WA, 1991.

38. P. Stadelmann, Java Electron Microscopy Software (JEMS), [Computer Program] CIME-EPFL, Lausanne, Switzerland, 2009.

39. C.-T. Inc. and GTT-Technologies, FactSage™, [Computer Program], Montreal, Canada, 2009.

40. B. Kibbel and A.H. Heuer, "Exaggerated Grain Growth in ZrO_2-toughened Al_2O_3," *J. Am. Ceram. Soc.,* **69** [3] 231-6 (1986).

41. T. Traoré, T.S. Kabré, and P. Blanchart, "Gehlenite and Anorthite Crystallisation from Kaolinite and Calcite Mix," *Ceram. Int.,* **29** [4] 377-83 (2003).

3. GRAIN BOUNDARY CHEMISTRIES IN THE SINTERING OF ALUMINA WITH CALCIA AND SILICA ADDITIVES REVISITED: INVERT GLASS FORMATION BOUNDARY

3.1. ABSTRACT

Alumina samples, with additive ratios of $CaO:1.5SiO_2$ and $CaO:0.8SiO_2$ were sintered at 1400°C, 1600°C, and 1700°C. Scanning electron microscopy (SEM) and transmission electron microscopy (TEM) were used for microstructural evaluation. At 1400°C secondary phases of anorthite and gehlenite were observed. At temperatures above 1600°C amorphous grain boundaries of invert glass compositions and anorthite were found. The observed phases can be explained by the proposed model of an invert glass formation boundary. The model explains the secondary phases observed in steady state non-equilibrium sintering of alumina for a system of additives $CaO:xSiO_2$, with $x \leq 1.5$.

3.2. INTRODUCTION

In the sintering of alumina with calcia and silica additives one of the more commonly reported ratios used is a 1:1 $CaO:SiO_2$ (additive ratios of calcia to silica will be referred to as CS, with ratios normalized to molar calcia). Various findings have been reported for this ratio. Brydson et al., in transmission electron microscopy (TEM) analysis of sintered samples ranging from 2-10 weight percent (wt%) CS additive ratio at 1400°C for varying dwell times reported a tetragonal phase proposed to be gehlenite ($2CaO{\cdot}Al_2O_3{\cdot}SiO_2$). Two amorphous triple point chemistries were observed, one similar to anorthite and one similar to gehlenite.[1] Švančárek et al., in a hot pressing study at 1450°C, reported gehlenite as a secondary phase.[2] Seabaugh et al. conducted a templated growth study and detected anorthite ($CaO{\cdot}Al_2O_3{\cdot}2SiO_2$) by X-ray diffraction (XRD) and scanning electron microscopy (SEM) analysis when samples were sintered to 1550°C.[3] TEM studies by Powell-Dogan and Heuer found predominantly amorphous grain boundaries without anorthite or gehlenite in samples sintered between 1560°C and 1600°C. Powell-Dogan's and Heuer's study was not a pure CS ratio, impurities of 0.4 wt% MgO and 0.05 wt% Na_2O were present and hence yielded an intragranular phase of β-alumina ($11Al_2O_3{\cdot}xNa_2O$, $1.0 \leq x \geq 1.6$) and an intergranular phase of spinel

($MgO{\cdot}Al_2O_3$). Calcium hexaluminate ($CaO{\cdot}6Al_2O_3$) was also a secondary phase found as an intergranular phase.[4] Upon subsequent heat treatment, calcium hexaluminate was observed to have partially resorbed from the grain boundary. Anorthite was the primary phase crystallized upon heat treatments.[5] Kositć et al. in sintering studies near the CS ratio up to 1550°C also reports calcium hexaluminate confirmed by XRD.[6] Song and Coble studied additive levels 0.3, 1.0, 3.0, and 10 wt% sintered at 1650°C for various intervals and also reported amorphous boundaries with calcium hexaluminate as intragranular and intergranular phases.[7] The summary of the varying findings at the CS ratio are presented in Table 3.I. The sintering temperature at this ratio appears to be a variable of interest.

Table 3.I. Review of the Reported Crystalline Secondary Phases for the CS Ratio

Sintering Temperature	Secondary Phases Observed	Chemical Formula	Reference Number
1400°C	Gehlenite	$2CaO{\cdot}Al_2O_3{\cdot}SiO_2$	1
1450°C	Gehlenite	$2CaO{\cdot}Al_2O_3{\cdot}SiO_2$	2
1550°C	Anorthite	$CaO{\cdot}Al_2O_3{\cdot}2SiO_2$	3
1550°C	Calcium Hexaluminate	$CaO{\cdot}6Al_2O_3$	6
1560°C to 1600°C	Calcium Hexaluminate*	$CaO{\cdot}6Al_2O_3$	4
1650°C	Calcium Hexaluminate	$CaO{\cdot}6Al_2O_3$	7

*β-alumina and spinel were present due to minor levels of Na_2O and MgO present

Sintering experiments with additive ratios of greater calcia in the CS ratio are of interest to the glass formation boundary approach since the calcium aluminosilicate system can produce glasses free of silica.[8-10] Glasses with less than 50 mole percent (mol %) silica are termed as an "invert" glasses where the calcium ions present no longer exist as modifying ion but play a role in glass forming network.[11] Figure 3.1 shows the region of invert glass compositions as adapted from Shelby.[10]

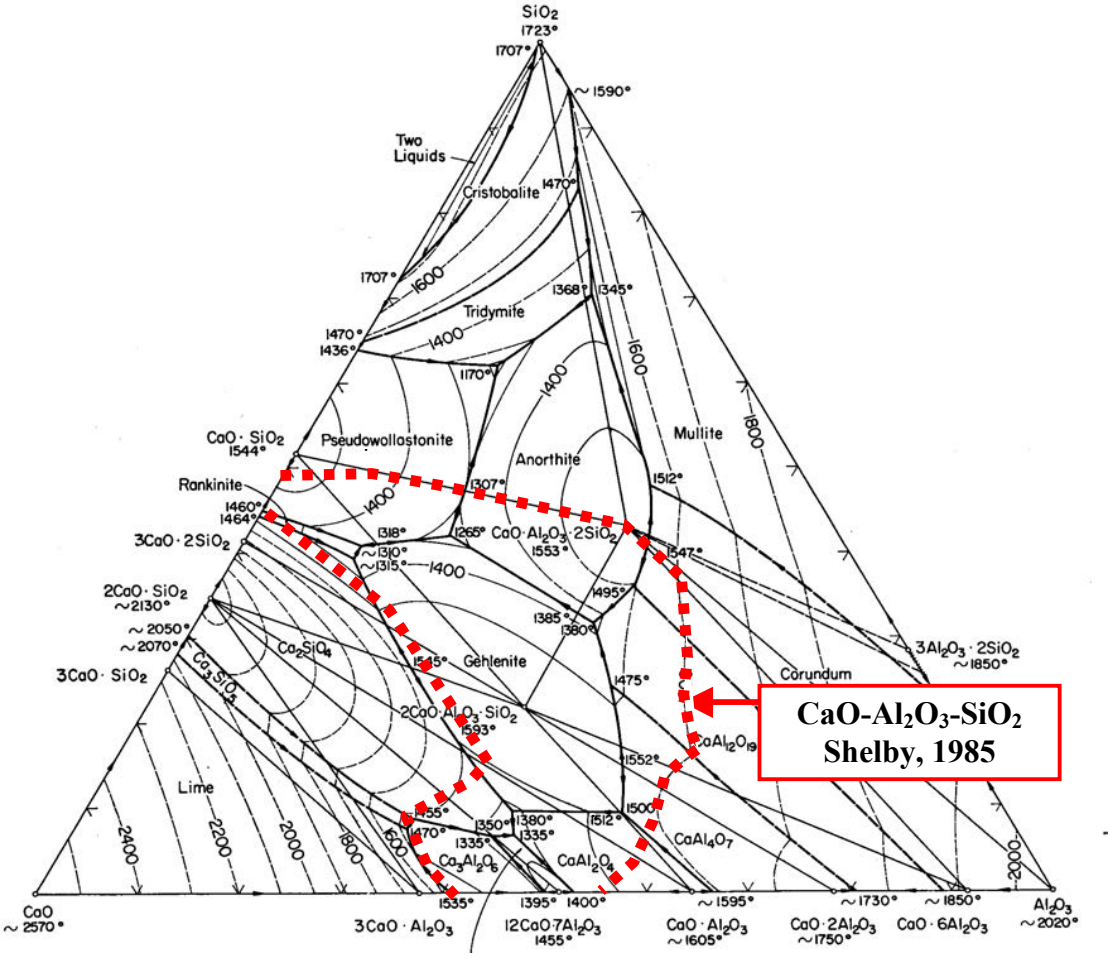

Figure 3.1. Glass formation region of invert glasses, adapted from Shelby.[10, 12]

A review of the literature shows that microstructural studies of co-dopant additives with ratio concentrations greater of calcia than silica in the CS ratio were less common. This is possibly because the use of glass frits for liquid phase sintering is a common practice and the compositions of greater calcia than silica in the CS ratio are not within common range of glass compositions of calcium aluminosilicate (the anorthite glass composition, $CaO{\cdot}Al_2O_3{\cdot}2SiO_2$, being the most common) or magnesium calcium aluminosilicate glasses generally applied.[13-18] In Švančárek et al. in a hot pressing study at 1450°C also included ratios of approximately C0.5S, C0.3S and C0.1S. At the additive ratios C0.5S and C0.3S gehlenite was the phase crystallized at the grain boundaries. At C0.1S grossite ($CaO{\cdot}2Al_2O_3$) was reported. The liquid phases reported were deficient in silica when compared to crystalline phases. The authors attributed the deficiency to

extensive crystallization of the grain boundaries.[2] Song's and Coble's sintering study at 1650°C also included a C0.3S and reported amorphous boundaries and calcium hexaluminate as intragranular and intergranular phases.[7] Kositć et al. in research using a glass additive of C0.1S ratio sintered to 1550°C also reported calcium hexaluminate as a secondary phase confirmed by XRD.[6]

3.3. EXPERIMENTAL PROCEDURE

Colloidal processing and sintering experimental procedures were similar to those described in the previous high silica to calcia ratios study (Section 2).[19] The only difference was the use of a finer colloidal silica source (NALCO® 1130, NALCO Chemical Company, Naperville, IL.). Chemical analysis using inductively couple plasma emission spectroscopy (ICP-ES), scanning electron microscopy (SEM), and transmission electron microscopy (TEM), energy dispersive spectroscopy (EDS) analysis were also performed as described in a previous higher silica to calcia ratios study (Section 2).[19]

3.4. RESULTS

Table 3.II presents the chemistries of the samples attained from ICP-ES in mole percent (mol%) oxide. Samples A-F were discussed in a previous study (Section 2).[19] Samples G, H, and I correspond to the C1.5S series. Samples J, K, and L belong to the C0.8S series. The heterocoagulation process with NALCO® 1130 colloidal silica, yielded suspensions with an average of 5.22 ± 0.19 mol% silica (94.78 mol% alumina).

Table 3.II. ICP-ES Chemistries of the Sintered Samples

Sample	Average Mole Ratio	Actual Mole Ratio	Sintering Temperature	Al_2O_3 (mol%)	CaO (mol%)	SiO_2 (mol%)	Other (mol%)
G	C1.5S	1.50	1400°C	91.60	3.35	5.04	0.02
H	C1.5S	1.42	1600°C	91.76	3.38	4.81	0.05
I	C1.5S	1.49	1700°C	91.84	3.26	4.86	0.03
J	C0.8S	0.80	1400°C	88.64	6.33	5.03	<0.01
K	C0.8S	0.90	1600°C	89.22	5.65	5.08	0.02
L	C0.8S	0.78	1700°C	88.63	6.40	4.97	<0.01

Figure 3.2 shows bright-field TEM micrographs of both C1.5S and C1.2S additive ratios. The microstructure of anorthite (twinned) and gehlenite were identified as secondary phases in Sample G (sintered at 1400°C) shown in Figure 3.2A. The morphology of the gehlenite was consistent with findings reported by Powell and Heuer and was further confirmed by electron diffraction and energy dispersive spectroscopy (EDS) chemistries.[5] A spherical inclusion was commonly observed within the gehlenite. However, the size of the phase was not suitable for selected area electron diffraction and the EDS only showed it to be of a higher alumina concentration within the gehlenite chemistry matrix. The phase could possibly be calcium hexaluminate or (less likely based on strain arguments) alumina, the clear identification of this phase is a topic for future work. Sample H (sintered at 1600°C) shows only amorphous triple points as seen in Figure 3.2B. Anorthite and an amorphous phase were found within the triple points of Sample I (sintered at 1700°C) as seen in Figure 3.2C. The anorthite was confirmed by electron diffraction and EDS chemistry.

Anorthite, gehlenite, and the unidentified spherical inclusion were also found in Sample J (sintered at 1400°C) for the C0.8S ratio shown in Figure 3.2D. The microstructures found in Sample J were similar to G for the C0.8S ratio sintered at 1400°C. Sample K (sintered at 1600°C) shows only amorphous triple points as seen in Figure 3.2E. Sample L (sintered at 1700°C) also shows only amorphous triple points as seen in Figure 3.2F.

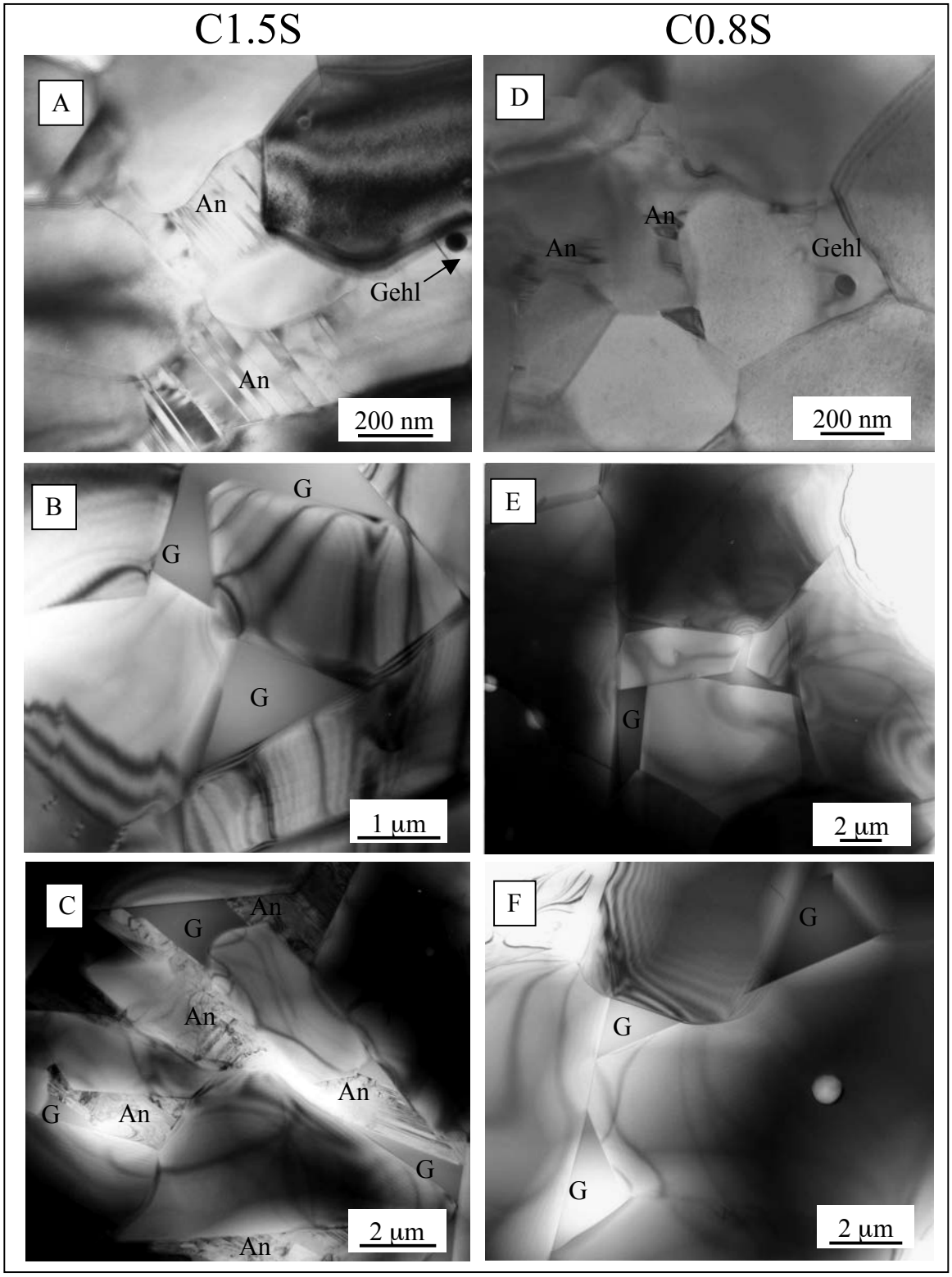

Figure 3.2. Bright-field TEM micrographs are shown for C1.5S (left column) and C0.8S (right column). Phases labeled G are amorphous (glassy) triple points, An are anorthite, and Gehl are gehlenite.

Table 3.III tabulates the chemistries of the amorphous triple points collected by TEM EDS in wt% for Samples H, I, K and L. Samples I, K and L had triple point chemistries of invert glass compositions. Amorphous triple points were not detected for Samples G and J at 1400°C. The triple point chemistries of this study have lower standard deviations when compared to higher silica to calcia ratios (Section 2). The lower standard deviations are likely due to the fact that the EDS measurements were from larger triple points.[19] Figure 3.3 is the plot of EDS chemistries expressed with the range of standard deviations overlaid on the CaO-SiO_2-Al_2O_3 phase diagram.[12] Figure 3.3A shows that the C1.5S ratio falls between Sample H and I. Figure 3.3B for the C0.8S ratio shows the triple point chemistries in Samples K and L to be similar in composition and corresponds to the C0.8S additive ratio used in processing. Additionally a slight solubility of chlorine, which is an artifact of the processing (from CaO source, a $CaCl_2$ solution), was observed within the amorphous triple points of Samples H and K for both ratios at 1600°C. Sample H had an additional 0.42 atomic percent (at%) chlorine and Sample K had an additional 2.58 at% chlorine. Chlorine solubility within the amorphous triple points was not observed for Samples I and L (sintered at 1700°C).

Table 3.III. TEM EDS Analysis of the Triple Points

Sample	Al_2O_3 (wt%)	CaO (wt%)	SiO_2 (wt%)	Cl (At%)*
H	26.39 ± 1.18	19.84 ± 3.21	53.76 ± 4.10	0.42 ± 0.17
I	27.61 ± 0.95	37.02 ± 2.10	35.37 ± 2.75	0
L	26.37 ± 1.40	37.56 ± 2.48	36.07 ± 3.23	2.58 ± 0.19
K	28.83 ± 1.80	33.92 ± 1.46	37.26 ± 1.72	0

* Cl concentrations have been reported as an additional amount to the amorphous phase.

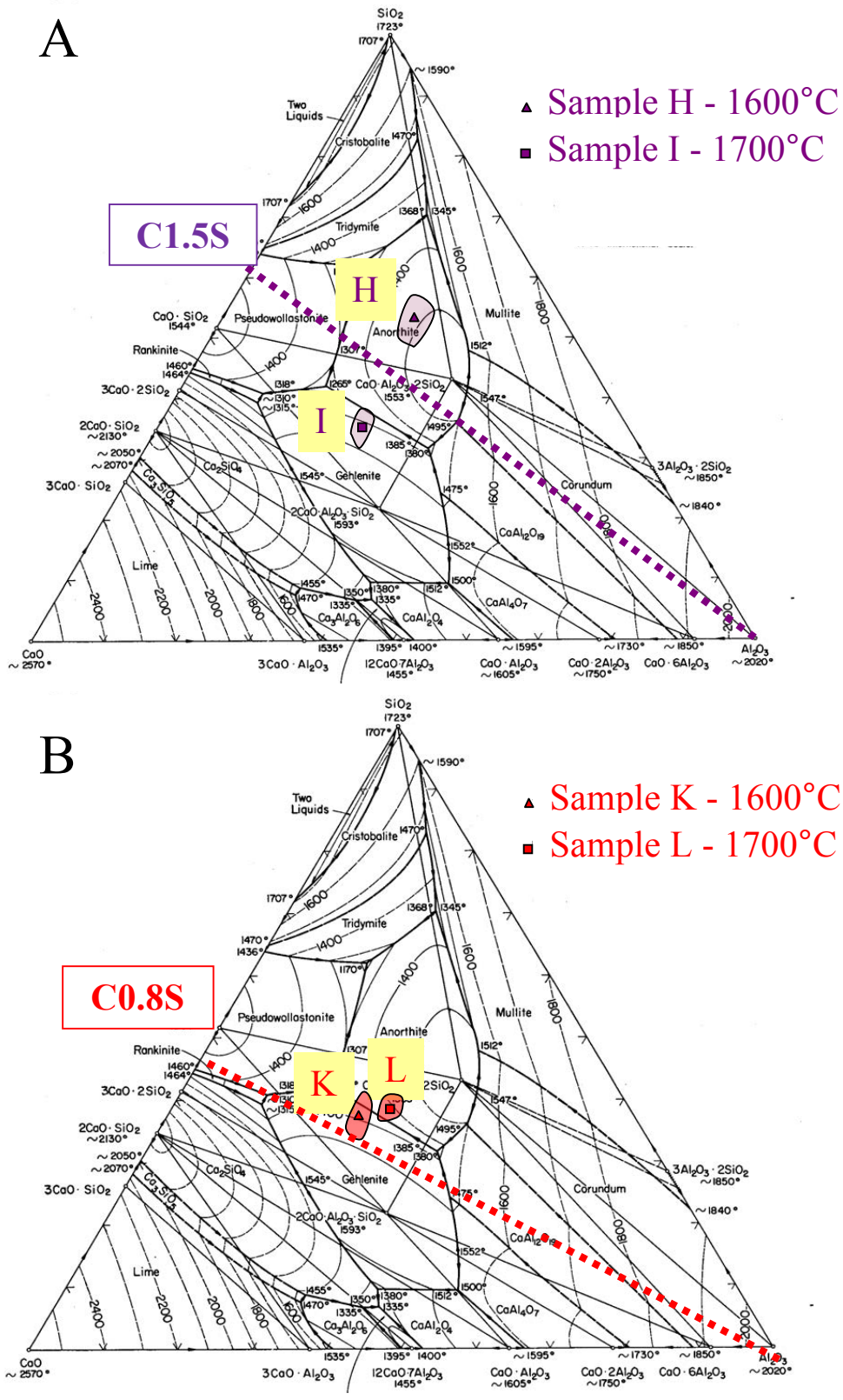

Figure 3.3. TEM EDS chemistries of the triple point analysis (A) C1.5S and (B) C0.8S ratio.[12]

The analyses from the SEM are separated into columns of C1.5S and C0.8S ratio additives. SEM analyzes in Figure 3.4A for Sample G and Figure 3.4D for Sample J did not reveal grain growth for samples sintered to 1400°C for either series of C1.5S or C0.8S. The backscatter electron micrographs in Figure 3.4A and 3.4D showed a secondary phase with a difference of contrast from the alumina grains. The observed phase has a similar morphology to the spherical phase within the gehlenite as seen in the TEM micrographs from Figure 3.2A and 3.2D. Samples sintered at 1600°C and 1700°C that were thermally etched (as shown in Figure 3.4B, 3.4C, 3.4E, and 3.4F), exuded a liquid from the grain boundary to the surfaces of the grain, similar to that reported by Ravishankar et al.[20] For Sample H in Figure 3.4B and Sample K in Figure 3.4E, sintered to 1600°C, abnormal grain growth was observed. The abnormal grain growth appears to create a higher population of plate-like grains in comparison to the microstructures observed with higher silica to calcia ratios (Section 2) which is consistent with Dillion's and Harmer's grain growth studies involving additives of only CaO and only SiO_2.[19, 21-23] For Sample I in Figure 3.4C and Sample L in Figure 3.4F, sintered to 1700°C, abnormal grain growth was again observed and also the crystallization of whisker like phases on the surfaces of the grains, the morphology of which is similar to the anorthite found by Seabaugh et al.[3]

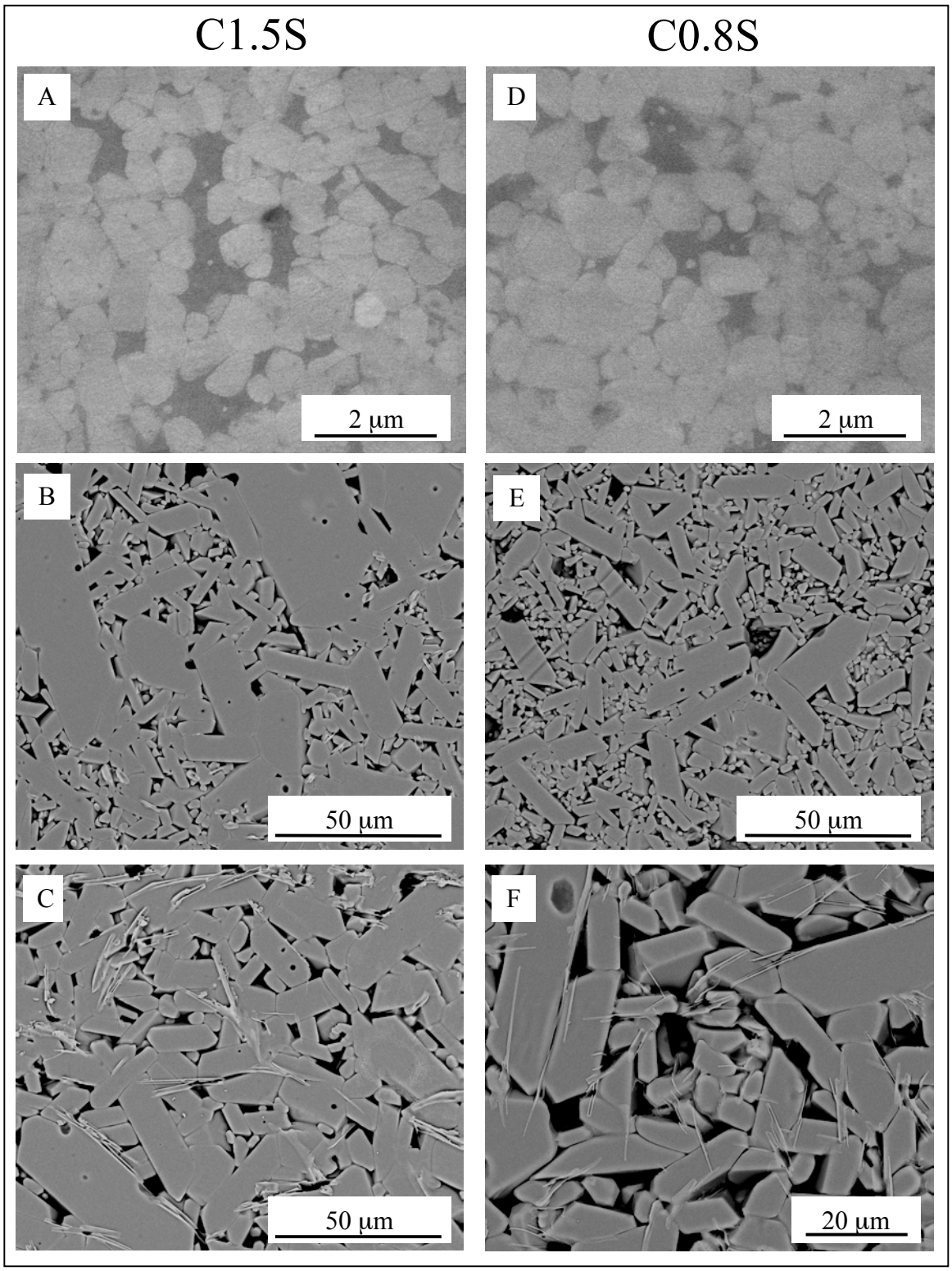

Figure 3.4. Backscatter electron micrographs are shown for the C1.5S (left column) and C0.8S (right column). Samples were thermally etched. Imaging was performed in low vacuum mode for A and D. An Au-Pd coating was used for B, C, E, and F.

3.5. DISCUSSION

Samples G (C1.5S) and J (C0.8S) were sintered at 1400°C and show similar microstructures with anorthite and gehlenite as secondary phases. At 1400°C alumina dissolution into a calcia base grain boundary is not the same as that of a silicate base grain boundary. In a study of up to 5 wt% CaO additive at 1330°C as a function of time, Wu et al. showed that the reaction behavior between calcia and alumina is quite different than that of alumina dissolution into silicate based grain boundary. Even at 60°C below the eutectic the secondary phase of calcium aluminate ($CaO{\cdot}Al_2O_3$) transitions to grossite as the main secondary phase in approximately four hours, and eventually transitions into calcium hexaluminate as the main secondary phase after 10 hours.[24] The transitions without the formation of a liquid phase suggest that the diffusion of Al^{3+} ions may be quite different than that of alumina dissolution into an amorphous silicate that was demonstrated by DeCarlo et al.[25] Based on the lack of amorphous triple points observed in Samples G and J at 1400°C for ratios of CxS with $x \leq 1.5$, the crystallized phases evolved in this microstructure are proposed to come from subeutectic solid state reactions rather than the crystallization from a triple point due to alumina dissolution into a silicate base liquid. Similarly, the phase of grossite at C0.1S reported by Švančárek et al. is also likely a result of a subeutectic solid state reaction.

At a bulk glass composition of approximately 34.5% CaO, 34.2% SiO_2, and 31.3% Al_2O_3 wt% chlorine solubility of 1.9 at% has been reported, which is consistent with the observed chlorine solubilities observed in the glassy triple points of Samples H and K sintered at 1600°C. The solubility of chlorine in a glass structure has been shown to be dependent on the fraction of nonbridging oxygen (NBO) to total oxygen present in the host glass matrix and chloride ions were proposed to occupy the site around the NBO. In the calcium aluminosilicate glass system, when the $CaO:Al_2O_3$ ratio is equal to one, all the oxygens are expected to be bridging oxygens. At ratios greater than one for $CaO:Al_2O_3$, excess Ca^{2+} ions will form NBO's.[26] Even though the triple point chemistries of samples sintered to 1700°C should theoretically generate a similar glass structure, Samples I and L did not show solubility for chlorine. This would suggest that at 1700°C the chlorine can be liberated from the liquid boundaries as a gaseous phase. In the samples sintered to 1400°C (Samples G and J), the crystalline secondary phases of

anorthite and gehlenite in the samples do not have a solubility for chlorine. It is proposed that the solid state reactions of anorthite and gehlenite occur during the dwell of the sintering and chlorine is liberated at this stage. In sintering (10K/min ramp) to 1600°C the secondary phases do not form, therefore the chlorine can still exist in the amorphous grain boundary.

C2S is another ratio (anorthite composition liquid) used in the sintering of alumina. For the majority of the cases, the literature reported that sintering with high purity alumina sources created only amorphous grain boundaries sintering in the range of 1550°C to 1650°C.[16-18, 27] A dielectric loss study of industrial alumina by Floyd sintered with C2S ratio at 1650°C reported anorthite.[14] For the C1.5S additive ratio a similar microstructural change is observed. Sample H has only amorphous grain boundaries when sintered to 1600°C and sample I crystallizes anorthite when sintered to 1700°C. It is proposed that sintering at temperatures above 1650°C, the melt will saturate with alumina resulting in the crystallization of anorthite.

Within the CaO-Al_2O_3-SiO_2 system, the location of the calcium hexaluminate phase field had been uncertain even after Osborn and Muan proposed the diagram.[12, 28] Proposed in the previous higher silica to calcia ratio additive study (Section 2), once the liquid forms the isotherms are relative indicators of sintering temperatures.[19] At the C0.8S ratio sintered to 1700°C the Osborn and Muan diagram would place the composition in the calcium hexaluminate phase field shown in Figure 3.5A. Through a combination of solid state sintering (phases of the compatibility triangle) and quenching experiments, Gentile and Foster show a narrower detailed region surrounding the invariant point within the gehlenite-anorthite-calcium hexaluminate compatibility triangle with a larger corundum phase field and would place the C0.8S ratio sintered at 1700°C composition within the corundum phase field shown in Figure 3.5B. For this region of the phase diagram, the Gentile and Foster diagram (Figure 3.5B) is in relatively decent agreement with Mao et al. modified ionic two-sublattice model assessed by the calculation of phase diagram using the computer coupling of phase diagrams and thermochemistry (CALPHAD) technique which is shown Figure 3.5C.[29] For C1.5S and C0.8S additive ratios in this study, calcium hexaluminate was not found at the grain boundaries. In particular, the C1.5S ratio sintered to 1700°C (sample I) yielded anorthite

rather than calcium hexaluminate at the grain boundary. The Gentile and Foster diagram is supportive of this study's analysis at 1700°C. Based on the glass formation boundary approach, Sample I would first crystallize out corundum (which could be kinetically difficult and indistinguishable from the matrix grains) at grain boundaries. Depending on the cooling path and the actual glass formation boundary, the crystallization of anorthite is still a feasible reaction.

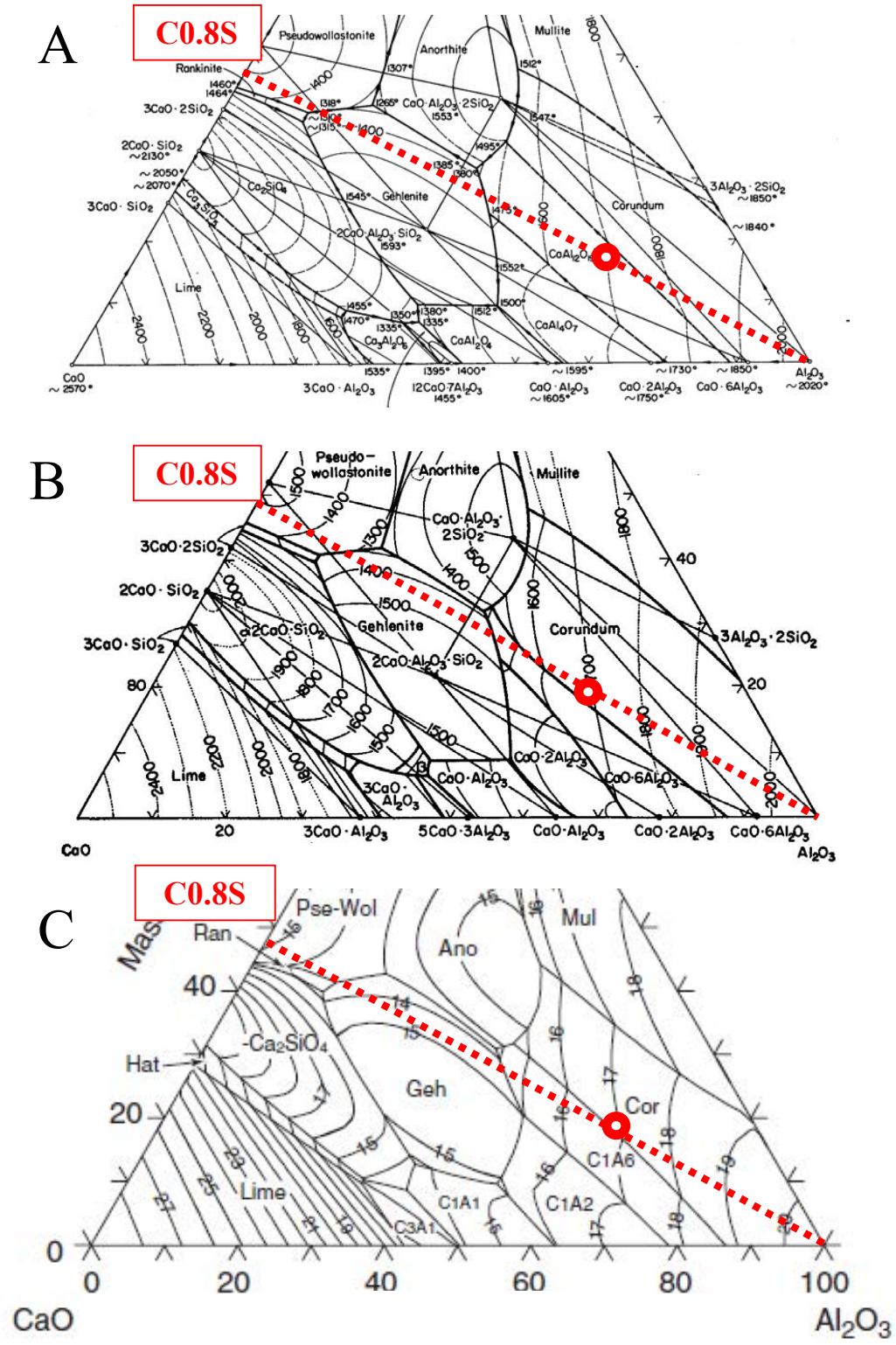

Figure 3.5. Differences of the calcium hexaluminate phase field in the CaO-Al_2O_3-SiO_2 system, adapted with interpretations to the C0.8S ratio at 1700°C. (A) Diagram from Osborn and Muan (B) Diagram from Gentile and Foster (C) CALPHAD technique by Mao et al.[12, 27, 28]

The low alumina concentration of the EDS analysis of the amorphous triple points suggests the isotherms do not work as relative indicators of sintering temperature for the additive ratios C1.5S and C0.8S. The lower concentration of alumina at the grain boundary could be the result of an unquenched system.

From Samples I, K and L of this study an invert glass formation boundary is proposed in Figure 3.6 on the phase diagram from Gentile and Foster.[28] The proposed invert glass formation boundary approach provides an explanation for the varying phases reported in the literature at the CS ratio. Sintering at 1400°C is proposed to be dominated by solid state subeutectic reactions. As sintering temperature exceeds 1600°C the grain boundaries become amorphous. The crystallization of anorthite within the amorphous triple point suggests a portion of the anorthite phase field must reside outside the glass formation boundary. It its therefore proposed that the upper dashed line region of the invert boundary and the lower region of the glass formation boundary form two separate boundaries and not one continuous glass formation boundary .

Amorphous grain boundaries were observed at 1700°C and it should be noted that the glasses tested in Shelby's study only extend to the regions along the 1600°C liquidus.[10] The dashed line region of the invert glass formation boundary for ratios below C0.8S at 1700°C is predicted to still be amorphous.

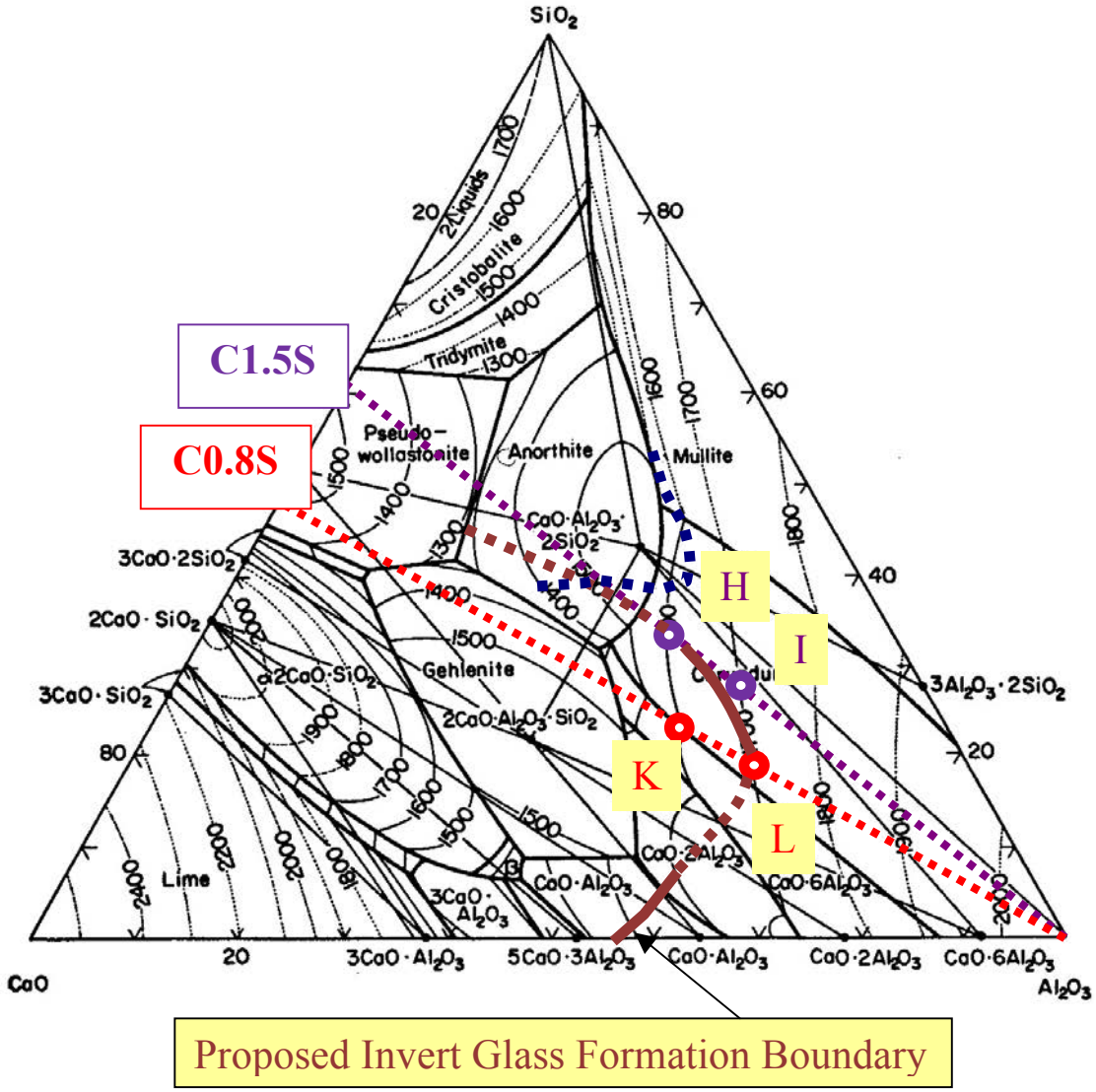

Figure 3.6. Proposed invert glass formation boundary in the sintering of alumina of calcia and silica additives.[27]

3.6. CONCLUSION

The dissolution of alumina into a silicate amorphous grain boundary and that of calcia based grain boundary are different and result in the phases of anorthite and gehlenite when sintered at 1400°C. Sintering above 1600°C resulted in the formation of amorphous triple points of invert glass compositions exhibiting properties of the bulk glass (specifically the solubility of chlorine). The invert glass formation boundary is applicable to sintering above 1600°C. The proposed formation of subeutectic reactions at the grain boundaries and invert glass formation boundary gives a plausible explanation of

the varying secondary phases reported literature, specifically for the one to one calcia to silica ratio that has been commonly reported.

3.7. REFERENCES

1. R. Brydson, S.-C. Chen, F.L. Riley, S.J. Milne, X. Pan, and M. Rühle, "Microstructure and Chemistry of Intergranular Glassy Films in Liquid-phase-sintered Alumina," *J. Am. Ceram. Soc.,* **81** [2] 369-79 (1998).

2. P. Švancárek, D. Galusek, F. Loughran, A. Brown, R. Brydson, A. Atkinson, and F. Riley, "Microstructure-stress Relationships in Liquid-phase Sintered Alumina Modified by the Addition of 5 wt.% of Calcia-silica Additives," *Acta Mater.,* **54** [18] 4853-63 (2006).

3. M.M. Seabaugh, G.L. Messing, and M. Vaudin, "Texture Development and Microstructure Evolution in Liquid-phase-sintered α-Alumina Ceramics Prepared by Templated Grain Growth," *J. Am. Ceram. Soc.,* **83** [12] 3109-16 (2000).

4. C.A. Powell-Dogan and A.H. Heuer, "Microstructure of 96% Alumina Ceramics: I, Characterization of the As-sintered Materials," *J. Am. Ceram. Soc.,* **73** [12] 3670-6 (1990).

5. C.A. Powell-Dogan and A.H. Heuer, "Microstructure of 96% Alumina Ceramics: III, Crystallization of High-calcia Boundary Glasses," *J. Am. Ceram. Soc.,* **73** [12] 3684-91 (1990).

6. E. Kostić, S. Bošković, and S.J. Kiss, "Reaction Sintering of Al_2O_3 in the Presence of the Liquid Phase," *Ceram. Int.,* **19** [4] 235-40 (1993).

7. H. Song and R.L. Coble, "Morphology of Platelike Abnormal Grains in Liquid-phase-sintered Alumina," *J. Am. Ceram. Soc.,* **73** [7] 2086-90 (1990).

8. W.M. Carty, "Observations on the Glass Phase Composition in Porcelains," *Ceram. Eng. Sci. Proc.,* **23** [2] 79-94 (2002).

9. B. Quinlan, "The Unity Molecular Formula Approach to Glaze Development"; M.S. Thesis. Alfred University, Alfred, NY, 2002.

10. J.E. Shelby, "Formation and Properties of Calcium Aluminosilicate Glasses," *J. Am. Ceram. Soc.,* **68** [3] 155-8 (1985).

11. H. Rawson, *Inorganic Glass-forming Systems;* pp. 91-4. Academic Press, New York, 1967.

12. Phase Diagrams for Ceramists, Vol. 1; Fig. 630. Edited by E.F. Osborn and A. Muan. American Ceramic Society, Westerville, OH, 1964.

13. J.S. Reed, *Introduction to the Principles of Ceramic Processing,* 2nd ed.*;* pp. 608-9. John Wiley & Sons, New York, 1988.

14. J.R. Floyd, "Effect of Secondary Crystalline Phases on Dielectric Losses in High-alumina Bodies," *J. Am. Ceram. Soc.,* **47** [11] 539-43 (1964).

15. P.L. Flaitz, "Some Aspects of Liquid-phase Sintering of Alumina"; Ph.D. Thesis. University of California, Berkeley, CA, 1982.

16. J.E. Marion, C.H. Hsueh, and A.G. Evans, "Liquid-phase Sintering of Ceramics," *J. Am. Ceram. Soc.,* **70** [10] 708-13 (1987).

17. N.P. Padture and H.M. Chan, "Improved Flaw Tolerance in Alumina Containing 1 vol% Anorthite via Crystallization of the Intergranular Glass," *J. Am. Ceram. Soc.,* **75** [7] 1870-5 (1992).

18. M.J. Kim and D.Y. Yoon, "Effect of Magnesium Oxide Addition on Surface Roughening of the Alumina Grains in Anorthite Liquid," *J. Am. Ceram. Soc.,* **86** [4] 630-3 (2003).

19. T.F. Lam, K.J. DeCarlo, and W.M. Carty, "Grain Boundary Chemistries in the Sintering of Alumina with Calcia and Silica Additives Revisited: High Silica to Calcia Ratios and the Glass Formation Boundary," *J. Am. Ceram. Soc.,* (submitted for publication).

20. N. Ravishankar and C.B. Carter, "Exuding Liquid from the Grain Boundaries in Alumina," *J. Am. Ceram. Soc.,* **84** [4] 859-62 (2001).

21. S.J. Dillon and M.P. Harmer, "Relating Grain-boundary Complexion to Grain Boundary Kinetics I: Calcia-doped Alumina," *J. Am. Ceram. Soc.,* **91** [7] 2304-23 (2008).

22. S.J. Dillon and M.P. Harmer, "Relating Grain Boundary Complexion to Grain Boundary Kinetics II: Silica-doped Alumina," *J. Am. Ceram. Soc.,* **91** [7] 2314-20 (2008).

23. S.J. Dillon and M.P. Harmer, "Diffusion Controlled Abnormal Grain Growth in Ceramics," *Mater. Sci. Forum,* **558-559**, 1227-36 (2007).

24. S.J. Wu, L.C. DeJonghe, and M.N. Rahaman, "Subeutectic Densification and Second-phase Formation in Al_2O_3-CaO," *J. Am. Ceram. Soc.,* **68** [7] 385-8 (1985).

25. K.J. DeCarlo, T.F. Lam, and W.M. Carty, "Dissolution of Alumina in Silicate Glasses and the Glass Formation Boundary," *Ceram. Trans.,* **209**, 61-9 (2010).

26. S. Siwadamrongpon, M. Koide, and K. Matusita, "Prediction of Chlorine Solubility in CaO-Al_2O_3-SiO_2 Glass Systems," *J. Non-Cryst. Solids,* **347** [1-3] 114-20 (2004).

27. E. Kostić, S.J. Kiss, and S. Bošković, "Liquid Phase Sintering of Alumina," *Powder Metall. Int.,* **19** [4] 41-3 (1987).

28. A.L. Gentile and W.R. Foster, "Calcium Hexaluminate and Its Stability Relations in the System CaO-Al_2O_3-SiO_2," *J. Am. Ceram. Soc.,* **46** [2] 74-6 (1963).

29. H. Mao, M. Hillert, M. Selleby, and B. Sundman, "Thermodynamic Assesment of the CaO-Al_2O_3-SiO_2 System," *J. Am. Ceram. Soc.,* **89** [1] 298-308 (2006).

4. GRAIN BOUNDARY CHEMISTRIES IN THE SINTERING OF ALUMINA WITH CALCIA AND SILICA REVISITED: VOLUME ANALYSIS AND PHASE CORRELATIONS

4.1. ABSTRACT

Recent studies investigating grain boundary evolution in 93-95 weight percent (wt%) alumina doped with CaO and SiO_2 indicate that the grain boundary chemistry and mineralogy can be adequately predicted by invoking the glass formation boundary in the calcium-alumino-silicate system. Two separate glass formation boundaries were identified: one of a silica-based glass and one composed of invert glass. To further evaluate the feasibility of this approach, the volume fraction of secondary phases existing at the grain boundaries (by scanning electron microscopy (SEM)) and triple points chemistries (using transmission electron microscopy (TEM)) data, and inductively couple plasma emission spectroscopy (ICP-ES) analyses of the bulk samples were analyzed. These results confirmed the glass formation boundary approach. Based on the volume fraction correlation with the triple point chemistries, a quantification model correlating additive levels and secondary phase volume is proposed.

4.2. INTRODUCTION

In the liquid phase sintering literature the data is often discussed in terms of volume percent (vol%) when a glass frit is used as the sintering aid. The volume liquid phase is calculated from the density of glass additive, although even in this case alumina dissolution is still possible.[1-3] The vol% of secondary phases (7 to 28 vol%) has been reported to have a varying effect on the mechanical behavior of alumina.[4-10] The exact chemistry of grain boundaries has been generally concluded to be "transient" and the density of the grain boundary liquid would be unknown.[3, 11-13] Several studies have investigated the influence of varying additive concentrations on the microstructure and densities from the range of 0.3 to 15 wt%. These studies concluded that an increase in grain size occurred with increasing concentration of additives but without a changes in the observed secondary phases.[11, 14, 15] In fact, an electron microscopy study by Brydson et al. found that the grain boundary composition was not dependent on the amount of additives in the range of 2-10 wt%.[11] Since the glass formation boundary approach views

the additives as a localized segregation of glass-forming oxides, a relationship of the amount of additives to the volume of secondary phases observed should exist that could potentially provide for a better understanding to use additives in the sintering of alumina. Figure 4.1 shows the conclusions of the previous two revisited studies in the sintering of alumina with calcia and silica additives (Section 2 and 3). Figure 4.1A is the proposed glass formation boundaries based boundary and Figure 4.1B shows the grain boundary chemistries.[16, 17]

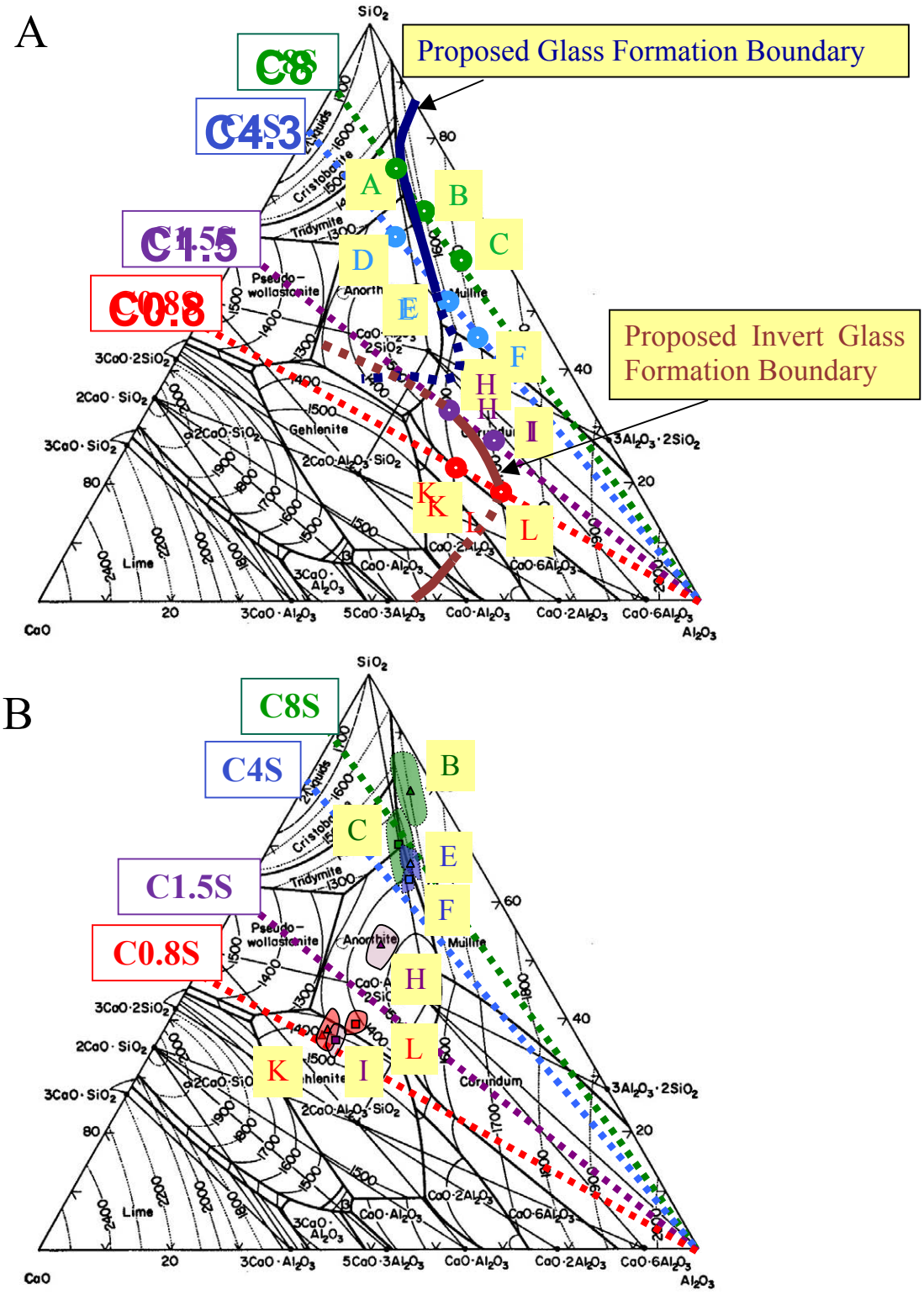

Figure 4.1. (A) Proposed glass formation boundaries in the sintering alumina. (B) Triple point grain boundary chemistries from for samples sintered above 1600°C.[16-18]

4.3. EXPERIMENTAL PROCEDURE

Scanning electron microscopy (SEM) was performed on polished unetched samples B, C, E, F, H, I, K and L processed in previous grain chemistry studies (Section 2 and 3).[16, 17] Stereological analyses to measure the volume fraction of the phases present were performed using ImageJ (Image Processing and Analysis in Java) software.[19] Chemical analysis data from inductively couple plasma emission spectroscopy (ICP-ES) of the samples were applied in this study. Calculated densities were obtained from SciGlass software using the average compositions of glassy triple points from transmission electron microscopy energy dispersive spectroscopy (TEM EDS) analyses of the sintered samples.[20] The densities of the glasses were applied to convert the average calculated volume fractions to the average wt% of secondary phases observed in the microstructures.

4.4. RESULTS AND DISCUSSION

The amorphous grain boundaries of the samples sintered at 1400°C (Samples A, D, G, and J) were not resolvable by SEM and therefore were not used in the volume fraction analysis. Table 4.I presents the densities of the observed secondary phases, these densities were calculated or obtained from literature. The density of mullite was applied for Samples B and C based on the large area of mullite matrices observed in these samples. SciGlass software offers several different calculation methods to predict the properties of glasses. However, the accuracy of a selected method depends on the type of glass.[20, 21] Being that glasses of high aluminosilicate, calcium aluminosilicate, and invert (below 50 mol% silica) glass compositions were observed at the triple points, the use of more than one method was required. The amorphous compositions in Samples E and F were calcium aluminosilicates with compositions most similar to feldspathic ceramic glazes. The Gan Fuxi-74 database has been confirmed to provide accurate property calculations of feldspathic ceramic glazes and was therefore used in the density calculation for Samples E and F.[21] The Priven 98 method was the only method that could calculate properties for glasses with below 50 mol% silica and was applied to Samples H, I, K, and L. As noted in the table, an average value was used for Sample I since phases of both anorthite and glass were commonly observed within the same triple point (and further confirmed in the microstructure presented later in this paper).

Table 4.I. Densities of Secondary Phases Observed in the Sintered Samples

Sample	Additive Ratio	Sintering Temperature	Density of Secondary Phase (g/cm^3)	Database or Reference Number
B	C8S	1600°C	3.06	19
C	C8S	1700°C	3.06	19
E	C4S	1600°C	2.58	Gan Fuxi-74
F	C4S	1700°C	2.61	Gan Fuxi-74
H	C1.5S	1600°C	2.61	Priven 98
I	C1.5S	1700°C	2.81*	Priven 98 and 20
K	C0.8S	1600°C	2.86	Priven 98
L	C0.8S	1700°C	2.82	Priven 98

*An average was applied for sample I. The density of the glass was 2.86 and the anorthite has been referenced at 2.76.[20, 22]

For the C8S ratio, Sample B (sintered at 1600°C) is shown in the top left quadrant of Figure 4.2 and displays a bimodal distribution of grain size and a region of a mullite matrix (in the contrasted area in the lower left hand corner of the micrograph). Previous TEM analysis, showed the finer grains to be connected by amorphous film which was difficult to resolve with SEM because it was so thin (on the nanometers scale).[16] Sample C (sintered at 1700°C) also shows a bimodal distribution of grain size but with a drastic change in the microstructure from 1600°C there are larger regions of mullite (bottom left quadrant in Figure 4.2). The volume fraction/vol% of secondary phase was calculated to be 9.6% for sample B and 13.9% for Sample C as shown in Table 4.II.

In the C4S ratio series, Sample E (sintered at 1600°C) is shown in the top right quadrant of Figure 4.2 and again shows a bimodal distribution of grain size with a region of mullite matrix in the top right corner of the micrograph. Fewer mullite matrices were observed in Sample E in comparison to Sample B. Sample F (sintered at 1700°C) is shown in the lower right quadrant of Figure 4.2. The mullite matrix morphologies were not observed as frequently and the secondary phase was concluded to be predominantly amorphous. A bimodal distribution of grain size was still observed in Sample F. The TEM micrographs for Samples E and F from a previous study (Section 2) displayed an increasing size of triple points between the grains. Samples E and F were both calculated

to have 10.5-10.6 vol % (Table 4.II) which is possible and consistent because the grain size also increases.

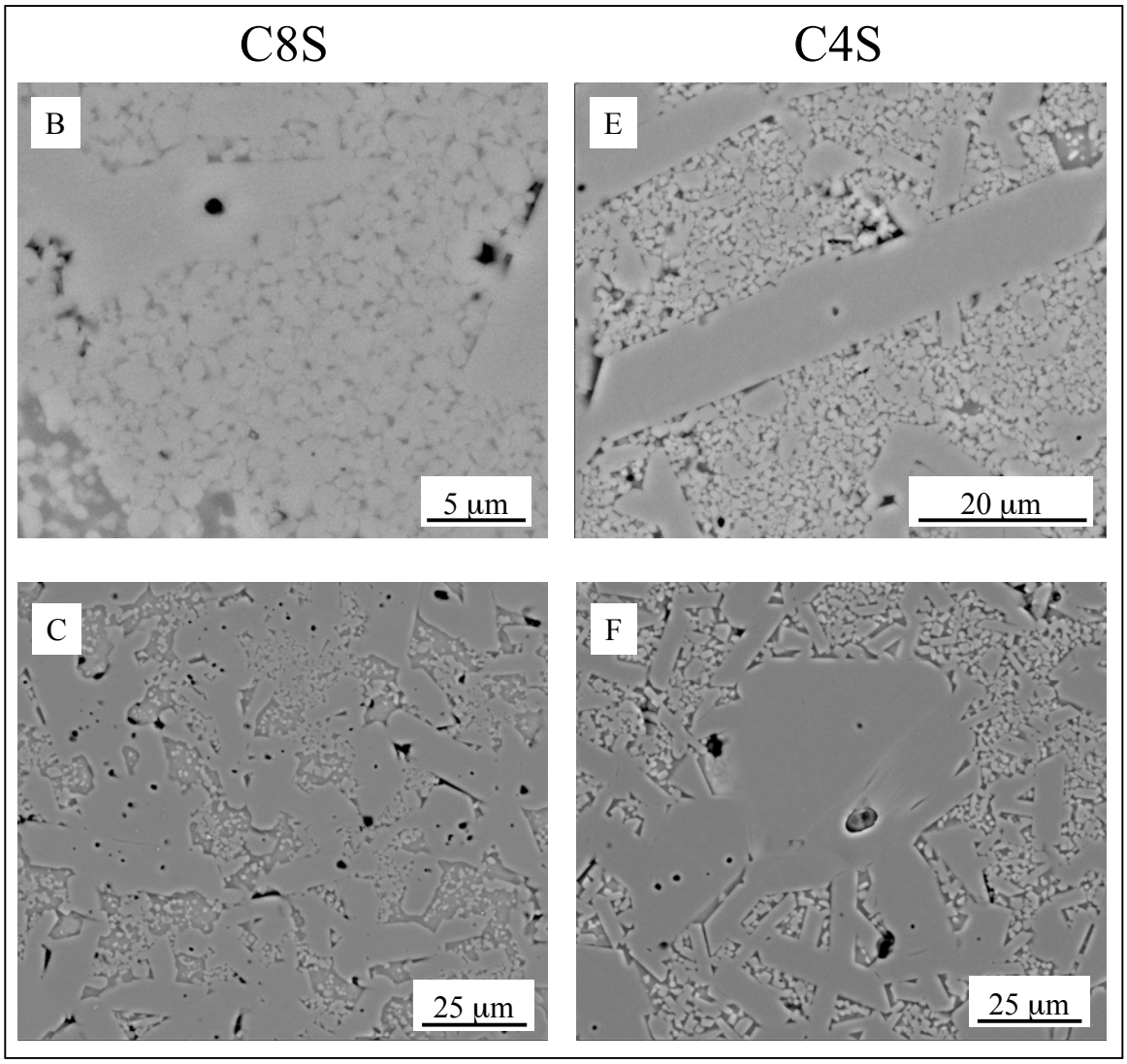

Figure 4.2. SEM micrographs for C8S (left column) and C4S (right column), Samples B and E were sintered at 1600°C and samples C and F were sintered at 1700°C.

Table 4.II. ImageJ Volume Analysis and Wt% Conversion for Samples B, C, E, and F

Sample	Vol% of Secondary Phases	Vol% Porosity	Vol% of Alumina	Wt% of Alumina
B	9.6 ± 2.9	0.5 ± 0.4	89.9 ± 2.9	92.41
C	13.9 ± 2.2	1.4 ± 0.8	84.7 ± 2.1	88.78
E	10.5 ± 0.9	0.6 ± 0.3	88.9 ± 0.9	92.90
F	10.6 ± 1.2	0.5 ± 0.2	88.9 ± 1.2	92.77

Using the difference calculated from the bulk chemical analysis and the observed wt% from the microstructure, Table 4.III presents the raw data used to calculate the alumina concentration at the grain boundary for Samples B, C, E, and F. As proposed, the volume analysis calculations show an increase in alumina dissolution with increasing sintering temperature in C8S (Sample B and C) and C4S (Sample E and F). The large change in the calculated alumina concentration at the grain boundary from B to C is consistent since most of the secondary phase observed was the mullite matrix (the compositional make up of 3-2 mullite is ~68 wt% alumina).[23]

Table 4.III. Calculated Al_2O_3 Concentration in Grain Boundary - Samples B, C, E, and F

Sample	Al_2O_3 (wt%)	CaO (wt%)	SiO_2 (Wt%)	Observed Al_2O_3 (wt%)	Calculated Difference of Al_2O_3 (wt%)	Al_2O_3 (wt%) at Grain Boundary
B	94.39	0.73	4.74	92.41	1.98	26.58
C	94.54	0.49	4.92	88.78	5.76	51.57
E	93.86	1.12	4.87	92.90	0.96	13.81
F	94.34	1.02	4.59	92.77	1.57	21.87

The C1.5S ratio series Sample H (sintered at 1600°C) is shown in the top left quadrant of Figure 4.3 and shows a bimodal distribution of grain size. Sample I (sintered at 1700°C) appears to be less bimodal in alumina grain size distribution (bottom left quadrant in Figure 4.3). The inset in the micrograph (bottom left quadrant in Figure 4.3) shows anorthite crystallization within the glassy triple point which is consistent with

previous TEM observations (Section 3).[17] The vol% of secondary phase was calculated to be 8.8% for Sample H and 9.0% for sample I as shown in Table 4.IV.

Sample K (sintered at 1600°C) of the C0.8S ratio is shown in the top quadrant of Figure 4.3. Sample L (sintered at 1700°C) of the C0.8S ratio is shown in the bottom right quadrant of Figure 4.3. The volume fraction/vol% of secondary phase was calculated to be 12.0% for Sample K and 11.4% for Sample L as shown in Table 4.IV.

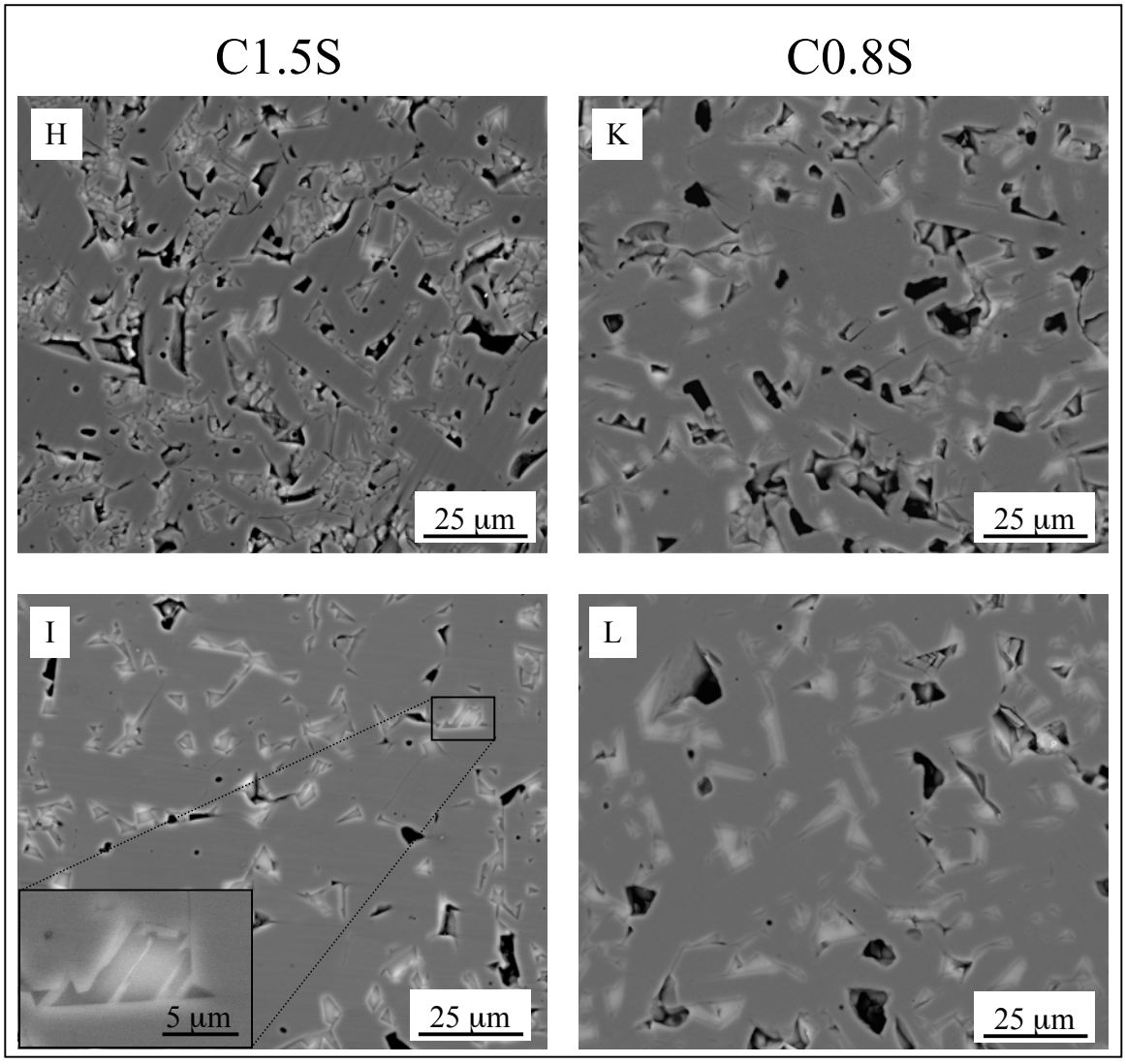

Figure 4.3. SEM micrographs for C1.5S (left column) and C0.8S (right column), Samples H and K were sintered at 1600°C and samples I and L were sintered at 1700°C.

Table 4.IV. ImageJ Volume Analysis and Wt% Conversion for Samples H, I, K, and L

Sample	Vol% of Secondary Phases	Vol% Porosity	Vol% of Alumina	Wt% of Alumina
H	8.8 ± 1.2	5.2 ± 1.1	86.0 ± 1.8	93.75
I	9.0 ± 0.8	3.7 ± 0.9	87.3 ± 1.0	93.21
K	12.0 ± 1.2	7.8 ± 0.8	80.3 ± 1.6	90.33
L	11.4 ± 0.8	4.3 ± 0.9	84.4 ± 1.2	91.29

Table 4.V tabulates the calculated grain boundary compositions from the difference of bulk chemical analyses and the observed wt% from the microstructure in Samples H, I, K, and L. The calculated alumina concentration for Samples H and I were within 4 wt% of EDS chemistry reported previously (Section 3).[17] For the C0.8S additive ratio, the calculated alumina for Sample K is approximately 7 wt% greater than EDS chemistry and the calculated alumina for Sample L is approximately 6 wt% less than EDS chemistry. Based on the compounded errors of standard deviations used in determining the vol% of secondary phases, the calculated chemistries for Sample K and L would be approximately one standard deviation greater or less than chemistries reported by TEM EDS.

Table 4.V. Calculated Al_2O_3 Concentration in Grain Boundary - Samples H, I, K, and L

Sample	Al_2O_3 (wt%)	CaO (wt%)	SiO_2 (Wt%)	Observed Al_2O_3 (wt%)	Calculated Difference of Al_2O_3 (wt%)	Al_2O_3 (wt%) at Grain Boundary
H	95.14	1.93	2.94	93.75	1.39	22.20
I	95.15	1.86	2.97	93.21	1.94	28.39
K	93.6	3.26	3.14	90.33	3.27	33.82
L	93.21	3.70	3.08	91.29	1.92	22.07

Powell-Dogan et al. observed that the grain boundary of an alumina substrate of approximately 99.5 wt% with glass forming impurities could be devitrified to crystallize microstructures similar to devitrification studies of 94 wt% alumina suggesting that the concept of a glass formation boundary could be applicable to sintering alumina up to at

least 99.5 wt%.[24] The correlations of vol% with the grain boundary chemistry in this study and the observation by Brydson et al. of a constant grain boundary composition independent of additive concentration, suggests that the volume of secondary phases can be controlled.[11] Figure 4.4 presents the proposed additive concentrations to the volume fraction relationship. The volume percent of secondary phases formed in relation to the composition of the glasses were similar in all the samples with the exception of sample B. The volume fraction of secondary phases observed in Sample B was greater than the rest of the sample analyzed due the extensive crystallization of a mullite matrix.

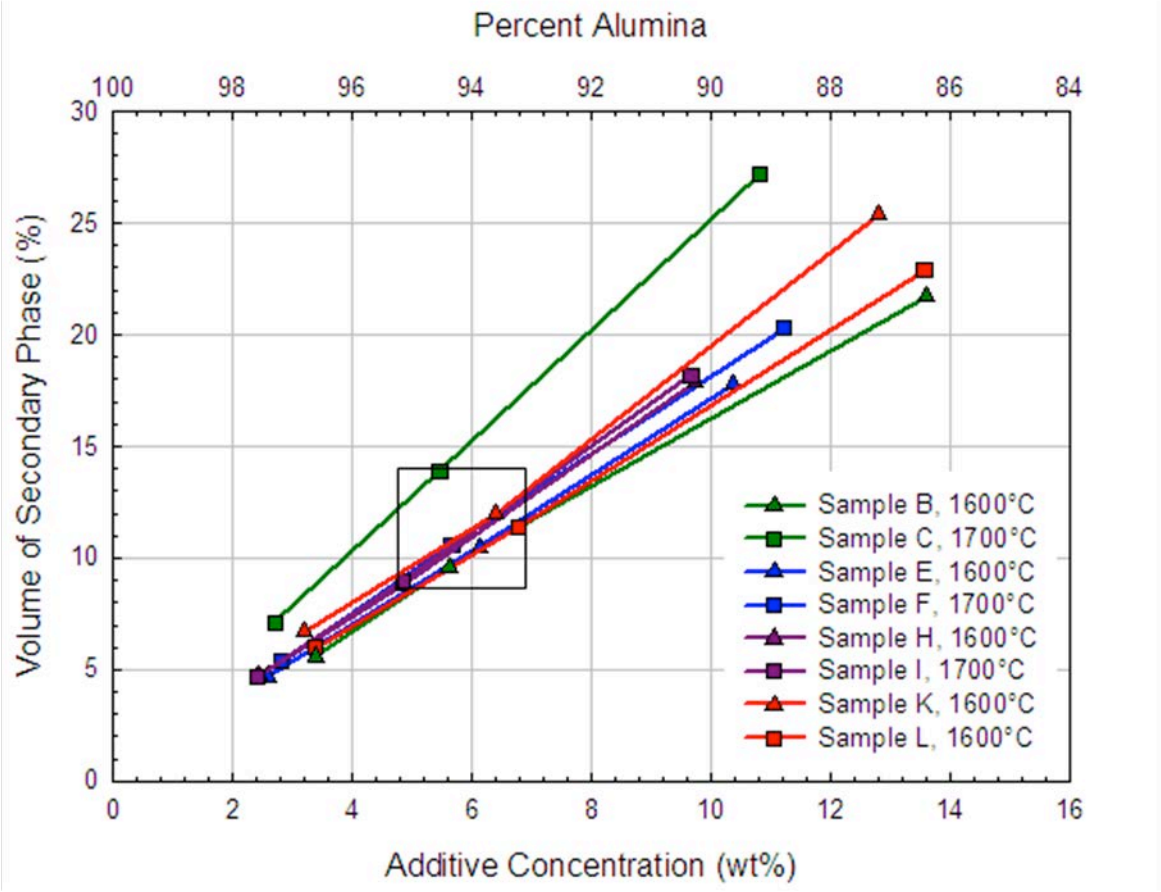

Figure 4.4. Calculated additive concentration relationship with volume fraction of observed secondary phases. The box regions of which contain the experimental points.

4.5. CONCLUSION

Microstructural observations of alumina sintered with calcia and silica additions to yield 93-95 wt% alumina show the volume of secondary phases is consistent with a glass formation boundary approach. From the volume fraction correlation with the triple point chemistries a quantification model for additive levels to desired volume percent has been proposed.

4.6. REFERENCES

1. J.S. Reed, *Introduction to the Principles of Ceramic Processing,* 2nd ed.*;* pp. 608-9. John Wiley & Sons, New York, 1988.

2. P.L. Flaitz, "Some Aspects of Liquid-phase Sintering of Alumina"; Ph.D. Thesis. University of California, Berkeley, CA, 1982.

3. R.E. Chinn, M.J. Haun, C.Y. Kim, and D.B. Price, "Microstructures and Properties of Three Composites of Alumina, Mullite, and Monoclinic $SrAl_2Si_2O_8$," *J. Am. Ceram. Soc.,* **83** [11] 2668-72 (2000).

4. N.P. Padture and H.M. Chan, "Improved Flaw Tolerance in Alumina Containing 1 vol% Anorthite via Crystallization of the Intergranular Glass," *J. Am. Ceram. Soc.,* **75** [7] 1870-5 (1992).

5. C.A. Powell-Dogan and A.H. Heuer, "Microstructure of 96% Alumina Ceramics: III, Crystallization of High-calcia Boundary Glasses," *J. Am. Ceram. Soc.,* **73** [12] 3684-91 (1990).

6. S.J. Bennison, H.M. Chan, and B.R. Lawn, "Effect of Heat Treatment on Crack-resistance Curves in a Liquid Phase Sintered Alumina," *J. Am. Ceram. Soc.,* **72** [4] 677-9 (1988).

7. N.A. Travitzky, D.G. Brandon, and E.Y. Gutmanas, "Toughening of Commercial 85 wt% Al_2O_3 by Controlled Heat Treatments," *Mater. Sci. Eng.,* **71**, 65-70 (1985).

8. Y. Yeshrun, Z. Rosenburg, D.G. Brandon, and N.A. Travitzky, "Effect of Heat Treatment on the Dynamic Response of Commercial 85 wt% Al_2O_3," *Mater. Sci. Eng.,* **71**, 71-5 (1985).

9. W.A. Zdaniewski and H.P. Kirchner, "Toughening of a Sintered Alumina by Crystallization of the Grain-boundary Phase," *Adv. Ceram. Mater.,* **1** [1] 99-103 (1986).

10. H. Tomaszewski, "Effect of the Intergranular Phase Structure on the Thermomechanical Properties of Alumina Ceramics," *Ceram. Int.,* **14** [2] 93-9 (1986).

11. R. Brydson, S.-C. Chen, F.L. Riley, S.J. Milne, X. Pan, and M. Rühle, "Microstructure and Chemistry of Intergranular Glassy Films in Liquid-phase-sintered Alumina," *J. Am. Ceram. Soc.,* **81** [2] 369-79 (1998).

12. A. Nakajima and G.L. Messing, "Liquid-phase Sintering of Alumina Coated with Magnesium Aluminosilicate Glass," *J. Am. Ceram. Soc.,* **81** [5] 1163-72 (1998).

13. H.-Y. Kim, J.-A. Lee, and J.-J. Kim, "Densification Behaviors of Fine-alumina and Coarse-alumina Compacts during Liquid-phase Sintering with the Addition of Talc," *J. Am. Ceram. Soc.,* **83** [12] 3128-34 (2000).

14. H. Song and R.L. Coble, "Morphology of Platelike Abnormal Grains in Liquid-phase-sintered Alumina," *J. Am. Ceram. Soc.,* **73** [7] 2086-90 (1990).

15. M.M. Seabaugh, G.L. Messing, and M. Vaudin, "Texture Development and Microstructure Evolution in Liquid-phase-sintered α-Alumina Ceramics Prepared by Templated Grain Growth," *J. Am. Ceram. Soc.,* **83** [12] 3109-16 (2000).

16. T.F. Lam, K.J. DeCarlo, and W.M. Carty, "Grain Boundary Chemistries in the Sintering of Alumina with Calcia and Silica Additives Revisited: High Silica to Calcia Ratios and the Glass Formation Boundary," *J. Am. Ceram. Soc.,* (submitted for publication).

17. T.F. Lam, K.J. DeCarlo, and W.M. Carty, "Grain Boundary Chemistries in the Sintering of Alumina with Calcia and Silica Additives Revisited: Invert Glass Formation Boundary," *J. Am. Ceram. Soc.,* (submitted for publication).

18. A.L. Gentile and W.R. Foster, "Calcium Hexaluminate and Its Stability Relations in the System CaO-Al_2O_3-SiO_2," *J. Am. Ceram. Soc.,* **46** [2] 74-6 (1963).

19. W. Rasband, ImageJ (Image Processing and Analysis in Java), [Computer Program] National Institutes of Health, Bethesda, MD, 1997.

20. SciVision, SciGlass 6.5, [Computer Program], Lexington, MA, 2005.

21. A.I. Priven and O.V. Mazurin, "Comparison of Methods Used for the Calculation of Density, Refractive Index and Thermal Expansion of Oxide Glasses," *Glass Technol.,* **44** [4] 156-66 (2003).

22. C.S. Hurlbut, *Dana's Manual of Mineralogy,* 18^{th} ed.*;* pp. 466-8. John Wiley & Sons, New York, 1971.

23. Phase Diagrams for Ceramists, Vol. 1; Fig. 630. Edited by E.F. Osborn and A. Muan. American Ceramic Society, Westerville, OH, 1964.

24. C.A. Powell-Dogan, A.H. Heuer, and H.M. O'Bryan, "Devitrification of the Grain Boundary Glassy Phase in a High-alumina Ceramic Substrate," *J. Am. Ceram. Soc.,* **77** [10] 2593-8 (1994).

5. SUMMARY OVERVIEW

5.1. COMPARISON TO LITERATURE

In the sintering of alumina various compositions of additives have been reported, resulting in a variety of mineralogies at the grain boundaries that have lacked an overall explanation of grain boundary evolution in alumina. The glass formation boundary approach for sintering in alumina proposes that the additives be viewed as a localized concentration in contact with alumina particles, where alumina dissolution will proceed as a function of sintering temperature allowing for predictable grain boundary chemistries and mineralogies resulting from alumina saturation of the amorphous grain boundary.[1] This study concludes that the grain boundary mineralogies and chemistries are not random and fall within the concept of a proposed glass formation boundary approach that is applicable to the sintering of alumina.[1, 2]

In this study, controlling the choice of additives was a focus in this study due to reported variability and complexity of additives in the literature. Additives of Na_2O and K_2O were not chosen for the study due to the high potential for alkali migration by the electron beam.[3] MgO was not tested as an additive due to foreseeable issues in quantifying the MgO solubility within an alumina lattice at the alumina grain edges and the complex issues surrounding the exact role of MgO in alumina, which is not fully understood.[4-7] Being that a sufficient amount of sintering literature was available for a direct comparison of these results with the sintering of alumina containing the co-dopants CaO and SiO_2 and the well established glass formation boundary in the CaO-Al_2O_3-SiO_2 system, CaO and SiO_2 additives was an ideal system to test the hypothesis of using the glass formation boundary approach to sintering alumina.[8-22]

The apparent randomness and confusion found within the sintering of alumina occurs because sintering temperatures are not as simple as they appear, the prime example being the comparison of microstructures of 1400°C and 1600°C are fundamentally different. Figure 5.1 shows the conclusions of data this study, the proposed glass formation boundary and the invert glass formation boundary in relation to previous reported literature.

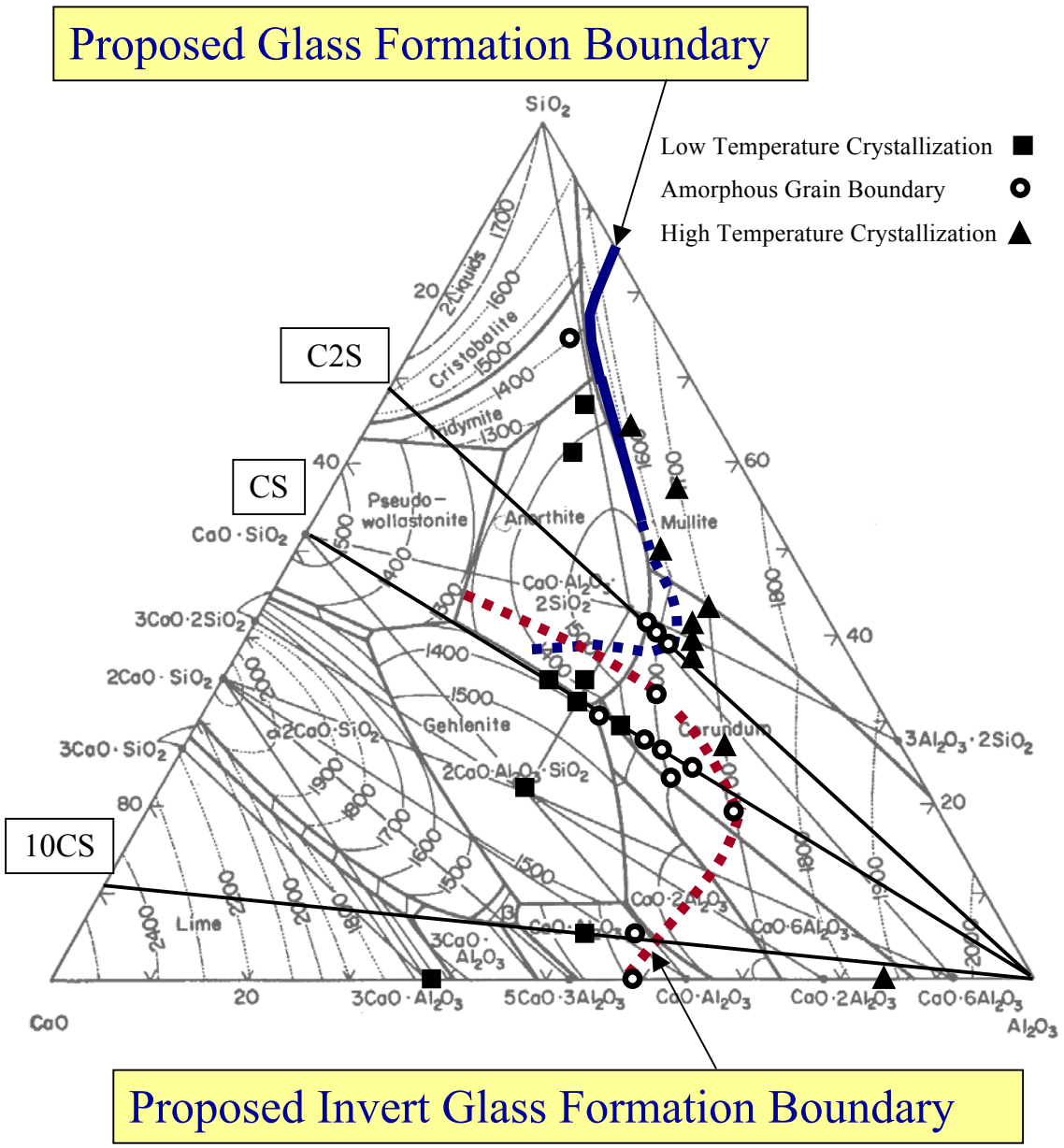

Figure 5.1. The glass formation boundaries in the sintering of alumina in comparison with the reviewed literature.[1, 2, 8-11, 14, 15, 17, 18, 20, 23-26]

As Švančárek et al. had previously shown, varying additive ratios within a 1400°C system will result in crystalline secondary phases relating to corresponding phase fields of the additive ratios.[20] However, when compared with microstructures of above 1600°C these results appear to be random. The resulting randomness is because the observed crystalline secondary phases at 1400°C are not believed to be caused by a

saturation of alumina at the grain boundary but rather a by competing localized low temperature solid state reaction at the grain boundaries. These localized low temperature solid state reactions that were also demonstrated in Wu et al. study of alumina sintering with calcia where subeutectic sintering temperatures of 1330°C yielded crystalline secondary phases.[12] The pseudobinary simulations from FactSage™ of this study further explain the occurrence and explain the dissolution of the secondary phase back into an amorphous grain boundary with increasing temperature.[1]

Above 1600°C, the crystalline secondary phases that occurs result from alumina saturation of amorphous grain boundary obeying the glass formation boundary concept. Two types of glasses were observed, resulting in the proposal of a glass formation boundary and an invert glass formation boundary and not a single continuous glass formation boundary. In the sintering of alumina with calcia and silica additives, a common additive ratio is anorthite glass composition with the ratio of $CaO:2SiO_2$ (C2S). In the range of 1550°C to 1620°C, studies by Kostić et al., Marion et al., Padture et al., and Kim et al. all report amorphous grain boundaries.[14, 17-19] Floyd's sintering study performed at 1650°C in 1964 correlated secondary phases, specifically anorthite, with dielectric loss measurements.[11] At this temperature anorthite should be the result of alumina saturation, however based on the fact the anorthite phase field is within the glass formation boundary this could be the result of crystallization from the slow cool of an industrial process or the shift of glass formation boundary by impurity alkali concentrations allowing for anothite formation.[2] Through dilution experiments (80 wt% alumina, to yield greater quantities of secondary phases), mullite, gehlenite, and calcium hexaluminate were observed by X-ray diffraction that proposed to form at the 94 wt% alumina samples when varying the ratios CaO to SiO_2, the range of the ratios correlating to the specific phases of which were not reported.[11] This study observed the microstructures of mullite and amorphous grain boundaries to occur where $x>4$ in ratios $CaO:xSiO_2$ for sintering temperatures above 1600°C.[1]

Samples sintered at 1550°C yielding amorphous grain boundaries are within the glass formation boundary but will crystallized by heat treatments or annealing processes which enable nucleation and growth as demonstrated by Powell-Dogan et al. and Padture et al.[8, 17] Phases outside of the glass boundary that did not appear during sintering will not

crystallize at the heat treatment temperatures within the glass formation boundary. This provides an explanation for why Powell-Dogan et al. did not find mullite as a crystallized phase in their heat treatment studies.[8, 27, 28]

Another common additive ratio in the sintering of alumina is $CaO:SiO_2$ (CS), studies of which have been performed by Seabaugh et al., Powell-Dogan and Heuer, Kostić et al., and Song and Coble.[8, 10, 15, 18] This study found that the amorphous compositions of the grain boundaries of the ratios with greater CaO to SiO_2 were of an invert compositions and have similar to properties of the observed bulk glasses, specifically the solubility of chloride ions (an artifact of $CaCl_2$ as the source of CaO). Though the triple points chemistries of the amorphous grain boundaries did not appear to correlate sintering temperature with the prescribed liquidus of the phase diagram by the glass formation boundary approach as they did in higher silica systems, this could be the result of an unquenched system.[2] A similar difference has been observed in Single Crystal Conversion studies where the observance of the grain boundary is dependent on cooling. This study proposes a plausible explanation for structurally undetectable alumina crystallization (from the grain boundary) back on to interfaces of the alumina grains, resulting in the differences of grain boundary thickness previously noted by Dillon et al. and Scott et al.[2, 25, 26]

In comparison to literature, the sintering experiments of this study did not find calcium hexaluminate that have been reported Powell-Dogan et al., Kostić et al., and Song and Coble.[2, 15, 16] As pointed out in the discussion of this study, specifically the varying findings of Gentile et al. and Obsorn phase diagrams, the stability of calcium hexaluminate is a topic of uncertainty.[2, 23, 29] Even in Powell-Dogan study, it was noted that the calcium hexaluminate appears to resorb from the sintered sample upon heat treatments.[16]

It should be noted that the compilation of the literature of this study involved studies that reported phases from X-ray diffraction alone, without a microstructural study from Transmission Electron Microscopy or reconfirmation chemical analysis in many cases. Even with this being the case, the glass formation boundary approach to sintering in alumina proposed in this study is very consistent with the reviewed literature.

5.2. REFERENCES

1. T.F. Lam, K.J. DeCarlo, and W.M. Carty, "Grain Boundary Chemistries in the Sintering of Alumina with Calcia and Silica Additives Revisited: High Silica to Calcia Ratios and the Glass Formation Boundary," *J. Am. Ceram. Soc.,* (submitted for publication).

2. T.F. Lam, K.J. DeCarlo, and W.M. Carty, "Grain Boundary Chemistries in the Sintering of Alumina with Calcia and Silica Additives Revisited: Invert Glass Formation Boundary," *J. Am. Ceram. Soc.,* (submitted for publication).

3. A.K. Varshneya, A.R. Cooper, and M. Cable, "Changes in Composition During Electron-microprobe Analysis of K_2O-SrO-SiO_2 Glass," *J. Appl. Phys.,* **75** [4] 2199-202 (1966).

4. J.E. Blendell and C.A. Handwerker, "Effect of Chemical Composition on Sintering Ceramics," *J. Cryst. Growth,* **75** [1] 138-60 (1986).

5. S.J. Bennison and M.P. Harmer, "A History of the Role Magnesia in the Sintering of α-Alumina," *Ceram. Trans.,* **7**, 13-49 (1990).

6. W. Jo, D.-Y. Kim, and N.-M. Hwang, "Effect of Interface Structure on the Microstructural Evolution of Ceramics," *J. Am. Ceram. Soc.,* **89** [8] 2369-80 (2006).

7. S.J. Dillon and M.P. Harmer, "Comment on "Effect of Interface Structure on the Microstructural Evolution of Ceramics," *J. Am. Ceram. Soc.,* **90** [7] 2291-2 (2007).

8. C.A. Powell-Dogan and A.H. Heuer, "Microstructure of 96% Alumina Ceramics: III, Crystallization of High-calcia Boundary Glasses," *J. Am. Ceram. Soc.,* **73** [12] 3684-91 (1990).

9. R. Brydson, S.-C. Chen, F.L. Riley, S.J. Milne, X. Pan, and M. Rühle, "Microstructure and Chemistry of Intergranular Glassy Films in Liquid-phase-sintered Alumina," *J. Am. Ceram. Soc.,* **81** [2] 369-79 (1998).

10. M.M. Seabaugh, G.L. Messing, and M. Vaudin, "Texture Development and Microstructure Evolution in Liquid-phase-sintered α-Alumina Ceramics Prepared by Templated Grain Growth," *J. Am. Ceram. Soc.,* **83** [12] 3109-16 (2000).

11. J.R. Floyd, "Effect of Secondary Crystalline Phases on Dielectric Losses in High-alumina Bodies," *J. Am. Ceram. Soc.,* **47** [11] 539-43 (1964).

12. S.J. Wu, L.C. DeJonghe, and M.N. Rahaman, "Subeutectic Densification and Second-phase Formation in Al_2O_3-CaO," *J. Am. Ceram. Soc.,* **68** [7] 385-8 (1985).

13. E. Kostić, S.J. Kiss, and S. Bošković, "Liquid Phase Sintering of Alumina," *Powder Metall. Int.,* **19** [4] 41-3 (1987).

14. J.E. Marion, C.H. Hsueh, and A.G. Evans, "Liquid-phase Sintering of Ceramics," *J. Am. Ceram. Soc.,* **70** [10] 708-13 (1987).

15. H. Song and R.L. Coble, "Morphology of Platelike Abnormal Grains in Liquid-phase-sintered Alumina," *J. Am. Ceram. Soc.,* **73** [7] 2086-90 (1990).

16. C.A. Powell-Dogan and A.H. Heuer, "Microstructure of 96% Alumina Ceramics: I, Characterization of the As-sintered Materials," *J. Am. Ceram. Soc.,* **73** [12] 3670-6 (1990).

17. N.P. Padture and H.M. Chan, "Improved Flaw Tolerance in Alumina Containing 1 vol% Anorthite via Crystallization of the Intergranular Glass," *J. Am. Ceram. Soc.,* **75** [7] 1870-5 (1992).

18. E. Kostić, S. Bošković, and S.J. Kiss, "Reaction Sintering of Al_2O_3 in the Presence of the Liquid Phase," *Ceram. Int.,* **19** [4] 235-40 (1993).

19. M.J. Kim and D.Y. Yoon, "Effect of Magnesium Oxide Addition on Surface Roughening of the Alumina Grains in Anorthite Liquid," *J. Am. Ceram. Soc.,* **86** [4] 630-3 (2003).

20. P. Švancárek, D. Galusek, F. Loughran, A. Brown, R. Brydson, A. Atkinson, and F. Riley, "Microstructure-stress Relationships in Liquid-phase Sintered Alumina Modified by the Addition of 5 wt.% of Calcia-silica Additives," *Acta Mater.,* **54** [18] 4853-63 (2006).

21. A.P. Goswami, S. Roy, M.K. Mitra, and G.C. Das, "Influence of Powder, Chemistry and Intergranular Phases on the Wear Resistance of Liquid-Phase-Sintered Al_2O_3," *Wear,* **244** [1-2] 1-14 (2000).

22. J.E. Shelby, "Formation and Properties of Calcium Aluminosilicate Glasses," *J. Am. Ceram. Soc.,* **68** [3] 155-8 (1985).

23. Phase Diagrams for Ceramists, Vol. 1; Fig. 630. Edited by E.F. Osborn and A. Muan. American Ceramic Society, Westerville, OH, 1964.

24. D.S. Phillips and Y.R. Shiue, "Grain Boundary Microstructure in Alumina Ceramics," *Adv. Ceram,* **10**, 357-67 (1983).

25. S.J. Dillon and M.P. Harmer, "Mechanism of "Solid State" Single Crystal Conversion in Alumina," *J. Am. Ceram. Soc.,* **90** [3] 993-5 (2007).

26. C. Scott, M. Kaliszewski, C. Greskovich, and L. Levinson, "Conversion of Polycrystalline Al_2O_3 into Single Crystal Sapphire by Abnormal Grain Growth," *J. Am. Ceram. Soc.,* **85** [5] 1275-80 (2002).

27. C.A. Powell-Dogan and A.H. Heuer, "Microstructure of 96% Alumina Ceramics: II, Crystallization of High-magnesia Boundary Glasses," *J. Am. Ceram. Soc.,* **73** [12] 3677-83 (1990).

28. C.A. Powell-Dogan, A.H. Heuer, and H.M. O'Bryan, "Devitrification of the Grain Boundary Glassy Phase in a High-alumina Ceramic Substrate," *J. Am. Ceram. Soc.,* **77** [10] 2593-8 (1994).

29. A.L. Gentile and W.R. Foster, "Calcium Hexaluminate and Its Stability Relations in the System CaO-Al_2O_3-SiO_2," *J. Am. Ceram. Soc.,* **46** [2] 74-6 (1963).

6. CONCLUSIONS

The microstructural observations of this study showed that the concept of glass formation boundary approach is applicable to the sintering of alumina with glass forming additives. At the 1400°C sintering temperatures, competing localized low temperature solid state reactions are proposed to occur. Above 1600°C two types of glasses were observed, resulting in the proposal of a glass formation boundary and an invert glass formation boundary. The amorphous compositions of the grain boundaries appear to have similar to properties of the observed bulk glasses, specifically the solubility of chloride ions. The proposed model of the glass formation boundaries allow for the explanation for the various crystalline secondary phases reported in the literature and phase predictions in steady state non-equilibrium conditions of sintering in alumina with calcia and silica additives.

The volume of the observed secondary phases correlates with the grain boundary chemistries at the triple points which were consistent with the glass formation boundary approach. Being that the glass formation boundary approach works with the hypothesis of localized concentrations from the sintering additives and the reported observations of grain boundary compositions to be independent of the concentration additives within a sintering system, the volume of secondary phases would be directly limited by the concentration of additives used in sintering. The glass formation boundary concept proposed is applicable to sintering alumina with other glass forming additives.